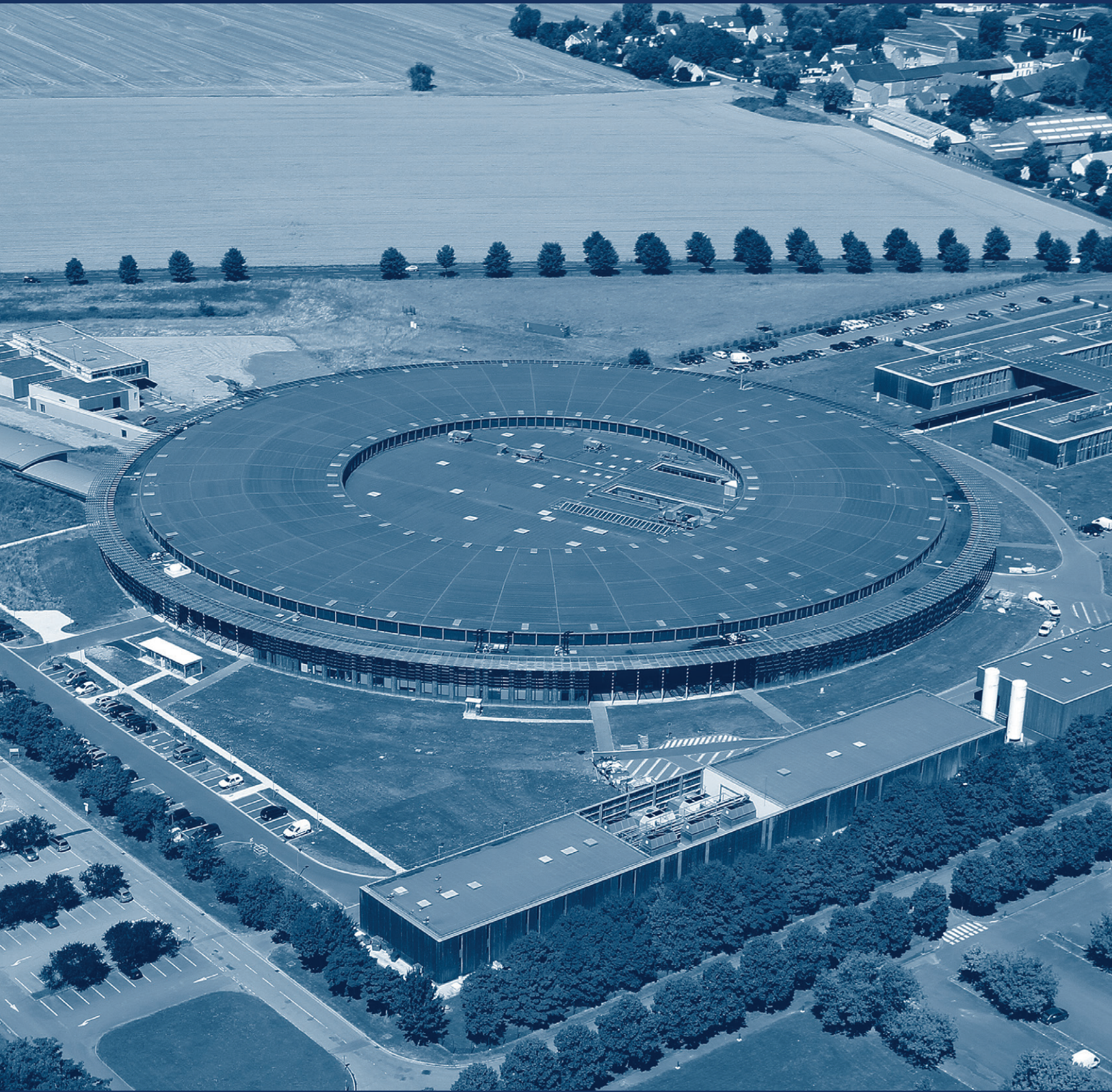




SOLEIL
HIGHLIGHTS 2013
Through the prism of science



ÉDITORIAL

Pour cette quatrième édition des faits scientifiques marquants de SOLEIL la sélection des articles s'est avérée encore plus difficile que les années précédentes, avec un nombre de publications toujours en forte augmentation, tant en quantité qu'en qualité. Cette augmentation reflète le dynamisme et l'excellence des recherches menées par les scientifiques des lignes de lumière de SOLEIL et leurs utilisateurs, également accueillis en nombre croissant, et ce dans tous les domaines de la recherche couverte par SOLEIL. De tels résultats sont bien sûr rendus possibles grâce aux performances et à la fiabilité de « la machine », et donc à l'implication constante des équipes des Sources ainsi que des différents groupes support. Ces derniers réalisent un travail de R&D, transversal à toutes les divisions de SOLEIL, qui apporte des réponses sur mesure - parfois même de façon anticipée - aux demandes des chercheurs sur les lignes afin de toujours faciliter et améliorer leurs prises de résultats.

2014 voit avancer les différents projets en cours à SOLEIL, avec notamment les quatre dernières lignes de lumière dont la construction et la mise au point se déroulent selon le calendrier prévu. Leurs utilisateurs arriveront à partir de 2015, pour une moisson de résultats toujours plus riche.

Ces Highlights paraissent au cœur de l'Année Internationale de la Cristallographie, science interdisciplinaire s'il en est, qui mobilise des techniques complémentaires mises en œuvre sur près de la moitié des lignes de lumière de SOLEIL. De quoi alimenter une partie de l'édition 2014 de nos Highlights.

Jean DAILLANT

Directeur Général de SOLEIL

EDITORIAL

For this fourth edition of the scientific highlights at SOLEIL, it turned out to be even more difficult to decide which articles to include, with the quantity and quality of publications increasing every year. This increase reflects the excellent vital research conducted by scientists responsible for the SOLEIL beamlines and also their users, arriving in increasing numbers to make use of beam time in all areas of research covered by SOLEIL. Such results are of course made possible primarily due to the performance and reliability of the "machine" and thus the constant involvement of the beam teams and the different support groups. The latter carry out R & D, linking together all the SOLEIL divisions and providing customized solutions - sometimes even in advance - at the request of researchers on the beamlines, in order to constantly facilitate and improve their results.

In 2014, several projects are in the pipeline at SOLEIL, notably the next four beamlines, with both their construction and optimization on schedule. These will be open to outside users from 2015, resulting in an ever richer panoply of results.

These Highlights are appearing during the International Year of Crystallography, an interdisciplinary science like no other and which requires complementary techniques set up on almost half the beamlines at SOLEIL. A good reason to dedicate part of the 2014 edition of our Highlights to this subject.

Jean DAILLANT

Director General of SOLEIL

SOLEIL EN 2013

La croissance significative de l'accueil des utilisateurs observée entre 2010 et 2012 s'est poursuivie en 2013. Les lignes de lumière et les laboratoires Chimie, Surfaces et Biologie de SOLEIL ont compté près de 4 000 visites d'utilisateurs, issus de 690 laboratoires différents, 486 de ces laboratoires utilisant SOLEIL pour la première fois. Les scientifiques en provenance des Etats-Unis sont entrés en 2013 dans le « Top Five » des communautés étrangères utilisatrices de SOLEIL, avec le Royaume-Uni, l'Allemagne, l'Italie et l'Espagne.

Le retour général des utilisateurs, en particulier sur la qualité des environnements expérimentaux et la qualité du support apporté par les scientifiques sur les lignes, est extrêmement positif au vue des « end of run reports » qui couvrent deux tiers des expériences réalisées en 2013.

En décembre, pour le 14^{ème} appel à projets, la ligne HERMES s'est ajoutée aux vingt-quatre lignes de lumière déjà ouvertes aux utilisateurs. Les quatre dernières lignes, NANOSCOPIUM, ANATOMIX, ROCK et PUMA, ouvriront graduellement d'ici 2015, la station d'imagerie par diffraction cohérente (CDI) de NANOSCOPIUM devant même être opérationnelle dès 2014.

D'autre part, le nombre des publications est en constante augmentation, en nombre et en qualité, avec une proportion importante de publications dans des revues à haut facteur d'impact. 545 articles ont ainsi été publiés en 2013, contre 404 sur l'ensemble de 2012.

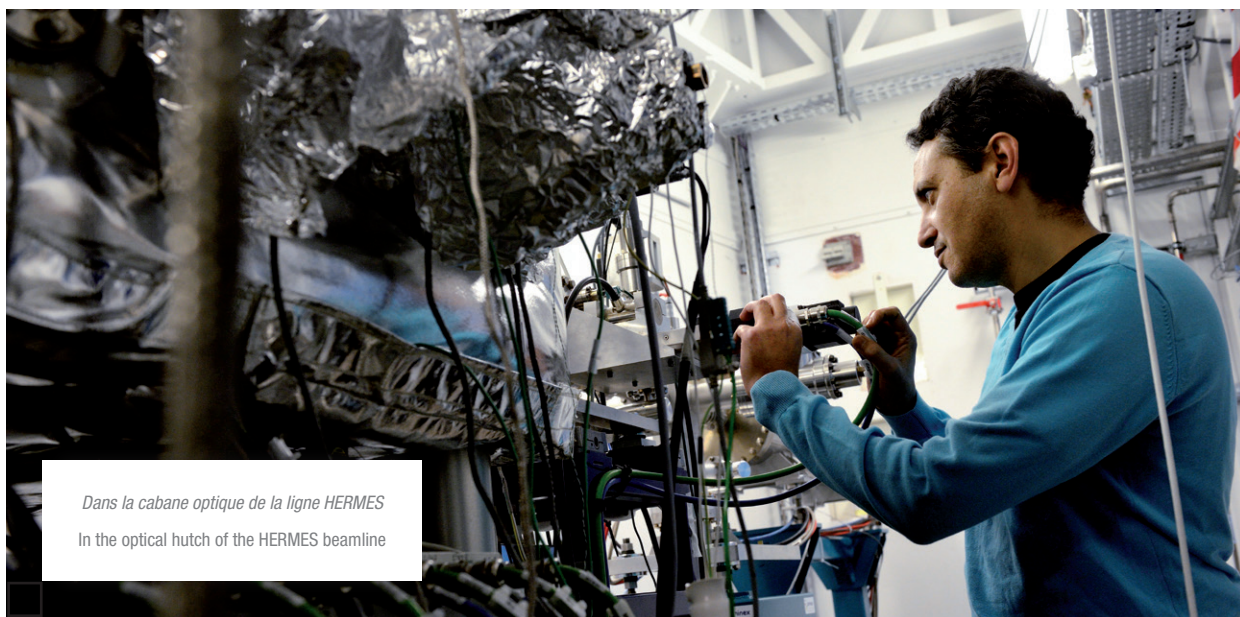
SOLEIL IN 2013

The strong growth in number of users, a trend seen between 2010 and 2012, continued in 2013. SOLEIL beamlines and Chemistry, Surfaces, and Biology laboratories had almost 4000 visits, by scientists from 690 different laboratories. Of these, 486 labs were using SOLEIL for the first time. In 2013, scientists from the USA joined the top five foreign users of SOLEIL, alongside the UK, Germany, Italy, and Spain.

On the whole, the feedback has been extremely positive. Our users especially appreciated the quality of the experimental environments and the support provided by the beamline scientists. This is reflected in the 'end of run reports' covering two thirds of the experiments carried out in 2013.

In December, for the 14th call for projects, the HERMES beamline joined the twenty-four beamlines already open to users. The last four beamlines, NANOSCOPIUM, ANATOMIX, ROCK and PUMA, will open between now and 2015. The coherent diffraction imaging (CDI) station on NANOSCOPIUM should even be operational in 2014.

The number of publications is also growing steadily, and quality is on the rise. Many of the articles are being published in high impact factor journals. 545 articles were published in 2013, compared to 404 the year before.



Dans la cabane optique de la ligne HERMES
In the optical hutch of the HERMES beamline



Le groupe Fonctionnement, en charge du pilotage des accélérateurs et de l'anneau de stockage, au grand complet.

The whole Operation team, in charge of running the accelerators and the storage ring.

TOUJOURS PLUS DE PHOTONS

L'opération de l'anneau de stockage avec les plus hautes performances reste la préoccupation collective des équipes de SOLEIL (lire également page 134). L'ensemble des résultats obtenus en 2013 met en évidence une très bonne fiabilité des accélérateurs malgré une dynamique continue d'installation de nouveaux équipements. La disponibilité du faisceau de photons pour les lignes de lumière, pourtant impactée par des microcoupures de l'alimentation électrique générale totalement indépendantes de SOLEIL, est remontée à 98 % (96,4 % en 2012) et le temps moyen entre deux pannes a atteint un record de 68 heures, contre 49 en 2012.

Le maintien au meilleur niveau des performances de SOLEIL passe également par le développement d'insertions innovantes et une veille sur les sources de rayonnement utilisant des accélérateurs. Dans ce cadre, des études pour un « wiggler sous-vide a périodique » et un « onduleur cryo-ready » sont en cours, en collaboration avec le synchrotron suédois MAX IV ainsi que pour des kickers d'injection multipôles innovants adaptés soit à SOLEIL, soit à MAX IV.

MORE AND MORE PHOTONS

Operation of the storage ring with the highest performance characteristics remains the joint concern of all SOLEIL teams (see also page 134). All the results obtained in 2013 show how very reliable the accelerators are, even though new equipment is constantly being installed. The availability of the photon beam for the beamlines has at times been affected by power supply problems beyond the control of SOLEIL, but it has come back up to 98% (compared to 96.4% in 2012). The mean time between failures has reached a record of 68 hours, compared to 49 in 2012.

Keeping SOLEIL at the highest possible level of performance also means that we need to develop innovative insertions and keep a watch on radiation sources using accelerators. With this in mind, studies for an aperiodic in-vacuum wiggler and a cryo-ready undulator are underway, in collaboration with the Swedish MAX IV synchrotron. We are also working on innovative multipole injection kickers for either SOLEIL or MAX IV.

DU CÔTÉ DES LIGNES DE LUMIÈRE

La construction des trois lignes de lumière financées sur projet avance : la première cabane optique de PUMA, optimisée pour les matériaux anciens, est achevée et le wiggler (W164), source de lumière de cette ligne, a été installé pendant l'arrêt technique du mois d'octobre.

La construction de ROCK, ligne d'absorption X dédiée aux études cinétiques dans les sciences de l'énergie (batteries) et de la catalyse, avance selon le calendrier prévu, avec notamment la mise en place du premier miroir dans le tunnel de l'anneau de stockage en octobre. Et un accueil des premiers utilisateurs en février 2015.

La construction de la ligne longue de nanotomographie ANATOMIX, qui est soutenue par des partenaires académiques et industriels dans les domaines du biomédical et des matériaux avancés, est bien lancée dans sa phase de conception avec des développements d'instruments originaux grâce aux compétences des différents groupes support.

Mais les lignes de lumière déjà fonctionnelles font également l'objet de toute l'attention des équipes de SOLEIL. Suite à une première autorisation d'utiliser la ligne de lumière MARS au-dessus des seuils d'exemption, délivrée par l'Autorité de Sécurité Nucléaire le 30 novembre 2012, des expériences sur des échantillons dépassant ces seuils ont été réalisées en septembre 2013 par un groupe du CEA. Le passage aux étapes ultérieures, pour l'étude d'échantillons de plus forte radioactivité, est en cours.

Pour rappel, le projet « femto-slicing » permettra de générer des pulses fs X à plus haute cadence combinant lasers femto-seconde (sur les lignes TEMPO, CRISTAL et, potentiellement, DEIMOS et GALAXIES) et rayonnement synchrotron afin de développer des expériences résolues en temps. Sa réalisation se poursuit dans le calendrier prévu, avec notamment de premiers essais du laser dans le tunnel de l'anneau de stockage effectués en août 2013, et la mise en place en octobre du wiggler W164 qui, outre son rôle de source de lumière pour la ligne PUMA (cf plus haut), servira de « modulateur » au processus de femto-slicing.

NEWS FROM THE BEAMLINES

The construction of the three project-financed beamlines is making progress. The first optical hut for PUMA, optimised for ancient materials, has been completed. The wiggler (W164), the light source for this beamline, was installed during the technical shutdown in October.

ROCK is an X-ray absorption beamline dedicated to kinetic studies in the fields of energy (batteries) and catalysis. Its construction is advancing on schedule; the first mirror was installed in the storage ring tunnel in October. And the first users are expected in February 2015.

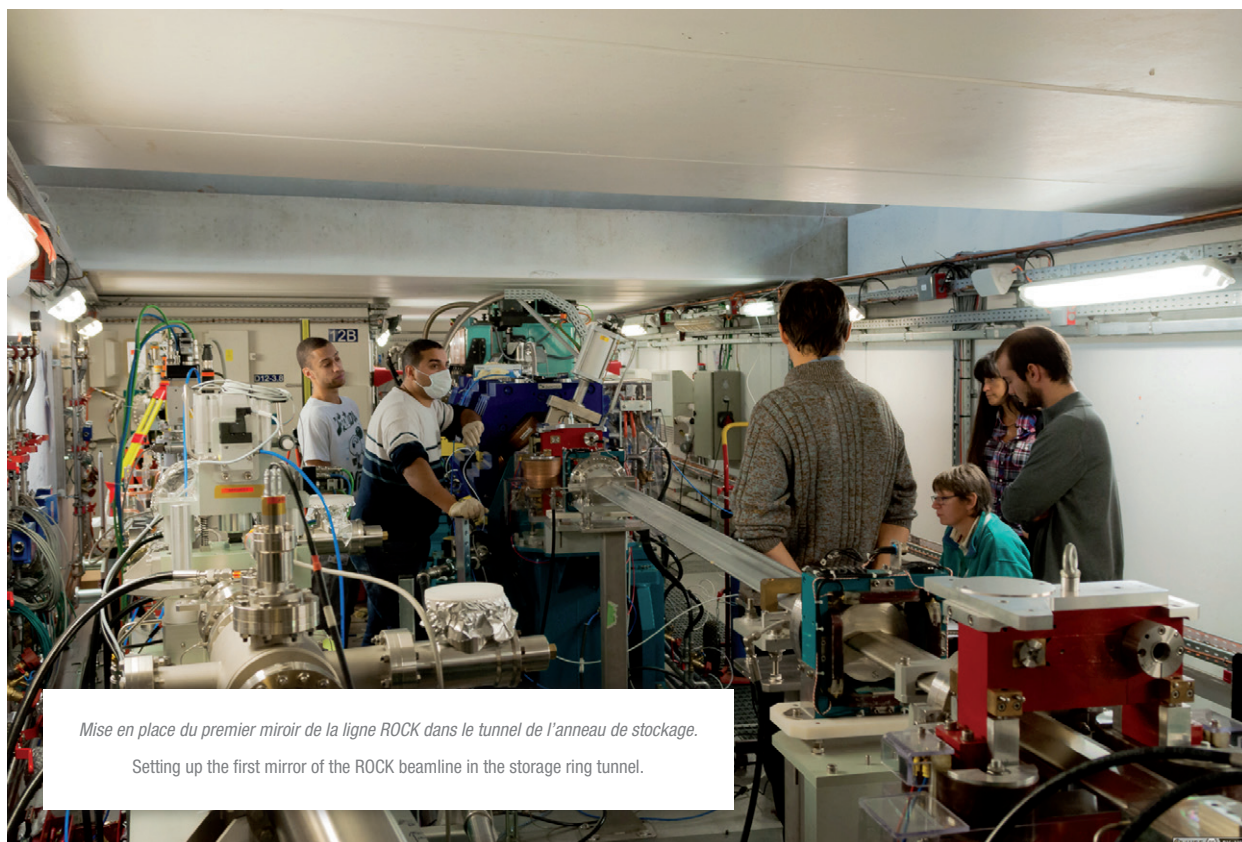
The design phase for the long nanotomography beamline, ANATOMIX, is well underway, with support from academic and industrial partners in the biomedical and advanced materials fields. The skills of the support groups are being used to develop original instruments.

But the teams at SOLEIL have not forgotten about the beamlines that are already operational. Following a first authorisation to use the MARS beamline above the exemption thresholds, issued by the ASN on 30 November 2012, experiments on samples exceeding those thresholds were carried out by a group from the CEA in September 2013. This project is now moving into the next phase, to study more highly radioactive samples.

The femto-slicing project will generate fs X-ray pulses at a higher rate, combining femto-second lasers (on the TEMPO, CRISTAL, and possibly the DEIMOS and GALAXIES beamlines) and synchrotron radiation to develop time-resolved experiments. This project is going according to schedule. The first tests of the laser in the storage ring tunnel were performed in August 2013, and the W164 wiggler was set up in October. In addition to being the light source for the PUMA beamline (see above), this will be a modulator for the femto-slicing process.

La mise en place de systèmes d'acquisition à haut flux de données sur les lignes de lumière est un enjeu important pour SOLEIL. Le prototype du système FlyScan, acquisitions multi-détecteurs sur des systèmes en mouvement et cadencés par une électronique unique, a été enrichi (voir également page 126) et mis en œuvre sur la ligne METROLOGIE, donnant des résultats prometteurs. Son optimisation se poursuit en vue d'une utilisation sur NANOSCOPIUM et, dans un second temps, sur des lignes de lumière déjà ouvertes aux utilisateurs : sept lignes pourraient être concernées dans un premier temps suivies potentiellement de huit autres.

The installation of high data rate acquisition systems on the beamlines is an important issue for SOLEIL. The prototype of the FlyScan system, providing multi-detector acquisition on moving systems, paced by a single electronic unit, has been enriched (see also page 126). This has been used on the METROLOGIE beamline, with promising results. It is still being optimised with a view to using it on NANOSCOPIUM. Later, it will also be used on beamlines that are already open to users: this could initially include seven beamlines, possibly followed by eight others.



Mise en place du premier miroir de la ligne ROCK dans le tunnel de l'anneau de stockage.

Setting up the first mirror of the ROCK beamline in the storage ring tunnel.

VERS LES SOURCES DE LUMIÈRE DE DEMAIN

De premiers résultats marquants ont été obtenus dans le cadre de la collaboration LUNEX5. La dernière réunion d'avancement a regroupé 36 participants de 7 laboratoires différents montrant la forte mobilisation autour de ce projet. Une excellente nouvelle a par ailleurs été annoncée en juillet 2013 : Marie-Emmanuelle Couprie, responsable du groupe Magnétisme et Insertions de la Division Sources et Accélérateurs de SOLEIL, a obtenu une bourse ERC (Advanced European Research Council grant) de 2,5 millions d'euros sur 5 ans pour le projet COXINEL, qui vise à démontrer, dans le cadre de la R&D de LUNEX, qu'en utilisant l'accélération par laser il est possible d'obtenir l'amplification Laser à Electrons Libres nécessaire au développement de sources de lumière plus compactes.

MAINTIEN ET DÉVELOPPEMENT DE NOS PARTENARIATS

Les partenariats scientifiques SOLEIL ont poursuivi leur dynamique en 2013, tant au niveau national avec le soutien de l'Agence Nationale de la Recherche (ANR) sur une quinzaine de projets de recherche collaborative et toujours un partenariat fort avec l'Institut National de la Recherche Agronomique (INRA), qu'au niveau européen avec l'obtention de la bourse européenne ERC citée plus haut.

La coopération internationale n'est pas en reste avec la conclusion d'un Memorandum of Understanding SOLEIL-SPring-8 en juin 2013, accord de coopération avec le synchrotron japonais qui confortera des échanges déjà fructueux entre nos deux centres en particulier pour les aspects d'utilisation du rayonnement synchrotron.

L'un des événements majeurs de 2013 a été, le 12 septembre dernier, l'inauguration officielle d'IPANEMA (plateforme européenne de recherche dédiée à l'étude des matériaux anciens), après un suivi sans faille de la construction par les groupes supports de SOLEIL et l'équipe IPANEMA. Etaient présents Madame la Ministre de l'Enseignement Supérieur et de la Recherche et Monsieur le Président de la Région Île de France entourés de nombreux élus locaux, des représentants du Ministère de la Culture et du CNRS.



*Signature du Memorandum of Understanding SOLEIL-SPring-8
Mme Fioraso, Ministre de l'Enseignement Supérieur et de la Recherche,
M. Yamamoto, Ministre d'Etat dédié à Okinawa aux Territoires du Nord, M.
Shirikawa, Président du JASRI, M. Ishikawa, Directeur du RIKEN Spring-8 Center
et M. Daillant, Directeur Général de SOLEIL.*

Signing of the Memorandum of Understanding between SOLEIL and Spring-8.
Mrs Fioraso, Minister for Research and Higher Education,
Mr Yamamoto, Minister for Okinawa and the Northern Territories,
Mr Shirikawa, Chairman of JASRI, Mr Ishikawa, Director of the RIKEN Spring-8
Center, and Mr Daillant, Director General of SOLEIL.

LOOKING AHEAD TO TOMORROW'S LIGHT SOURCES

Some initial exciting results have been obtained in the context of the LUNEX5 joint project. The last progress meeting was attended by 36 participants from seven different laboratories—which goes to show how many resources have been devoted to this project. And some excellent news was announced in July 2013: Marie-Emmanuelle Couprie, head of the Magnetism and Insertions group of the Sources and Accelerators Division at SOLEIL, has obtained an Advanced European Research Council grant of 2.5 million euros over five years for the COXINEL project. This project aims to show, in the context of LUNEX R&D, that laser acceleration can be used to obtain the free electron laser amplification required to develop more compact light sources.



Geneviève Fioraso, Ministre de l'Enseignement Supérieur et de la Recherche et Jean-Paul Huchon, président de la Région Île-de-France, accompagnés d'une délégation officielle d'élus locaux et régionaux, accueillis par Loïc Bertrand, directeur d'IPANEMA.

Geneviève Fioraso, Minister for Higher Education and Research, and Jean-Paul Huchon, President of the Île-de-France region, accompanied by an official delegation of local and regional elected officials, being greeted by Loïc Bertrand, Director of IPANEMA.

MAINTAINING AND EXTENDING OUR PARTNERSHIPS

The scientific partners at SOLEIL have maintained their momentum in 2013. Nationally, they have obtained support from the ANR (French National Research Agency) for about fifteen joint research projects and an ongoing strong partnership with INRA (the National Institute for Agricultural Research). On a European level, they have received the European ERC grant mentioned above. International cooperation is also on the agenda, with the signing of a Memorandum of Understanding between SOLEIL and SPring-8 in June 2013. This cooperation agreement with the Japanese synchrotron will give a further boost to the productive work we already do together, especially for aspects concerning the use of synchrotron radiation.

One of the biggest highlights of 2013 took place on 12th September: the official opening of IPANEMA (European research platform dedicated to the study of ancient materials). This was the culmination of the flawless work done by the SOLEIL support groups and the IPANEMA team in supervising its construction. In attendance were the Minister for Higher Education and Research and the President of the Île-de-France region, as well as many local elected officials and representatives of the Ministry of Culture and the CNRS.



La société Sigmaphi Electronics et SOLEIL ont signé le 5 décembre 2013 un accord de transfert de savoir-faire concernant des amplificateurs radio-fréquence à transistors.

On 5th December 2013, Sigmaphi Electronics and SOLEIL signed a technology transfer agreement concerning transistor RF amplifiers.

DES RELATIONS FORTES ET DURABLES AVEC L'INDUSTRIE

Les entreprises industrielles et de services à l'industrie sont de plus en plus nombreuses à travailler avec SOLEIL, aussi bien pour l'utilisation des lignes de lumière que dans le cadre de partenariats scientifiques, technologiques ou commerciaux.

Du point de vue des prestations d'analyse synchrotron, l'accélération de l'utilisation industrielle observée depuis le début de l'année 2012 s'est poursuivie en 2013, avec une croissance annuelle de plus de 80 % du nombre de projets industriels. Les secteurs industriels les plus utilisateurs de SOLEIL ont été en 2013, par ordre de volume décroissant : la pharmacie, les biotechnologies, la pétrochimie et les cosmétiques ; ces 4 secteurs ont représenté collectivement plus de 90 % des projets de recherche propriétaire. La moitié des lignes de lumière ouvertes aux utilisateurs est maintenant impliquée dans des projets d'expériences pour l'industrie. L'ensemble des projets à vocation industrielle, incluant les prestations de services évoquées précédemment et les projets déposés en comités de programme, dépasse pour la première fois la barre des 10 % du total des projets externes menés à SOLEIL.

La mise en place de nouvelles plateformes d'interface spécialisées s'est poursuivie au cours de l'année 2013, notamment pour répondre aux besoins de l'industrie cosmétique dans le cadre de la plateforme mutualisée d'innovation (PFMI) Cosmétomique et à l'attente des entreprises de la région Alsace dans le domaine des matériaux et nanotechnologies dans le cadre du projet MICASOL regroupant l'Institut Carnot MICA et des laboratoires alsaciens. Le lancement opérationnel de ces deux plateformes est prévu au cours du premier semestre 2014, pour permettre la réalisation des premières prestations de services d'analyses synchrotron ou de formation, et la mise en place des premiers partenariats de R&D.

Enfin SOLEIL a poursuivi en 2013 sa politique de mise à disposition des compétences technologiques de ses équipes auprès des PME et d'autres grandes infrastructures, en réalisant des prestations de services, de formation ou d'assistance technique dans les domaines de l'ultra-vide, des mesures magnétiques ou des aimants et alimentations pulsées.

STRONG AND DURABLE LINKS WITH INDUSTRY

There are more and more industrial and service companies working with SOLEIL, both to use the beamlines and in the context of scientific, technological, or commercial partnerships.

With regard to synchrotron analysis services, the increase in industrial use observed since the beginning of 2012 continued in 2013, with the number of industrial projects growing by more than 80% in a year. In decreasing order of volume, the industrial sectors that were the heaviest users of SOLEIL in 2013 were: pharmaceuticals, biotechnologies, petrochemicals, and cosmetics. These four sectors together accounted for more than 90% of proprietary research projects. Half of the beamlines open to users are now used for experiments related to industrial projects. All industrial projects, including the provision of service mentioned earlier and projects submitted to the programme committees, now account for more than 10% of the total number of external projects conducted at SOLEIL.

New specialist interface platforms continued to be set up throughout 2013. One was needed by the cosmetic industry in the context of the Cosmetomic mutualised innovation platform. The other was required to satisfy companies in the Alsace region in the field of materials and nanotechnologies, in the context of the MICASOL project involving Institut Carnot MICA and Alsatian laboratories. The operational launch of these two platforms is planned for the first half of 2014, at which point the first synchrotron testing or training services can be offered and the first R&D partnerships can be set up.

Finally, in 2013, SOLEIL pursued its policy of providing the technological skills of its teams to SMEs and other large infrastructures, to supply services, training, and technical support in the fields of ultra-high vacuum, magnetic measurements, and magnets and pulsed power supplies.

LA SCIENCE ENSEMBLE

SOLEIL a à cœur de mettre la science au cœur de la société, au travers de nombreuses actions de médiation scientifique. Nos équipes vont à la rencontre du public lors d'événements extérieurs classiques tels que la Fête de la Science, les Années Internationales, les Journées du Patrimoine ou la Nuit des Chercheurs. SOLEIL accueille également près de 5 000 visiteurs chaque année, de tous horizons, et leur propose des programmes et des outils pédagogiques documentaires et expérimentaux. Une ouverture quotidienne depuis la conception de SOLEIL, qui consolide l'importance pour SOLEIL de partager les connaissances au fur et à mesure qu'elles évoluent et familiarise également les scientifiques au débat science/société. Dans cet esprit, l'implication des nouvelles générations de chercheurs, et donc des doctorants, lors des visites du site, de lignes de lumière ou de témoignages dans le cadre de projets-métiers, est certainement essentielle. Cette dynamique s'est intensifiée grâce au dispositif des doctorants-conseils qui prévoit, en particulier avec notre partenaire de l'Université Paris-Sud, leur implication 32 jours par an pour des missions de médiation. Ainsi en 2013, depuis 10 ans et pour les années à venir, SOLEIL considère comme prioritaire et fertile l'ouverture du synchrotron à la société et aux partenariats de toute forme.

SCIENCE TOGETHER

SOLEIL wants to place science at the very heart of society through a variety of outreach actions to promote public awareness of science. Our teams go out to meet the public at classic outside events such as the Fête de la Science science fair, Années Internationales (international years), Journées du Patrimoine (heritage days), and Nuit des Chercheurs. SOLEIL also welcomes nearly 5000 visitors of all kinds every year, providing interesting programmes and educational materials (documents and experiments). An open approach that has been practiced ever since SOLEIL was first designed. It consolidates the importance to SOLEIL of sharing its knowledge as that knowledge grows, and engages scientists in a dialogue with society at large. In keeping with this spirit, it is essential to involve new generations of scientists and doctoral students in giving tours of the site or the beamlines, career talks, etc. The momentum of these actions has increased, thanks to the system of doctoral student-advisors, in particular with our partner from Université Paris-Sud. They spend 32 days per year working as science ambassadors. So, in 2013, SOLEIL can look back over the last ten years and look forward to the years to come, with the view that opening the synchrotron up to society and to all types of partnership is a top priority as well as a fertile approach.



Des élèves d'une classe de Première d'un Lycée de la Région Centre, attentives aux explications de Paul Dumas, responsable de la ligne SMIS.

Sixth form pupils from a high school in the central region of France listening to Paul Dumas, head of the SMIS beamline.

SURFACES, INTERFACES AND NANOSYSTEMS

- 16 The virtuous Graphene goes out of the Labs, increasing its production up to industrial scale
- 18 Approaching the Holy Grail of spintronics
- 20 "Bad metals" and "good superconductors"
- 22 Nitric acid on water ice: the chemical-physics behind a key pollutant of the Earth's cryosphere
- 24 Observation of topological electronic states in α -Sn films
- 26 Oxide electronics - Static and dynamic electronic properties of a ferroelectric device
- 28 Hydrogen-induced nanotunnel opening at the subsurface of an advanced semiconductor, Silicon Carbide

CHEMISTRY AND PHYSICAL CHEMISTRY, NANOCHEMISTRY

- 34 Active sites of metalloproteins in solution revealed by vibrational spectroscopy
- 36 Self-structuring of bridged silsesquioxanes through covalent and non-covalent bonding
- 38 New insights into short ordered Fe-Al oxyhydroxide coprecipitates
- 40 Bone growth regulation: how does osteopontin bind uranium?
- 42 High capacity Li-rich layered compounds for Li-ion batteries
- 44 Probing spin-spin interactions in surface-supported single-molecule magnets
- 46 Fluorescent nanoplatelets pile-up
- 48 Coupling XANES and DFT calculations to unravel the structure of heterogeneous catalysts

BIOLOGY AND HEALTH SCIENCES

- 54 Polymorphic and amyloid natures of neuronal inclusions of Huntington's disease brain revealed by IR microspectroscopy
- 56 Characterization of hydrophobic peptides by photoionization Mass Spectrometry
- 58 MAN1 at the nuclear envelope blocks TGF- β signaling by stimulating dephosphorylation of the Smad transcription factors
- 60 Synchrotron radiation - tandem mass spectrometry for proteomic and structural biology
- 62 Atomic structure of 14-subunit RNA polymerase I: insight into ribosomal RNA synthesis
- 64 The novel RNase P in action
- 66 The function of translation initiation factor IF2 analyzed by an integrated structural biology approach
- 68 Crystal structure of the crystallographer MamP

ATOMIC AND MOLECULAR PHYSICS, DILUTE MATTER, UNIVERSE SCIENCE

- 74 Advanced studies of molecular ions by resonant photoemission
- 76 Unravelling coupled electronic and nuclear angular momenta
- 78 Spectroscopy of the $^{15}\text{NH}_2$ radical
- 80 New routes to dissociation: the fourth way
- 82 Chirality reveals electronic/nuclear motion couplings
- 84 Young's double slit experiment revisited at the atomic level
- 86 Nanosolvation-induced stabilization of a protonated peptide dimer isolated in the gas phase
- 88 Photoelectron circular dichroism on gas phase alanine: a possible photophysical process at the origin of life's homochirality?

PHYSICS AND CHEMISTRY OF CONDENSED MATTER, EARTH SCIENCES

- 94 Synchrotron UV/visible imaging discriminates historical pigments
- 96 Programming the self-assembly of alloy nanowires: a combinatorial approach
- 98 Why do γ -Fe nanoparticles inside carbon nanotubes abnormally expand at high temperature?
- 100 Terahertz magneto-electric excitations in a chiral compound
- 102 Molecular refrigerators
- 104 Caffeine in cosmetics – optimizing its release into the body by means of "MOFs"
- 106 Resonant magnetic x-ray scattering on artificial spin ice
- 108 $\text{LuFe}_2\text{O}_{4+x}$: from multi-ferroicity to oxygen storage

MODELING, METHODOLOGY AND INSTRUMENTATION

- 114 SPI Boards Package a flexible multipurpose set of boards for various scientific applications
- 116 An in-house developed X-ray imaging detector for synchrotron based micro-tomography
- 118 A new double charged particle imaging spectrometer for gas phase VUV photoionization studies
- 120 Development of high performance heat transfer devices for synchrotron facilities
- 122 A new tool for greenhouse gases Infrared absorption modelling
- 124 A versatile source to make complex nanoscopic objects fly under vacuum
- 126 Simultaneous fast-scanning XRF, dark field, phase-, and absorption contrast tomography
- 128 The secondary source of NANOSCOPIUM

SOURCES AND ACCELERATORS DIVISION

- 134 Storage ring operation status: performance and evolutions
- 136 News on the storage ring optics: operation performance improvement
- 138 W164: one insertion device for two purposes



SURFACES, INTERFACES AND NANOSYSTEMS

- 16** The virtuous Graphene goes out of the Labs, increasing its production up to industrial scale
- 18** Approaching the Holy Grail of spintronics
- 20** “Bad metals” and “good superconductors”
- 22** Nitric acid on water ice: the chemical-physics behind a key pollutant of the Earth’s cryosphere
- 24** Observation of topological electronic states in α -Sn films
- 26** Oxide electronics - Static and dynamic electronic properties of a ferroelectric device
- 28** Hydrogen-induced nanotunnel opening at the subsurface of an advanced semiconductor, Silicon Carbide

SURFACES, INTERFACES AND NANOSYSTEMS

2013 highlights of the Surfaces, Interfaces and Nanosystems Scientific Section are characterized by the discovery of new and exciting electronic properties. Surfaces, interfaces and 2D materials are a key step in nanotechnology with the aim to engineer and fabricate low-dimensional materials and nano-objects.

The research activity on graphene was applied to new 2D materials and produced several SOLEIL highlights in 2012. All of them take advantage of electron spectroscopy in determining the electronic properties of materials. One of them deals with organic semiconductors, another on the role played by surfaces of aerosols in atmospheric chemistry. All of them were possible thanks to specific properties of synchrotron radiation and/or to the development of new kind of experiments. Real time synchrotron-radiation-based photoemission experiment during hydrogen exposure could identify nanotunnel opening within the subsurface region of silicon carbide (Soukiassian et al.). In analogy with the graphene electronic properties, nearly massless electrons belonging to 2D surface states were measured in Ultrathin α -Sn(001) Films grown on InSb(001) substrates: high flux and circular polarization of soft X-rays were used to show helical spin polarization of the Dirac-cone-like surface states (Ohtsubo et al.).

High flux and light polarization were also used to study electronic properties in 2D systems during a phase transitions from a paramagnetic to an antiferromagnetic state (Lin et al.). Variable photon energy of X-ray absorption spectroscopy was applied to atmospheric chemistry to study the surfaces of supercooled aerosols (Marcotte et al.).

Photoelectron spectroscopy was used to study the effective barrier height of ferroelectric material under in-situ bias voltage and to probe the transient response of the upper electrode/ferroelectric interface to polarization reversal (Rault et al.). Activity on graphene continues on special samples and exploiting new experimental tools available at SOLEIL: a high resolution angle and lateral resolved photoelectron spectroscopy (nano-ARPES) (Avila et al.).

Finally, spin polarized experiments were performed on organic semiconductors: a model spinterface between phthalocyanine molecules and a Co single crystal surface showed a high degree of spin polarization at room temperature (Djeghloul et al.).

Fausto SIROTTI

Head of the "Surfaces, Interfaces and Nanosystems" Scientific Section

SURFACES, INTERFACES ET NANOSYSTÈMES

Les Highlights 2013 de la section scientifique Surfaces, Interfaces et Nanosystèmes se distinguent par la découverte de propriétés électroniques nouvelles et surprenantes. Les surfaces, les interfaces et les matériaux 2D constituent une étape clé en nanotechnologie, avec pour objectif de concevoir et fabriquer des nouveaux matériaux et des nano-objets.

L'activité de recherche sur le graphène, qui a figuré dans plusieurs numéros des Highlights de SOLEIL en 2012, a été appliquée à de nouveaux matériaux 2D. Tous ces résultats tirent parti de la spectroscopie électronique pour déterminer les propriétés électroniques des matériaux. L'un d'eux concerne les semi-conducteurs organiques, tandis qu'un autre est en lien avec le rôle joué par les surfaces des aérosols en chimie atmosphérique. Ces résultats ont tous été rendus possibles par les propriétés spécifiques du rayonnement synchrotron et/ou par le développement de nouveaux types d'expériences.

Les expériences de photoémission en temps réel basées sur le rayonnement synchrotron pendant l'exposition à de l'hydrogène ont permis d'identifier l'ouverture de nanotunnels dans la région proche de la surface du carbure de silicium (Soukiasian et al.). Par analogie avec les propriétés électroniques du graphène, des électrons avec faible masse effective et appartenant aux états de surface 2D ont été mesurés dans des films ultra-fins de α -Sn(001) produits sur des substrats de InSb(001). Le flux élevé et la polarisation circulaire de rayons X mous ont été utilisés pour mettre en évidence la polarisation hélicoïdale du spin des états de surface de type cône de Dirac (Ohtsubo et al.).

Le flux élevé et la polarisation de la lumière ont aussi été utilisés pour étudier les propriétés électroniques dans les systèmes 2D pendant une transition de phase entre un état paramagnétique et un état antiferromagnétique (Lin et al.).

Une énergie de photon variable en spectroscopie d'absorption des rayons X a été appliquée à la chimie atmosphérique pour étudier les surfaces d'aérosols en surfusion (Marcotte et al.). La spectroscopie de photoélectrons a été utilisée pour étudier la hauteur de barrière effective d'un matériau ferroélectrique soumis à une tension de biais in-situ ainsi que pour sonder la réponse transitoire de l'interface électrode supérieure/ferroélectrique à l'inversion de polarisation (Rault et al.).

Les activités avec le graphène continuent en exploitant de nouveaux outils expérimentaux disponibles à SOLEIL : une spectroscopie de photoélectrons à haute résolution, résolue angulairement et latéralement (nano-ARPES) (Avila et al.).

Enfin, des expériences polarisées en spin ont été effectuées sur des semi-conducteurs organiques : une spinterface modèle entre des molécules de phthalocyanine et une surface de cristal unique de Co a présenté un degré élevé de polarisation en spin à température ambiante (Djeghloul et al.).

Fausto SIROTTI

Responsable de la Section Scientifique « Surfaces, Interfaces et Nanosystèmes »

The virtuous Graphene goes out of the Labs, increasing its production up to industrial scale

Composed of a few sheets of carbon atoms, graphene is the strongest material ever measured, it has a thermal conductivity more than doubled that of the diamond and has its charge mobility, which is among the highest of all semiconductors. But just as their properties are remarkable, this material likewise has accelerated the speed to which it has left the research laboratory for the market. The exceptional electrical properties of graphene have been discovered only five years ago, but today the yield of total production of different types of graphene is greater than 15 tons per year, and this is expected to increase to more than 200 tons per year within a year or two. In SOLEIL, the ANTARES research groups in collaboration with Wallard's group from the IEMN, Lille has created single large polycrystalline graphene sheets by a simple synthesis method and comprehensively characterized using Nano Angle Resolved Photoelectron Spectroscopy (NanoARPES).



Recently isolated, this material with amazing properties began to be manufactured following more industrial processes. Still expensive to produce, the graphene could soon be used for flat screens, batteries, transistors as well as several other applications. The idea, in the medium term, is to replace the transparent conductive layers of ITO (indium tin oxide), by a layer of graphene, less fragile, which may lend itself well to the production of flexible displays.

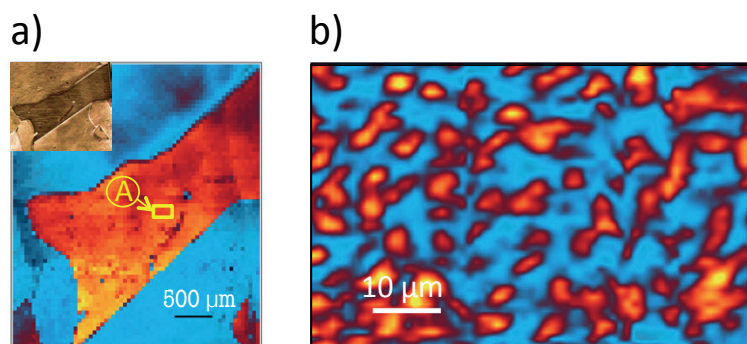
Chemical vapor deposition (CVD) of single layer graphene (SLG) on Cu has recently emerged as a powerful technique for realizing large scale graphene films in a cheap readily achievable fashion, enabling to produce continuous SLG sheets up to meter scale fully compatible with industrial processes [1,2]. However, these films do not exhibit crystalline alignment over distances critical to the large-scale production of spatially uniform vertical heterostructures. Specifically, current CVD grown graphene films are usually comprised of randomly rotated small grains [3]. Indeed, for electronic applications, when graphene is deposited on a metal support, it is needed to transfer it to a non-conductive substrate after the synthesis. The whole manipulation is difficult to control and electronic characterization using NanoARPES is required to detect the

eventual degradation of this polycrystalline material as well as the optimization and effectiveness of every step.

NanoARPES is the ideal technique to probe the electronic structure of both polycrystalline graphene films and Cu substrate directly underneath it. Our results [4] show the robustness of the Dirac relativistic-like electronic spectrum as a function of the size, shape and orientation of the single-crystal pristine grains in the graphene films investigated. Moreover, by mapping grain by grain the electronic dynamics of this unique Dirac system, we show that the single-grain gap-size is 80 % smaller than the multi-grain gap recently reported by classical ARPES.

In addition, it allows the investigation of the spatial uniformity of the lattice and electronic structures of graphene and their correlation with that of Cu.

In Figure 1, laterally resolved nano-ARPES data taken with a 100 nm beam spot [4] vividly illustrate the single-crystal islands of our graphene films as well as the register with the granular Cu substrate. To locate and compare different graphene islands, we generate spatial maps (figure 1a and 1b), where an ARPES spectrum was measured at each point in a 150 x 200 μm^2 grid.



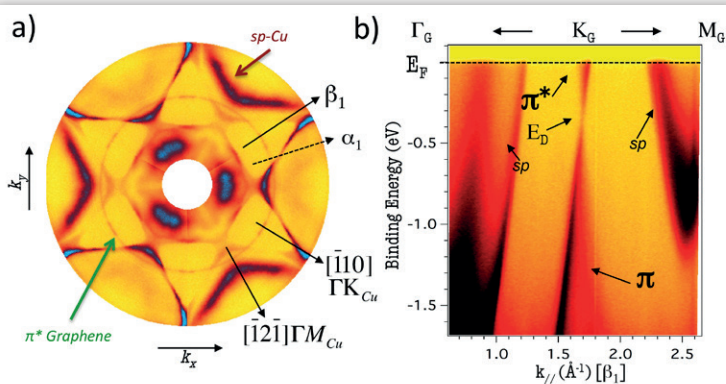
1 Real-space image of the copper states intensity obtained by nano-ARPES mapping presented on a linear scale as a false-color image. The inset of panel (a) shows the optical image of the sample. Panel (b) shows real-space images of graphene grains by monitoring the graphene states intensity at the "A" yellow rectangle indicated in panel (a).

Figure 2 shows a Fermi surface map subsequently measured probing hundreds of graphene islands together. It displays a circle instead of six bright spots (associated to a single graphene orientation), corresponding to the cross-sections of graphene's Dirac cones near the K points of many grains randomly oriented. Moreover, fainter star-like curves originated by the underlying copper substrate electronic states.

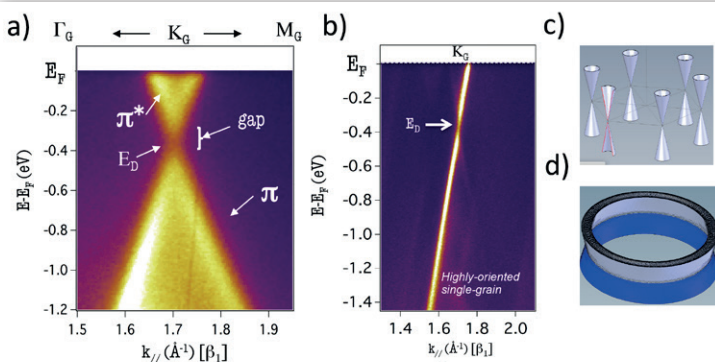
ARPES results show, that both multi- and single-grain ARPES spectra present a well-defined conical Dirac dispersion, with n-type extrinsic doping (Figure 2a-c). More importantly, the nano-ARPES gap-

size determination reveals the origin of the discordances between experimental gap-size values previously reported by classical ARPES and theoretical predictions, confirming that the graphene-copper interaction is rather weak, which gives rise to the opening of a mini-gap of only ~ 50 meV.

Our recent findings [4,5] certainly open the door to a direct evaluation of the mesoscopic structure and influence on the electronic properties of graphene films. These results offer new avenues for implementing graphene in real-world devices and exploring new phases of electronic materials.



Panel (a) shows the Fermi surface (FS) map of a graphene multi-grain film recorded at the A-box of figure 1(a). Panel (b) displays the energy-momentum dispersion relations of π and π^* bands near E_F of graphene along the β direction, using linearly polarized light of 100 eV.



Panel (a) displays the energy-momentum dispersion relations of π and π^* bands near E_F of multi-grain graphene film along the β direction, using circularly polarized light of 30 eV. Panel (b) shows E-k dispersion measured by nano-ARPES in a single pristine graphene grain oriented along the β direction (see Fig. 2a). Panel (c) and (d) show the reciprocal space of single- and multi-graphene grain. Moreover, the superposition of Dirac cones of graphene grains randomly oriented has been schematized.

ANTARES beamline

ASSOCIATED PUBLICATION

Exploring electronic structure of one-atom thick polycrystalline graphene films: A nano angle resolved photoemission study

J. Avila, I. Razado, S. Lorcy, R. Fleurier, E. Pichonat, D. Vignaud, X. Wallart and M.C. Asensio*

Scientific Reports 3 (2013): art.n° 2439

CORRESPONDING AUTHOR

*Synchrotron SOLEIL, l'Orme des Merisiers, St Aubin BP48, 91192 Gif sur Yvette Cedex, France

maria-carmen.asensio@synchrotron-soleil.fr

REFERENCES

- [1] X. Li et al. Science 324 (2009), 1312
- [2] S. Bae et al. Nat. Nanotechnol. 5 (2010), 574 J
- [3] P. Y. Huang et al. Nature 469 (2011), 389
- [4] J. Avila et al. Sci. Rep. 3 (2013), 2438, DOI: 10.1038/srep02439
- [5] L. I. Johansson et al. Sci. Rep. 4 (2014), 4157, DOI: 10.1038/srep041

Approaching the Holy Grail of spintronics

At age 25, the field of spintronics, which conceptually takes into account the electron spin in electronics, is now an integral part of our daily lives. It for instance governs the operation of read/write heads within our computer hard drives and of magnetic random access memories (MRAM). Thus, from optoelectronic relays to artificial synapses, spintronics is an additional means to encode and process information. Until now, spintronics has shone particularly in the development of efficient electronic components. However, it is also necessary to transmit the encoded information over mesoscopic distances between these spintronics devices. This is best achieved when using a current source that is highly spin-polarized. An international group led by researchers at Strasbourg has discovered a promising candidate to fulfill this mission.

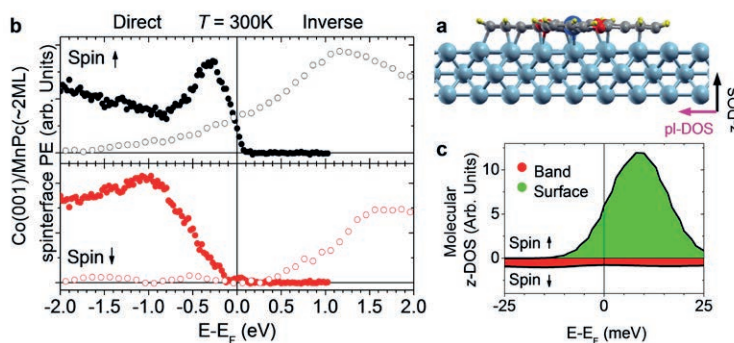
Within a spintronics paradigm, the transfer of information encoded by the electron spin shall be more efficient if the current is strongly spin-polarized. Indeed, while conventional electronics perform binary encoding based on the presence or absence of an electron, spintronics would encode this using the spin-up or spin-down property of this electron.

To achieve this strongly spin-polarized current source, various classes of materials (half-metals, diluted magnetic semiconductors, symmetry-preserving filters) have been explored. However, the spin polarization of the current supplied by these solutions does not remain strong in a nanodevice at the temperatures required by industry.

Cobalt and phthalocyanine

Researchers from the Strasbourg Institute of Physics and Chemistry of Materials (IPCMS) believe they have found a new way to overcome these obstacles. Leading an international group, they have worked over the past two years to understand a surprising phenomenon: combining commonplace materials such as cobalt (Co) and phthalocyanine (Pc) molecules, which are used as ink pigments, creates an interface (see Figure 1a) in a device that can spin-filter 84% of the current flowing through it. This prediction is based on measurements of spin-resolved photoemission, carried out on the CASSIOPEE beamline at the SOLEIL synchrotron starting in December 2010.

This experimental technique probes the number of occupied electronic states of each spin type, starting from the energy level at which electrical conduction level takes place (i.e. the Fermi level E_F). These measurements show that the interface between Co and Pc molecules is endowed with a strong spin asymmetry of electronic states at the E_F at room temperature (see Figure 1b). These results were then confirmed by additional spin-resolved inverse photoemission measurements (at the Politecnico di Milano, Italy), allowing the unoccupied electronic states above E_F to be probed.



1 The adsorption of phthalocyanine molecules on Co (a) would generate a strong spin asymmetry of the current at EF going through this interface (z direction) according to experimental measurements (b) and theoretical calculations (c).

Metal/molecule hybrid electron states

In order to understand these experimental results, the latest refinements in *ab initio* theory, such as the inclusion of van der Waals forces, were then deployed at the IPCMS. Referring to Figure 1c, in the absence of *d* band electrons in the Co spin up channel at E_F , Co surface states can hybridize with the electron orbitals of the molecule to provide metal/molecule

hybrid states that will intersect E_F . The large number of electrons that make up these hybrid spin up states (green in panel c) allows this interface interaction to dominate, in the expression of the spin polarization of the current, the metal/molecule hybridization induced by the Co *d* band in the spin-down channel (red in panel c).

An ideal spin-polarized current source?

This spin-polarized interface, or spinterface, seems to possess the properties of an ideal spin-polarized current source. Indeed, the high spin polarization of the current flowing through this interface comes from the Co magnetism, which remains robust against thermal disorder toward industrial applications. The effect requires only one molecule, which suggests possible nanodevices. Finally, the spin polarization of the molecule's orbitals forming the spinterface could allow better injection of these spins within organic semiconductors for inter-device spin transport.

These studies, published in January 2013 in *Scientific Reports*, thus reveal a promising candidate in the quest for the spintronics Holy Grail, which is discovering an ideal spin-polarized current source. The CNRS and Strasbourg University have, of course, already filed a patent application [1] concerning these industrially very promising interfaces. IPCMS researchers are currently exploring the fundamental and applied implications of this discovery, including the study of technological demonstration devices that would fully reveal the portency of this work.

CASSIOPEE beamline

ASSOCIATED PUBLICATION

Direct observation of a highly spin-polarized organic spinterface at room temperature

F. Djeghloul, F. Ibrahim, M. Cantoni, M. Bowen*, L. Joly, S. Boukari, P. Ohresser, F. Bertran, P. Le Fevre, P. Thakur, F. Scheurer, T. Miyamachi, R. Mattana, P. Seneor, A. Jaafar, C. Rinaldi, S. Javid, J. Arabski, J.P. Kappler, W. Wulfhekel, N.B. Brookes, R. Bertacco, A. Taleb-Ibrahimi, M. Alouani, E. Beaurepaire, and W. Weber
Scientific Reports 3 (2013) 1272

CORRESPONDING AUTHOR

* IPCMS-DMONS, 23 rue du Loess PB 43, 67034 Strasbourg, France

bowen@unistra.fr

REFERENCE

[1] FR 2012/ 12 53564 "Source de courant polarisée en spin", M. Bowen, W. Weber, L. Joly, E. Beaurepaire, F. Scheurer, S. Boukari, M. Alouani, *patent pending*.

“Bad metals” and “good superconductors”

Surprisingly, the best superconductors discovered to date are often not very good metals. This is true for the family holding the highest superconducting transition temperatures, the cuprates, but also for some iron superconductors discovered more recently. For physicists a “bad metal” is a complex object that is not well described by current theories. At the CASSIOPEE beamline, we have used Angle Resolved Photoemission to reveal some unexpected characteristic of the electronic structure of one of this bad metallic state, namely the formation of a “pseudogap”.

New iron superconductors

In the newly discovered iron superconductors, the origin of superconductivity still raises many questions. There is a close proximity between superconducting and magnetic phases. This reminds the situation in another family of high temperature superconductors, cuprates, and

suggests that, instead of destroying superconductivity, as it usually does, magnetism may help in certain cases to reach superconductivity at quite high temperatures. Understanding this in more details may help to create new types of superconductors, possibly at even higher temperatures.

Magnetism, superconductivity and metallicity

To go further, it is necessary to understand better the nature of magnetism itself and the role of magnetic correlations in the metallic state. In cuprates, magnetism sets in within an insulating background, with one electron localized at each copper site, which then order antiferromagnetically. The Coulomb repulsion is so strong in these systems that it would cost too much energy to have two electrons on the same site and the system chooses instead to localize one electron per site (this state

is called the Mott insulator). In iron superconductors, the situation is quite different. Magnetism sets in within a metallic background and there are six electrons per site. However, some of these phases are “bad metals” meaning it becomes very difficult for electrons to move from site to site. Why would “bad metals” become “good superconductors”? This apparent contradiction may be at the heart of the formation of high temperature superconductivity.

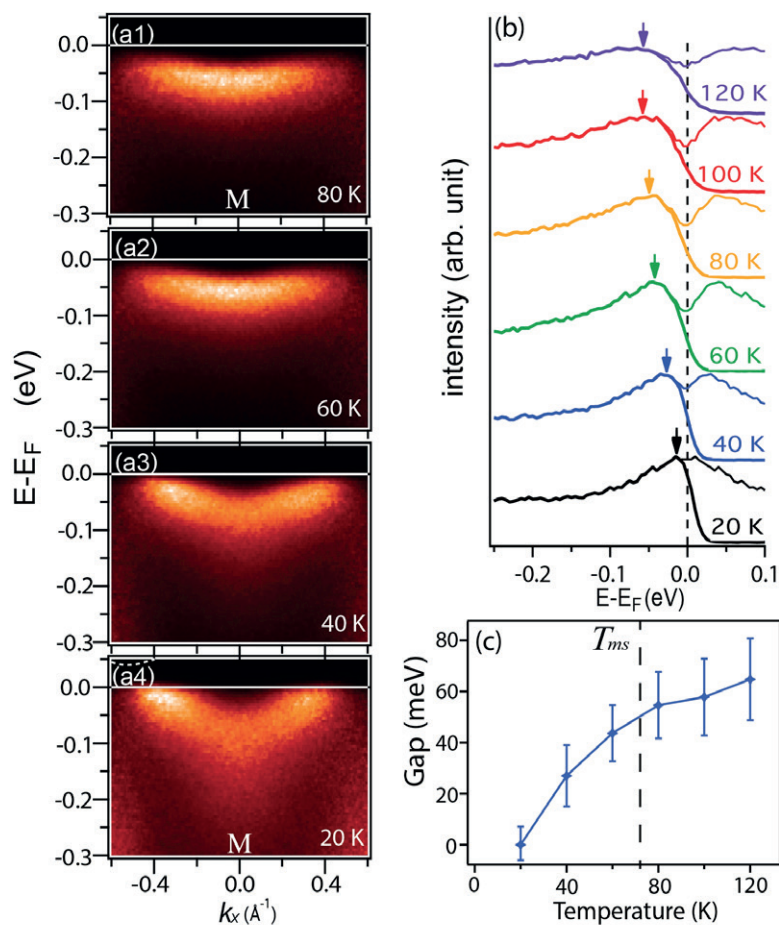
Anomalous metallic state in Fe_{1.06}Te

In a recent study, we investigated how this bad metallic behavior manifests itself in the electronic structure of Fe_{1.06}Te. We imaged the electronic structure with angle resolved photoemission spectroscopy at the CASSIOPEE beamline of the SOLEIL synchrotron, both in the metallic paramagnetic phase (i.e. magnetically disordered, which occurs for temperatures T above 76K) and in the magnetically ordered phase ($T < 76K$). Figure 1(a) shows the evolution of one electronic band in this compound. The Fermi level (the occupied state having the highest energy) is shown by the white line and the red intensity corresponds to states occupied with electrons. Normally, one gets a metal if there are bands crossing the Fermi level, meaning there are partially filled bands where electrons are free to move. This is the case for low temperatures: at 20K, in Fig. 1(a4), we see electrons up to the Fermi level and the spectra taken at this point (Fig. 1b) shows a “Fermi step” characteristic of the metal. At high

temperatures, the intensity is small at the Fermi level and the peak in Fig. 1(b) moves away from it. This situation can be called “pseudogap” as it is intermediate between the one expected for a metal (no gap) and an insulator (full gap). The fact that a good metallic state is recovered in the magnetic state is a very direct indication of the role of magnetic disorder to create the bad metallic state. The idea is that there is a local tendency at each Fe site to align the spins of the electrons in different orbitals and form a local magnetic moment. In the magnetic phase, these moments order in a way optimizing electronic conduction in certain directions and magnetic fluctuations are frozen. In the paramagnetic phase, the disordered moments interact with conducting electrons and hinder their motion. There is then in the heart of the paramagnetic metallic phase, strong magnetic correlations between electrons that impact the nature of the metallic state. How it creates a pseudogap remains

to be understood. These correlations appear quite different from those present in the cuprates, which are mostly based on Coulomb repulsion. On the other hand, the metallic phase of the cuprates is also

known to harbor a “pseudogap”. Whether there is any connection between these two new states of matter is an interesting challenge.



● (a) Energy vs momentum plot of one electron band in $\text{Fe}_{1.06}\text{Te}$ for different temperatures measured with ARPES. (b) ARPES spectrum at k_x for different temperatures. The thin line is symmetrized with respect to the Fermi level. The maximum should be at E_F if there was no pseudogap. (c) Value of the pseudogap as a function of temperature.

CASSIOPEE beamline

ASSOCIATED PUBLICATION

Nature of the bad metallic behavior of $\text{Fe}_{1.06}\text{Te}$ inferred from its evolution in the magnetic state

Ping-Hui Lin, Y. Texier, A. Taleb-Ibrahimi, P. Le Fèvre, F. Bertran, E. Giannini, M. Grioni and V. Brouet*

Physical Review Letters 111 (2013) 217002

CORRESPONDING AUTHOR

*Laboratoire de Physique des Solides, Université Paris-Sud, UMR 8502, Bâtiment 510, 91405 Orsay, France

veronique.brouet@u-psud.fr

Nitric acid on water ice: the chemical-physics behind a key pollutant of the Earth's cryosphere

Nitric acid HNO_3 is an important player in many environmental heterogeneous processes involving airborne icy particulates and snow. For example, nitric acid is a precursor of snow-bounded nitrate anion NO_3^- , an important photochemical source of NO_x and OH radicals in Polar Regions [1]. As the photolysis rates of HNO_3 and NO_3^- at actinic wavelength (>300 nm) are strongly different [2], whether nitric acid adsorbs molecularly or is dissociated at the surface of environmental ices is fundamental in the NO_x and OH atmospheric budget. NEXAFS spectroscopy performed on the TEMPO beamline revealed that the known propensity for HNO_3 to be extensively dissociated in aqueous solutions is preserved upon adsorption onto ice at cryogenic temperatures and concentration regimes relevant to environmental chemistry processes. Nitric acid should thus be expected to behave as a strong acid at the surface of supercooled aerosols and in the quasi-liquid layer of environmental ices.

Atmospheric chemistry of nitric acid depends on how it adsorbs on ice

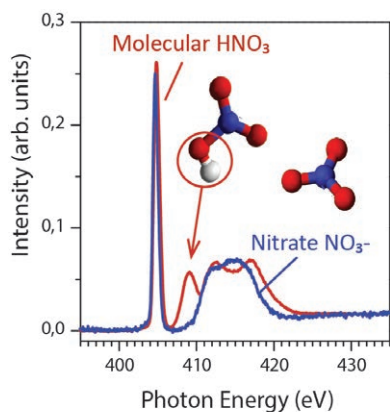
Given its major role in many environmental processes, the dissociative adsorption and acid–base chemistry of HNO_3 at aqueous interfaces continues to attract tremendous interest from both theoretical and experimental perspectives. Indeed, our understanding of several important atmospheric chemistry processes hinges on a quantitative description of the factors and parameters that control whether HNO_3

exists in its molecular or its dissociated form at the surface of atmospheric aerosols and of ice. For instance, this would impact our interpretation of the formation, stability, and reactivity of nitrates in urban particulate matter, the atmospheric reactive nitrogen budget, the NO_x photochemical fluxes from the snowpack, and the formation and lifetime of cirrus clouds.

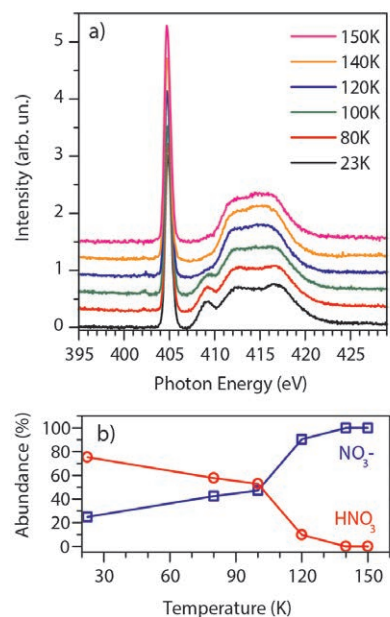
Nitric and HNO_3 easily converts into nitrate on ice

HNO_3 and NO_3^- have different electronic structures leading to distinct NEXAFS spectra [Figure 1], especially around 409 eV, where HNO_3 (red) displays a strong resonance (arrow) specific to the hydroxyl group OH, absent in NO_3^- (blue). Therefore, investigating the conversion of nitric acid HNO_3 into nitrate NO_3^- on water ice is particularly convenient. It allows the study of the extent of ionization of HNO_3 on the surface of a thin water ice film (100 monolayers thick) deposited on a gold substrate. Figure 2(a) displays the evolution of the N K-edge signal for 0.4 monolayer of HNO_3 adsorbed on ice at 23 K, then warmed to 150 K. The progressive disappearance of the resonance at 409 eV with the temperature indicates the gradual conversion of HNO_3 into NO_3^- . By fitting the NEXAFS spectra with a linear combination of the HNO_3 and NO_3^- spectra presented Figure 1, the relative abundance of these two species can be estimated as function of the temperature [Figure 2(b)]. Although the spectrum at 23 K looks like that of pure HNO_3 , the fit indicates that actually 25 % of nitric acid is already converted in NO_3^- . This shows that ionic dissociation of HNO_3 at the surface of ice occurs with

no thermal activation barrier. This occurs when HNO_3 sits on a favorable adsorption site, i.e. with enough water molecules to dissociate HNO_3 and solvate the nitrate anion. The molecular portion (75% @ 23 K) corresponds to HNO_3 molecules sitting on other surface sites with lower solvation capabilities. These molecules are in a metastable state and are progressively converted into NO_3^- when increasing the surface temperature, which provides the necessary energy for the optimization of the solvation shell and thus leads to dissociation. Around 110 K, the steep increase in the conversion rate is due to the diffusion of nitric acid molecules in the bulk of ice where they find enough water molecules for ionization and solvation. Those findings indicate that the known propensity for HNO_3 to be extensively dissociated in aqueous solutions is preserved upon adsorption onto ice at cryogenic temperatures and concentration regimes relevant to environmental chemistry processes. HNO_3 should thus be expected to behave as a strong acid at the surface of supercooled aerosols and in the quasi-liquid layer of environmental ices.



① N K-edge NEXAFS spectrum of molecular HNO_3 (red). The arrow indicates the transition specific to OH, absent in the dissociated form NO_3^- (blue).



② (a) N K-edge NEXAFS spectra of 0.4 monolayer of HNO_3 adsorbed on ice at 23 K, then progressively warmed at 150 K. (b) Quantitative analysis of the data allows the estimation of the relative abundance of HNO_3 and NO_3^- as function of the temperature.

TEMPO beamline

ASSOCIATED PUBLICATION

Nitric acid at the surface of amorphous solid water revealed by X-ray absorption spectroscopy

G. Marcotte, P. Ayotte, A. Bendounan, F. Sirotti, C. Laffon, and P. Parent*

Journal of Physical Chemistry Letters
4(16) (2013) 2643

CORRESPONDING AUTHOR

*Aix Marseille Université, CNRS, CINaM UMR 7325, campus de Luminy, case 613, 13288 Marseille, France

parent@cinam.univ-mrs.fr

REFERENCES

- [1] F. Dominé et al. Science 297 (2002), 1506
- [2] C. Zhu et al. J. Phys. Chem. A 114 (2010), 2561
- [3] P. Ayotte et al. J. Chem. Phys. 123 (2005), 184501/1

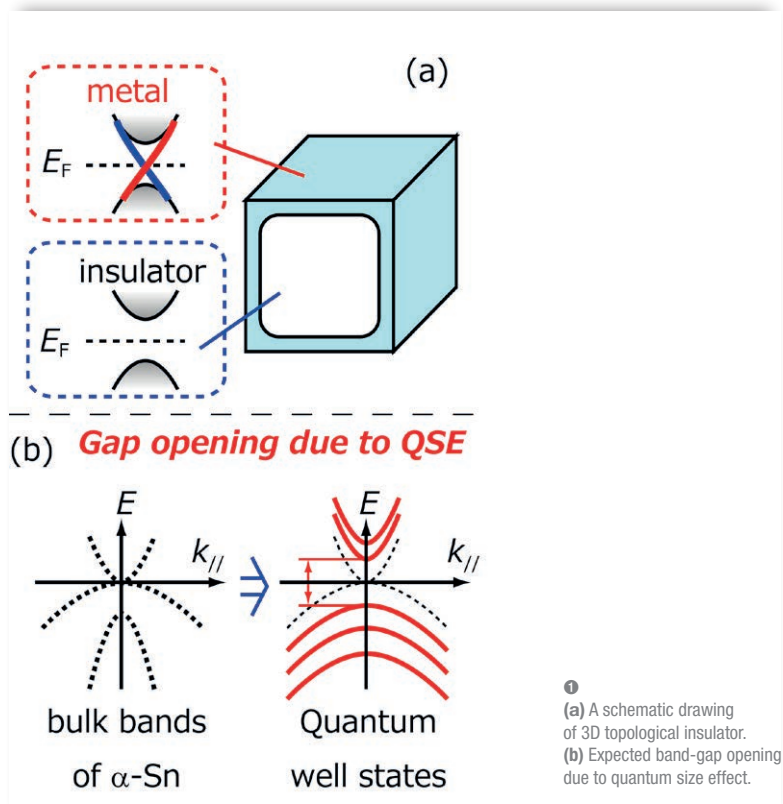
Observation of topological electronic states in α -Sn films

We combine angle-resolved photoelectron spectroscopy (ARPES), spin-resolved ARPES and ab initio DFT calculations to measure the spin-polarized surface electronic states of ultrathin α -Sn(001) films. Spin-integrated and spin-resolved ARPES show clear massless Dirac-cone dispersion and helical in-plane spin polarization, indicating non-trivial topological order of ultrathin α -Sn(001). The evolution of spin-polarized states with film thicknesses provides useful information that can be used to control the 3D band gap as well as the 2D gap and dispersion of spin-polarized states. This information is of potential importance for the fabrication of miniaturized spintronics devices made of ultrathin topological-insulator films.

Ultrathin films of topological insulators

Topological insulators (TI's) are emerging as a new state of quantum matter. While a TI has a finite size bandgap in its bulk band structure (thus it is "insulator"), a TI always holds metallic states on its surface/edge because of non-trivial parity invariants of its bulk bands [1]. These topological surface states (TSS) on a TI are characterized by spin-polarized massless Dirac-cone (DC) dispersion and hence TI's are an interesting template for spintronics devices as well as a playground to enhance new electronic phenomena.

Finite-size effects on TSS are very important. In particular, quantum-size effect (QSE) from film thicknesses can change the electronic structure of TI [2]. Once the electrons are confined in a very thin thickness, the bulk-band dispersion perpendicular to the film is no longer continuous but discrete, forming quantum-well states (see Figure 1). With QSE, one may control the bulk band structure to realize a new TI.



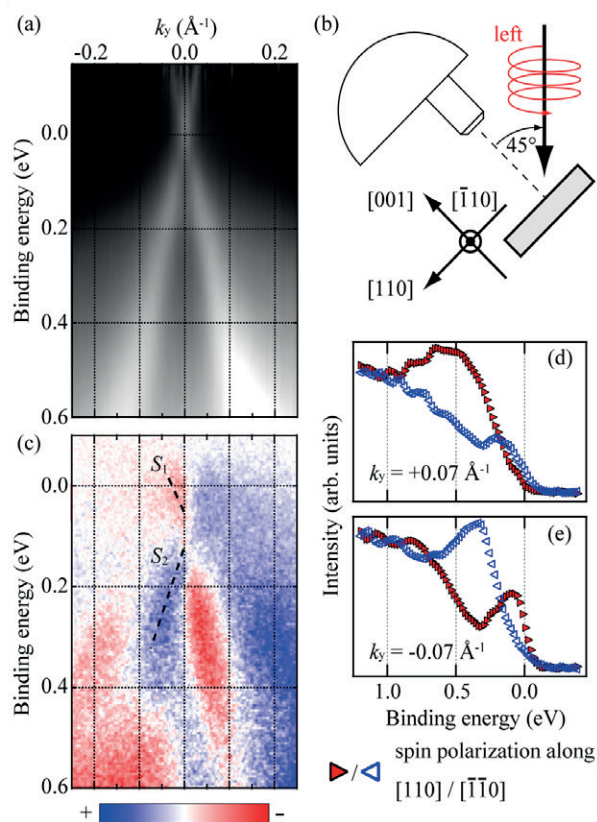
Spin-polarized Dirac cone on ultrathin Sn(001)

α -Sn is a zero-gap semiconductor and a possible candidate for such a new TI realized by QSE, since its bulk band structure is already non-trivial: if one can open a finite size bandgap on α -Sn, it becomes a TI. Although the phase of bulk Sn is not stable at room temperature (RT), the epitaxial Sn films grown on lattice-matched InSb(001) substrates [3] show the stable α phase even above RT.

On the epitaxial α -Sn (001) films grown by molecular beam epitaxy (MBE), we observed clear dispersion of surface bands by synchrotron-radiation angle-resolved photoelectron spectroscopy (ARPES), as shown in Figure 2a. Rather high-temperature measurement at 450 K enabled us to observe the surface electronic structure even above the Fermi level. Around the Fermi level, the surface

state showed almost massless linear dispersion. Furthermore, a following study by circular dichroism of ARPES and spin-resolved ARPES (Figure 2c-e) showed helical in-plane spin polarization of the surface state. Both features indicate that the surface states observed in this work are TSS, hence the epitaxial α -Sn film became a TI. We have also performed a density-functional-theory calculation and found a good agreement with what is observed. The theoretical calculation predicted a finite size bandgap of about 200 meV.

In summary, we could realize a new family of TI, epitaxial films of alpha-Sn, thanks to QSE. Its Dirac-cone-shape surface state dispersion and helical spin polarization were clearly observed by ARPES using Synchrotron Radiation.



2 ARPES results on the epitaxial α -Sn films. (a) ARPES intensity plot of the 24 monolayer film along $[-110]$ measured with $h\nu = 19$ eV, divided by the Fermi-Dirac distribution at 450 K function convolved with the instrumental resolution. (b) Experimental geometry in this work. (c) ARPES circular-dichroism plot of the 30 monolayers film taken with 19 eV photons at RT. Dichroism is obtained by subtracting the intensities of left-circularly polarized photons from those of right-circularly polarized ones. (d), (e) Spin-resolved ARPES spectra taken at RT with spin polarization toward $[110]/[-1-10]$. The acceptance angle for the spin-resolved ARPES corresponds to $k_y = \pm 0.06 \text{ \AA}^{-1}$.

CASSIOPEE beamline

ASSOCIATED PUBLICATION

Dirac cone with helical spin polarization in ultrathin α -Sn(001) films

Y. Ohtsubo, P. Le Fèvre, F. Bertran, and A. Taleb-Ibrahimi*

Physical Review Letters 111(21) (2013), art.n° 216401

CORRESPONDING AUTHOR

* Synchrotron SOLEIL, l'Orme des Merisiers, St Aubin BP48, 91192 Gif sur Yvette Cedex, France

amina.taleb@synchrotron-soleil.fr

REFERENCES

- [1] M.Z. Hasan & C.L.Kane, Rev. Mod. Phys. 2011 83, 1057; X. L. Qi & S. C. Zhang, Rev. Mod. Phys. 83 (2011), 1057
- [2] Y. Zhang et al. Nat. Phys. 6 (2010), 584
- [3] R. F. C. Farrow et al. J. Cryst. Growth 54 (1981), 507; M. G. Betti et al. Surf. Sci. 507-510 (2002), 335

Oxide electronics - Static and dynamic electronic properties of a ferroelectric device

Ferroelectric devices could be an alternative to magnetic based memories for future high-density data storage. Such devices have considerable advantages: they are non-volatile, have fast read-write times, low energy consumption and use realistic voltages. However, before considering future applications based on such materials, a better understanding of the electronic properties of nanometer-thick ferroelectric films is necessary. As this characterization is often impossible with standard techniques, we have studied ultra-thin films of ferroelectric materials on the TEMPO beamline, using classic and time-resolved photoelectron spectroscopy, an ideal tool for this kind of analysis.

In a ferroelectric device the local electric polarization is used to store information, either directly (FeRAMS) or by controlling another binary material state (resistive memories) [1].

The defining property of a ferroelectric (FE) material is a spontaneous macroscopic polarization which can be reversed under an applied electric field. Switching the polarization of such films requires a metallic contact, raising fundamental issues on the behavior of the interface

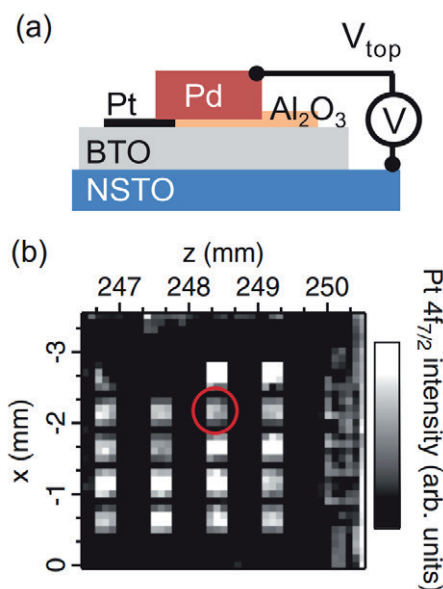
between the FE layer and the electrode. The polarization leads to fixed charge of opposite sign at the two metal-FE interfaces. Free charge carriers in the metal electrodes act to screen the polarization charge, however, the screening is usually imperfect and the residual depolarizing field inside the FE alters the electrostatic potential and can even suppress FE polarization below the so-called critical thickness [2].

In-operando PhotoEmission Spectroscopy

The key to better understand these systems is to probe their chemical and electronic properties under realistic operating conditions, *i.e.* application of d.c. or a.c. bias in the case of a ferroelectric. We developed a new experimental setup to allow such *in-operando* photoemission spectroscopy both in static and dynamic operations at TEMPO beamline.

The starting point is a Pt/BaTiO₃/SrTiO₃:Nb heterostructure (Pt/BTO/NSTO) grown by Molecular Beam Epitaxy. Electrodes 300 × 300 μm² in area and 3 nm thick were

patterned by ion beam etching. Thicker palladium pads overlapping part of the Pt electrodes were deposited to enable wire-bonding of the top electrodes for biasing. A highly insulating layer of Al₂O₃ was deposited onto bare BTO to suppress interference of the Pd pads with the capacitance (Figure 1a). At the TEMPO beamline, the 100 × 100 μm² beam could be directed onto a single top electrode located by a map of the whole sample using the Pt absorption edge (Figure 1b).



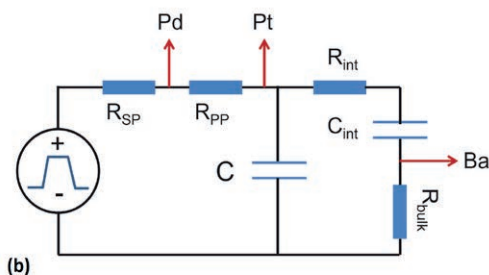
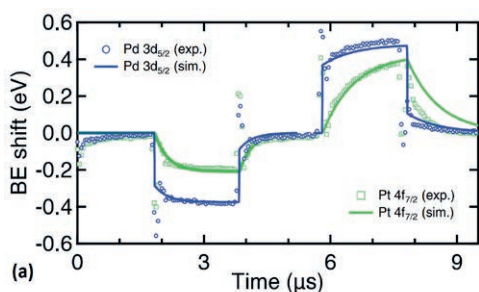
1 (a) Schematic of the capacitor; (b) Pt 4f intensity map for the Pt/BTO/NSTO sample showing 20 identical Pt/BTO/NSTO capacitors (300×300 μm²) on the 5×5 mm² surface, allowing location of the wired capacitor (red circle).

Electronic response to polarization switching at Pt/BaTiO₃ interface

Using this innovative setup, we directly measured the energy band alignment of the Pt/BTO interface as a function of the ferroelectric polarization. In the P+ state (FE polarization towards Pt), the structure can be modeled as back-to-back diodes showing Schottky-limited conduction. The experimental conduction-band offset is 0.40 eV at the Pt/BTO interface and 0.45 eV at the BTO/NSTO interface. In the P- state (FE polarization towards NSTO), the top interface band alignment remains Schottky-like (+0.90 eV) while at the bottom interface (BTO/NSTO) the conduction band offset reduces to zero leading to ohmic conduction, consistent with the current – voltage characteristic of the whole structure. The observed barrier heights depend on both the interface chemistry and the FE polarization [3].

Using the time-resolved detection system available at TEMPO beamline, the photoemission response of the capacitor to polarization switching induced by square voltage pulses has been measured. An equivalent circuit model has been developed which compares well with the photoemission response of the system (Figure 2). This shows the potential of time-resolved photoemission spectroscopy to follow the chemical/electronic changes in working model microelectronic devices, here a ferroelectric capacitor [4].

Electronic pump with synchrotron based XPS probe is the ideal tool and appears well-suited to the time-resolved capabilities of TEMPO. The next step is *in-operando* pump-probe measurements of the electron dynamics of the switch, focusing on the response of the ferroelectric near the electrode interface.



2 (a) Time-dependent evolution of the binding energy (BE) shifts for the Pd 3d_{5/2} (blue circles), Pt 4f_{7/2} (green squares) and results of the electrical simulations (solid lines) for the two core-levels. The blue dotted curve shows the pulse train applied on the top electrode; (b) Equivalent circuit model used to fit the experimental data to theoretical simulations.

TEMPO beamline

ASSOCIATED PUBLICATION

Interface electronic structure in a metal/ferroelectric heterostructure under applied bias

J.E. Rault*, G. Agnus, T. Maroutian, V. Pillard, P. Lecoeur, G. Niu, B. Vilquin, M.G. Silly, A. Bendounan, F. Sirotti, and N. Barrett

Physical Review B 87(15) (2013), 155146

CORRESPONDING AUTHOR

*Synchrotron SOLEIL, l'Orme des Merisiers, Saint-Aubin, 91192 Gif-sur-Yvette Cedex, France

julien.rault@synchrotron-soleil.fr

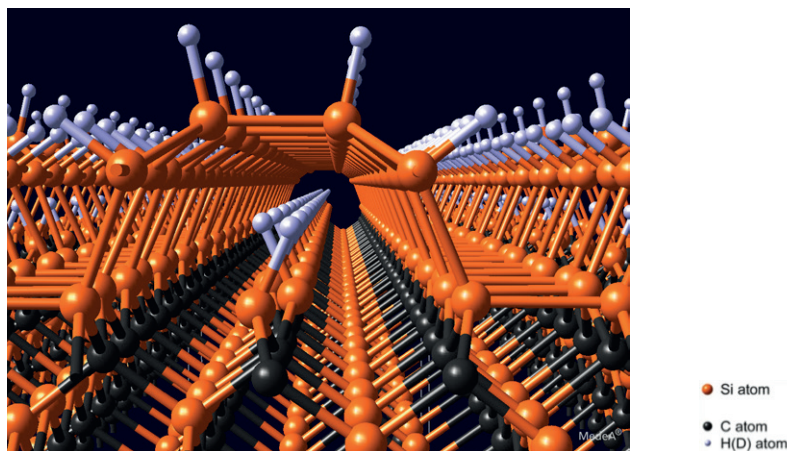
Hydrogen-induced nanotunnel opening at the subsurface of an advanced semiconductor, Silicon Carbide

Nanostructuring a surface is a key and mandatory engineering step towards advances in nanotechnology. A team of scientists from the Commissariat à l'Énergie Atomique et aux Énergies Alternatives, CEA-Saclay and the Synchrotron SOLEIL, Saint Aubin in France, from the University of Genoa and the Consiglio Nazionale delle Ricerche – CNR in Italy, and from the franco-american company Materials Design Inc., Angel Fire, New Mexico, USA & Materials Design sarl, Montrouge, France has shown that hydrogen/deuterium (H/D) induces the opening of nanotunnels below the surface of an advanced semiconductor, silicon carbide (SiC). This discovery is particularly interesting in view of the remarkable properties of SiC. These investigations have been performed using advanced experimental tools such as synchrotron radiation and vibrational spectroscopy techniques, and state-of-the-art theoretical simulations. Depending on the H/D SiC surface exposures, these nanotunnels undergo a sequence of semiconducting/metallic/semiconducting transitions. Therefore, they open very promising prospects towards applications in electronic, chemistry, storage, sensors and biotechnology.

■ Silicon carbide (SiC), a wide band-gap semiconductor, offers fascinating structural, thermal, mechanical, electronic and chemical properties, and is also especially resistant to radiation damages. SiC has a vast range of advanced applications including high-power, high-frequency, and high-temperature electronics devices and sensors. It has a remarkable biocompatibility making it useful for biomedical applications. SiC is also an especially suitable substrate for the growth of epitaxial graphene, with subsequent very promising potential applications in electronics and spintronics. Strain/stress interplay is the dominant driving force in SiC surface ordering, leading to more than 10 different surface reconstructions ranging from Si-rich to C-rich cubic SiC surfaces, and to the self-formation of highly stable massively parallel passive or active atomic lines and nanowires at the surface. Most interestingly, while H is very well known to passivate the

surface of semiconductors, the interaction of H/D atoms with the Si-rich 3C-SiC(001)-3x2 surface reconstruction leads to surface metallization, which is the first example of H/D-induced metallization of a semiconductor surface [1].

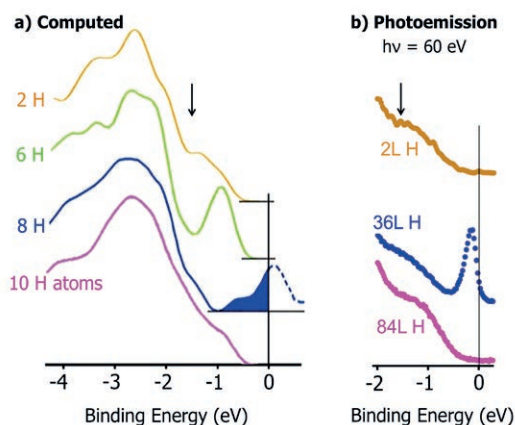
Although there are some examples of voids or nano-cavities generated at or below a surface, most are in the μm or sub- μm scales, and none exhibit spatial ordering. Here we report the first evidence of nanotunnel opening taking place within the subsurface region of a semiconductor, SiC, as depicted in Figure 1. Such an effect is induced by selective hydrogen/deuterium interaction at the surface, which possesses intrinsic compressive stress. This finding is established combining *ab-initio* total energy and vibrational computations using the VASP program within the MedeA® computational environment, and vibrational spectroscopy & synchrotron-radiation-based photoemission experiments.



1 3D view of a Nanotunnel. The nanotunnel opening induced by the interaction of H-atoms with the 3C-SiC(100)-3x2 surface is represented for the 8 H metallic structure. For clarity, the empty dangling bonds are not shown.

Hydrogen/deuterium-induced puckering of the subsurface Si atoms marks the critical step in this nanotunnel opening. Depending on hydrogen/deuterium coverage, the nanotunnels are either metallic or semiconducting as identified by density of states (DOS) calculations and photoemission experiments performed on the TEMPO beamline at the 3rd generation SOLEIL synchrotron. The experimental system is optimized to monitor live the electronic properties during hydrogen exposure, thereby leading to identify a semiconducting/metal/semiconducting transition as a function of hydrogen exposures as shown in Figure 2 comparing calculated and measured DOS, which appear to be in excellent agreement. For the metallic nanotunnel, the DOS build-up at the Fermi Level E_F (shown in blue) indicating metallization originates predominantly from the 3rd Si atomic layer below the surface while the combined contributions of the 1st and 2nd Si atomic layers remain marginal.

The vibrational frequencies for the clean and hydrogen-covered 3C-SiC(001)-3x2 surface measured by high-resolution electron energy loss spectroscopy (HREELS) are also in excellent agreement with the computed ones, providing deep insights and understanding into the nanotunnel opening. Dangling bonds generated inside the nanotunnel offer a promising template to capture atoms or molecules. These features open nano-tailoring capabilities towards advanced applications in electronics, chemistry, storage, sensors or biotechnology. Understanding and controlling such a mechanism open routes towards selective surface/interface functionalization.



2 Synchrotron radiation photoemission spectra and computed DOS for H-covered 3C-SiC(001)-3x2 surfaces. (a) Computed DOS for the 2 H, 6 H, 8 H atom and 10 H atom structures integrated over the top three Si layers and the first C layer and (b) SR-PES spectra recorded at photon energy of $h\nu = 60$ eV in the Fermi level region for exposures of 2L (Langmuir) H (semiconducting), 36L H (metallic) and 84L H (semiconducting) surfaces. Note the metallic–semiconducting transition upon higher H exposures to be in very good agreement with the calculated densities of states.

TEMPO beamline

ASSOCIATED PUBLICATION

Hydrogen-induced nanotunnel opening within semiconductor subsurface

P. Soukiassian*, E. Wimmer, E. Celasco, C. Giallombardo, S. Bonanni, L. Vattuone, L. Savio, A. Tejada, M. Silly, M. D'angelo, F. Sirotti, and M. Rocca

Nature Communications 4 (2013) 2800 & www.nature.com/ncomms/2013/131121/ncomms3800/pdf/ncomms3800.pdf

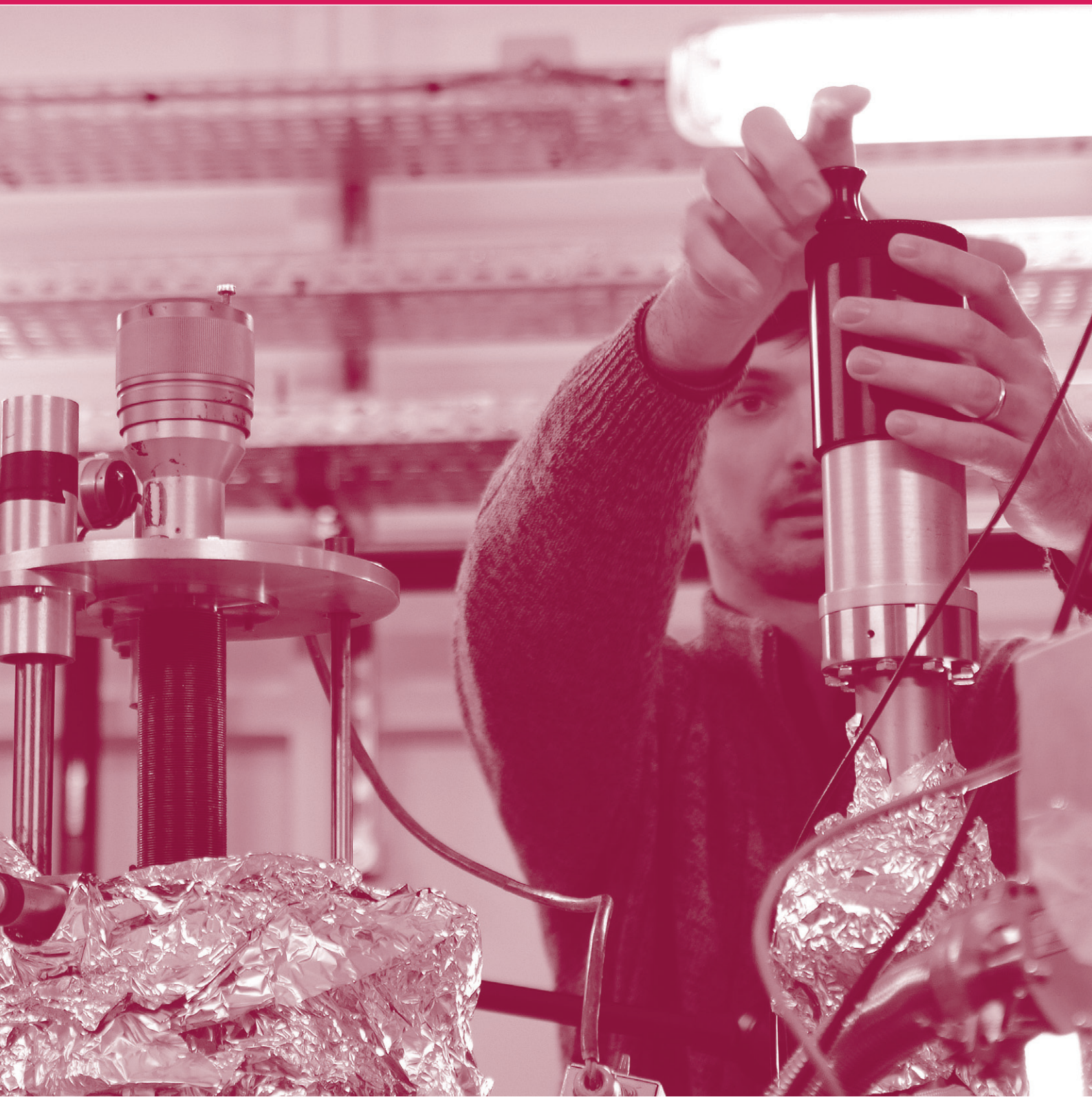
CORRESPONDING AUTHOR

* Commissariat à l'Énergie Atomique et aux Énergies Alternatives, SIMA, DSM-IRAMIS-SPEC, Saclay, Bât. 462, 91191 Gif sur Yvette, France

patrick.soukiassian@cea.fr

REFERENCE

[1] V. Derycke et al. Nature Materials 2 (2003), 253



CHEMISTRY AND PHYSICAL CHEMISTRY, NANOCHEMISTRY

- 34** Active sites of metalloproteins in solution revealed by vibrational spectroscopy
- 36** Self-structuring of bridged silsesquioxanes through covalent and non-covalent bonding
- 38** New insights into short ordered Fe-Al oxyhydroxide coprecipitates
- 40** Bone growth regulation: how does osteopontin bind uranium?
- 42** High capacity Li-rich layered compounds for Li-ion batteries
- 44** Probing spin-spin interactions in surface-supported single-molecule magnets
- 46** Fluorescent nanoplatelets pile-up
- 48** Coupling XANES and DFT calculations to unravel the structure of heterogeneous catalysts

CHEMISTRY AND PHYSICAL CHEMISTRY, NANOCHEMISTRY

The research in the fields of Condensed Matter Chemistry, soft matter and liquids benefits from the synchrotron radiation-based probes for describing and understanding a variety of systems and their changes under well-controlled conditions. This research thus concerns fundamental studies on model materials, as well as studies related to applications.

Within the fields of energy, the understanding of the performances of electrodes is essential to improve the cycling and rate capability of batteries. To address this issue, electrode material based on Lithium oxide composites were investigated under working conditions using the CRISTAL beamline by Sathiya et al.

The development of new smart materials such as high-spin molecules exhibiting a memory effect (single-molecule magnets) benefits from the information brought about by absorption and diffraction spectroscopies. On the DEIMOS beamline, Tancini et al. studied the superexchange coupling in surface-wired single-molecule magnets, a key step in the development of molecular spintronics. Another example of smart material concerns the search for new process for laser development. Self-assembly of colloidal nanoplatelets which provides such emission was studied by diffusion on the SWING beamline by Tessier et al.

Regarding environmental studies, the investigation of structures of soils sediments used for the scavenging of toxic material can take advantage on the sensitivity of X-Ray absorption on the LUCIA and SAMBA beamlines. In particular, the nature of Al-Fe oxyhydroxy co-precipitates playing such a role was determined by Hofmann et al.

At the border with lifescience, probing the active sites in metalloproteins has been characterized using Electrochemically-induced difference spectroscopy in a wide infrared domain on the AILES beamline. This study by Vita et al. points to the role of a hydrogen bond for tuning the active site. Health issues concerning the metal-environment characterization in biological material has been addressed on the MARS beamline by Safi et al. to investigate an uranyl binding site inside the osteopontin, a non-structured protein.

The control of the size and shape of nanomaterials is a necessary step for their development for optical, electronic, and catalytic applications. Such control during the synthesis of hybrid (organic-inorganic) material based on bridged silsesquioxanes was achieved by Creff et al. on the AILES beamline through measuring the far infrared absorption spectra during the material nanocrystallization.

Pascale Roy

Head of the "Chemistry and Physical Chemistry, Nanochemistry" Scientific Section

CHIMIE ET PHYSICO-CHIMIE, NANOCHEMIE

La recherche dans les domaines de la Chimie de la Matière Condensée, Matière Molle et Liquides utilise le rayonnement synchrotron pour sonder une large variété de systèmes et leurs changements dans des conditions bien contrôlées.

Ce type de recherche comprend aussi bien des études fondamentales sur des matériaux-modèles, que des études en vue d'applications.

Dans le domaine de l'énergie, la compréhension des performances des électrodes est essentielle à l'amélioration de la capacité de recharge des piles. Dans ce contexte, Sathiya et al. ont étudié des électrodes à base de composites d'oxyde de lithium dans les conditions de fonctionnement, sur la ligne CRISTAL.

La mise au point de nouveaux matériaux intelligents tels que les molécules à spin élevé présentant un effet mémoire (molécules-aimants) bénéficie des informations structurales fournies par la spectroscopie d'absorption et la spectroscopie de diffraction. Sur la ligne DEIMOS, Tancini et al ont étudié le couplage par super-échange dans des molécules-aimants en surface, étape essentielle au développement de la spintronique moléculaire. Un autre exemple relevant du domaine des matériaux intelligents est la recherche de nouveaux processus pour le développement de lasers. L'auto-assemblage des nanoplaquettes colloïdales susceptible de donner lieu à une telle émission a été étudié par diffusion sur la ligne SWING par Tessier et al.

Pour ce qui est des études environnementales, l'investigation des structures des sédiments de sol utilisés dans la récupération des déchets toxiques est basée sur la sensibilité de la spectroscopie d'absorption X sur les lignes LUCIA et SAMBA. En particulier, la nature des oxy-hydroxy co-précipités de Al-Fe jouant ce rôle a été déterminée par Hofmann et al.

A la frontière avec les sciences du vivant, sur la ligne AILES, les sites actifs des métalloprotéines ont été sondés et caractérisés par spectroscopie de différence induite par voie électrochimique dans un large domaine infrarouge. Cette étude de Vita et al. met en évidence le rôle de la liaison hydrogène dans le fonctionnement du site actif. Safi et al. se sont intéressés aux questions de santé liées à la caractérisation de l'interaction métal-environnement dans les matériaux biologiques, en étudiant sur la ligne MARS le site permettant de lier l'uranyle à l'intérieur de l'ostéopontine, une protéine non-structurée.

Le contrôle des dimensions et de la forme des nano-matériaux constitue une étape indispensable du développement des applications optiques, électroniques et catalytiques. Creff et al. ont obtenu ce type de contrôle sur la ligne AILES, au cours de la synthèse d'un matériau hybride (organique-inorganique) en mesurant le spectre d'absorption en IR lointain pendant la nano-cristallisation du matériau.

Pascale Roy

Responsable de la Section Scientifique « Chimie et Physico-Chimie, Nanochimie »

Active sites of metalloproteins in solution revealed by vibrational spectroscopy

New information on protein's structure, intra- and intermolecular hydrogen bonds, or metal-ligand bond properties can be unraveled in the Far IR and TeraHertz domain ($600 - 3 \text{ cm}^{-1}$ or $18 - 0.1 \text{ THz}$). Using Cu-azurin placed in a short path-length electrochemical cell adapted for transmission spectroscopy at the beamline, we show that the brilliance and stability of the Far-IR beamline AILES [1,2] enables to detail molecular properties of metal sites or metal redox states of proteins. Moreover it allows extracting from a complex background hydrogen bonding signatures directly relevant to the protein function.

Introduction

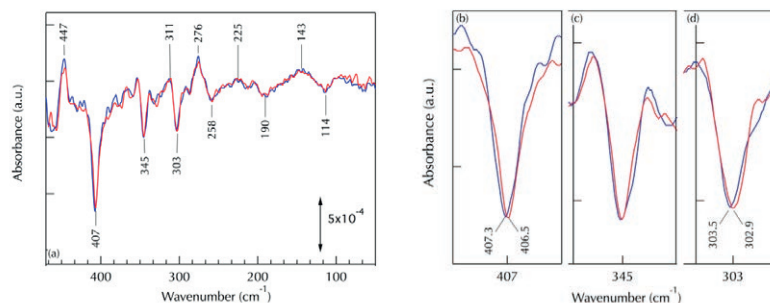
Vibrational analysis of proteins or biological molecules provides new information on biomolecular structures, dynamics and properties of intra- and intermolecular hydrogen bonds. Bending vibrational modes of amino acids as well as metal-ligand vibrations also absorb in the Far-IR, which is particularly appealing for probing metal active sites

in metalloproteins [3,4]. Far-IR absorption spectra of proteins in aqueous solution are dominated by the strong absorption of water. Due to the weakness of the signals to probe, typically of the order of 10^{-5} to 10^{-3} unit of absorbance, difference spectroscopy is needed to identify modes associated with active sites.

Identification of metal-ligand IR modes using metal isotope labelling

Only vibrations of chemical groups selectively perturbed by the Cu redox switch contribute in electrochemically-induced difference spectra. Indeed, in figure 1 and 2, well-defined bands are observed for the Cu^{II} state (negative) and for the Cu^I state (positive). To identify IR modes involving Cu-ligand vibrations, we compared spectra recorded with ⁶³Cu- and ⁶⁵Cu-azurin (Figure 1). With ⁶⁵Cu, two negative bands at 407

and 303 cm^{-1} (Cu^I state) are downshifted by 0.8 cm^{-1} and 0.6 cm^{-1} respectively (Figure 1b and 1d) suggesting that these bands correspond to modes involving Cu^I-ligand bond. DFT calculations allow to assign the band at 407.3 cm^{-1} to the $\nu(\text{Cu-SCys})$ mode strongly coupled with deformation modes of amino acids and the band at 303 cm^{-1} to the $\nu^{\text{as}}(\text{Cu-(NHis)}_2)$ IR mode, coupled with bending modes of the Cu ligands.



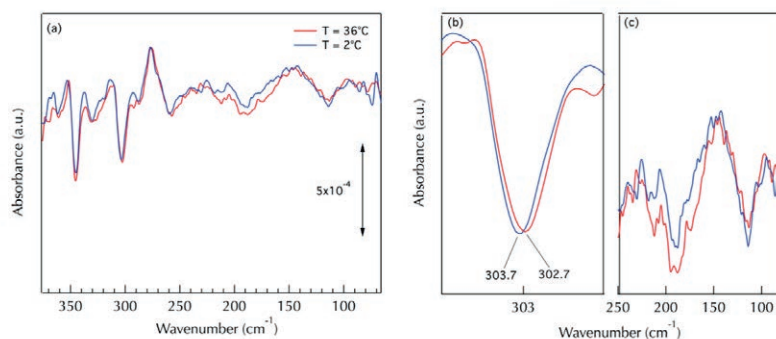
1 Effect of ⁶³Cu- and ⁶⁵Cu-azurin isotopic labelling on the reduced-minus-oxidized FTIR difference spectra. (a-d) Spectra recorded with ⁶³Cu- (blue) and ⁶⁵Cu- (red) azurin.

Probing hydrogen-bonding by the detection of temperature sensitive signatures in the Far-IR difference spectra

Hydrogen bonds in proteins, and notably those involving the water solvent, are highly temperature sensitive. Therefore, the thermal dependence of Far-IR absorption of Cu-azurin allows to specifically probe modes affected by hydrogen bonding.

Figure 2 shows a superimposition of reduced-minus-oxidized difference spectra recorded at 2°C and 36°C with Cu-azurin in H₂O. Temperature increase results in greater amplitude of the negative broad band at 225–150 cm⁻¹ and in a downshift of the 303.7 cm⁻¹ band to 302.7 cm⁻¹. The band frequency at 225–150 cm⁻¹ corresponds to intermolecular H bond stretching, arising from the longitudinal

motion of the hydrogen atom along the hydrogen bond axis. The band at 303 cm⁻¹ contains significant contribution from $\nu(\text{Cu}-(\text{NHis})_2)$ vibration. Interestingly, the histidine Cu ligand His¹¹⁷ is hydrogen bonded to a water solvent molecule in the crystallographic structure of Cu-azurin (Figure 2 inset). A weakening of this hydrogen bond at 36 °C may explain the temperature dependence of the 303 cm⁻¹ band frequency. The frequency downshift observed upon temperature increase is in line with a decreased electronegativity of the imidazole ligand due to a weakening of the imidazole NH₂...OH₂ intermolecular bond.



2 Temperature dependence of the FTIR difference spectra. Superimposition of reduced-minus-oxidized FTIR difference spectra recorded at 36 °C (red) and 2 °C (blue) on Cu-azurin samples. The main temperature effects are zoomed in (b) and (c).

Conclusions

The high resolution spectra obtained using synchrotron sources has allowed the first identification of metal-ligand IR modes using shifts induced by metal labelling, a strategy that overcomes metal substitution studies as it does not change the metal centre properties. Moreover, the Far-IR

data provide the first vibrational data on reduced CuI-azurin. Finally, coupling Far-IR difference spectroscopy with temperature changes allows detecting hydrogen bonding directly relevant to the protein function.

AILES beamline

ASSOCIATED PUBLICATION

Electrochemically-induced Far-Infrared difference spectroscopy on metalloproteins using advanced synchrotron technology

N. Vita, J-B. Brubach*, R. Hienerwadel, N. Bremond, D. Berthomieu, P. Roy and C. Berthomieu

Analytical Chemistry, 85 (2013), 2891

CORRESPONDING AUTHOR

* Synchrotron SOLEIL, l'Orme des Merisiers, St Aubin BP48, 91192 Gif sur Yvette Cedex, France

jean-blaise.brubach@synchrotron-soleil.fr

REFERENCES

- [1] Brubach, J. B et al. J Chem Phys 122 (2005), 184509
- [2] Roy, P. et al. Infrared Physics & Technology 49 (2006), 139
- [3] Marboutin, L. et al. J Phys Chem B 113 (2009), 4492
- [4] Marboutin, L. et al. Angew Chem Int Ed 50 (2011), 8062

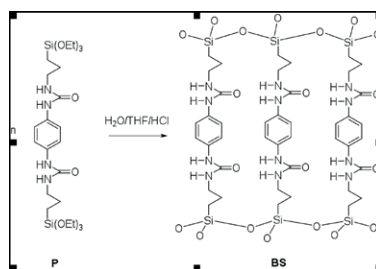
Self-structuring of bridged silsesquioxanes through covalent and non-covalent bonding

The self-structuring of a bridged silsesquioxane during sol-gel synthesis has been investigated by *in situ* optical microscopy (OM), light scattering (LS) and infrared spectroscopy (IR). The evolution of the system as a function of processing time was correlated with covalent interactions (polycondensation) and non-covalent interactions (H-bonding). A comprehensive mechanism based on the hydrolysis of the organosilane precursor **P** prior to the crystallization of the corresponding **BS** via H bonding and subsequent irreversible polycondensation is proposed.

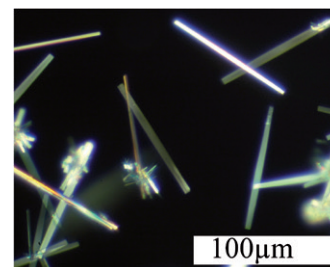
Introduction

Bridged silsesquioxane (**BS**) is an emerging class of hybrid material with—covalently Si-C bonded organic functions to silica. They are obtained by the sol-gel hydrolysis of molecular precursors in which the organic part is connected to several silicon atoms bearing hydrolysable alkoxy groups. New properties can be tuned to these materials according to the organic function which can also induce the self-structuring of the resulting hybrid. Indeed, it was found that during

the hydrolysis-condensation of **P**, self-assembly occurs with the formation of H-bonds resulting in a crystalline **BS** (Figure 1) as confirmed in former studies by TEM and PXRD studies [1,2]. Since two processes (H-bonds and Si-O-Si bond formation) may interfere in the structuring during the hydrolysis-condensation of **P**, *in situ* OM, LS and IR measurements have been performed to determine the key factors of the structuring processes.



1 Sol-Gel synthesis of crystalline BS



Results and discussions

OM analyses show the nucleation and growth of rectangular needles which display a strong and uniform birefringence indicating the formation of single crystals. In combination with LS experiments, three domains were determined (Fig. 2a): Domain I (10 min) indicates no molecular aggregation; nucleation of microcrystals occurs in Domain II and slows down into the final crystal shape in Domain III. The hydrolysis-condensation steps (covalent bonding) monitored by MFTIR ($900\text{--}1300\text{ cm}^{-1}$) to probe the $\nu_{\text{as}}\text{Si-O}$ (condensation) and the ρCH_3 (hydrolysis) vibrations reveal an increasing intensity of $\nu_{\text{as}}\text{Si-O}$ together with a decreasing intensity of ρCH_3 (Fig. 2b) [3,4]. These can be correlated to the 3 domains above: hydrolysis (up to 50%) of **P** (Domain I) with no polycondensation until 10 min after which time the hydrolysis rate decreases with a concomitant crystallization. Condensation then starts with a rapid crystal growth until 20 min (Domain II) and in Domain III no change of crystallite size is observed while

condensation continues (aging). The self-assembly via H-bonding formation (non-covalent interaction) was also monitored by MFTIR ($1350\text{--}1750$ for amide-1, ν_{CO} and for amide-2, δ_{NH}). The results (Fig. 2c-e) are again related with the 3 domains (Fig. 2c): only free molecules are present (Fig. 2d) in Domain I determined by the absence of H-bonding (free mode at around 1686 cm^{-1}). In Domain II, concomitant condensation and H-bonding formation occur (ν_{CO} shifts at lower frequency, 1635 cm^{-1}). The intensity variations of the amide-2 mode (Fig. 2e) are consistent with this interpretation (emergence of a band at around 1590 cm^{-1}). After 50 min (Domain III) a slight downshift of the H-bonded CO (4 cm^{-1}) as well as a narrowing and an increasing intensity of the peak with time is observed (Fig. 2d) indicating a strengthening of H-bonds while polycondensation proceeds and is consistent with further local rearrangement or intermolecular ordering in the system.

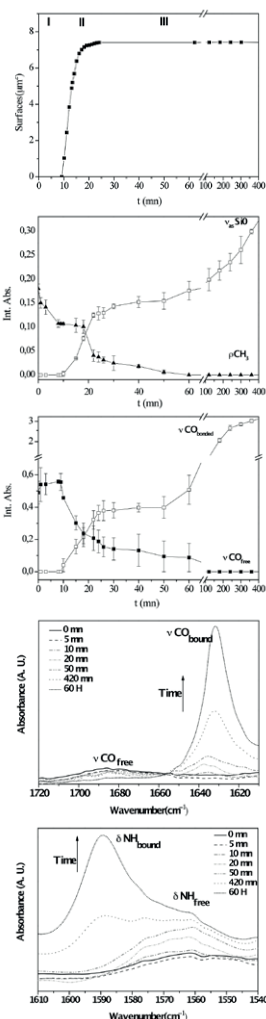
Conclusion

The techniques used (OM, IR and LS) to investigate the formation of a self-assembled **BS** during sol-gel processing clearly demonstrate a competition between covalent Si-O-Si bond and urea H-bonding interactions producing needle-like crystals.

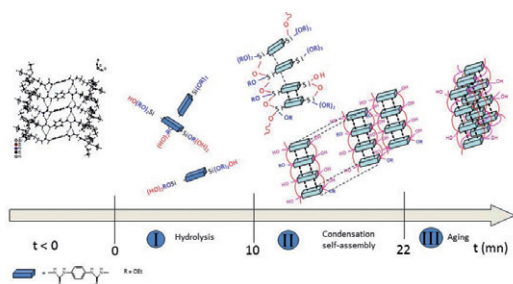
A mechanism describing the formation of the organized **BS** is proposed:

- Hydrolysis of **P** proceeds without significant condensation until around 50 % of the alkoxy groups are consumed;
- When the critical supersaturation concentration of the hydrolysed **P** is reached, formation of the organized **BS** starts via a concerted process involving intermolecular H-bonding of urea groups and condensation of adjacent silanol/alkoxy species to form siloxane species. Subsequent growth of the organized material is mediated by direct "attachment" of precursor molecules at the solid/solution interface;
- During aging, local reorganization occurs due to mechanical stress caused by increasing polycondensation within the needles leading to the crystals.

Figure 2 shows a tentative representation of the self-structuring of **BS** in the 3 domains.



2 Three domains obtained by OM, DLS and MFTIR experiments



3 Proposed mechanism for the self-assembled structure of **BS**

CRISTAL beamline

ASSOCIATED PUBLICATION

Self-assembly of bridged silsesquioxanes: modulating structural evolution via cooperative covalent and non-covalent interactions

G. Creff, B.P. Pichon, C. Blanc, D. Maurin, J.-L. Sauvajol, C. Carcel, J.J.E. Moreau, P. Roy, J.R. Bartlett, M. Wong Chi Man* and J.-L. Bantignies

Langmuir 29 (2013), 5581

CORRESPONDING AUTHOR

* Laboratoire Architectures Moléculaires et Matériaux Nanostructurés - ICG Montpellier (UMR 5253) CNRS- UMII-ENSCM- UMI, ENS de Chimie de Montpellier, 8 rue de l'École Normale, 34296 Montpellier Cedex 5, France
michel.wong-chi-man@enscm.fr

REFERENCES

- [1] J.J.E. Moreau et al. *Angew Chem. Int. Ed.*, 43 (2004), 203.
- [2] P. Dieudonné et al. *Small*. 2009, 5, 503.
- [3] J.L. Bantignies et al. *J. Phys. Chem. B*, 110 (2006), 15797
- [4] G. Creff et al. *PCCP* 14 (2012), 5672

New insights into short ordered Fe-Al oxyhydroxide coprecipitates

X-ray absorption spectroscopies at the $K\alpha$ edges of Fe and Al were conducted at LUCIA and SAMBA beamlines. They were decisive in understanding how these two cations interact during mineral phase formation by forced hydrolysis. The classical view of an oxyhydroxy-polymer with substitution between Al and Fe is now refined.



Low crystallinity iron oxyhydroxides are ubiquitous in environmental systems, where they act as strong sorbents, thus playing a dominating role for the distribution of trace compounds between solid and solution [1]. They are rarely present as a pure iron phase; the association of Fe(III) and Al in oxyhydroxides is particularly common

because of the abundance of both ions at the Earth surface and because of similarities in aqueous ion speciation. We investigated the products of hydrolysis of a solution containing both metal ions. The objective was to identify the interactions occurring between the cations during precipitation and to evaluate the effect of changes in Al/Fe ratio.

Fe and Al hydroxypolymers

The two solid phase end-members in the Fe-Al system, hydrous ferric oxide, HFO and hydrous aluminous oxide, HAO are quite distinct chemically and structurally. The solubility constants for HFO and HAO are 6 orders of magnitude apart and the two precipitates differ in the degree of polymerisation, Al remaining significantly more hydrated than Fe. Crystallinity of the pure end members is also different. HFO is

a 2-line ferrihydrite characterised by two diffuse diffraction lines on XRD patterns, also well identified by SAED. Conversely, HAO is amorphous towards X-rays and electrons. Despite these differences in the end-member phases, it has been claimed that hydroxide formation in solutions with both cations present, results in mixed phases (HFAO) with substitution between Fe and Al [2].

Location of Al in HFAO's

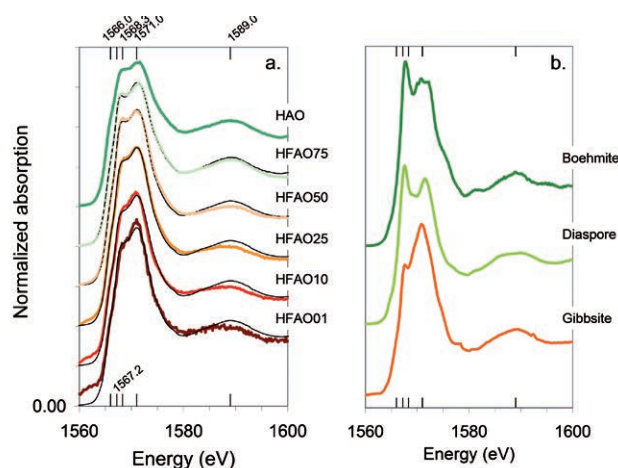
Fe-Al oxyhydroxy-coprecipitates were synthesized by forced hydrolysis of $\text{Fe}(\text{NO}_3)_3 \cdot 9\text{H}_2\text{O}$ and $\text{Al}(\text{NO}_3)_3 \cdot 9\text{H}_2\text{O}$ solutions. Solids containing 0, 1, 10, 25, 50, 75, 90 mol% Al were characterised for composition, texture, mineral structure and local atomic environment. EXAFS analyses at the Fe K-edge conducted on the co-precipitates were well fitted by assuming only Fe and O as close and distant neighbours of the target iron atom. Substituting Al for Fe in the local environment of Fe could not provide satisfactory EXAFS fits, suggesting that Al was not present in the local environment around iron atoms. Nonetheless Al was generally associated with HFO. At less than 50% Al, the Al/Fe ratio measured by TEM-EDXS on individual particle spots was homogeneous and representative of the

bulk ratio, suggesting that the Al-hydroxide forms a coating around the HFO nuclei [3]. Such a surface rim can be explained by $\text{Al}(\text{H}_2\text{O})_6^{3+}$ binding to hydroxy sites at the surface of the HFO nuclei, as soon as these are formed during synthesis. Al K-edge XANES spectra revealed the presence of structurally well organised Al-octahedra, best interpreted through a mono/multilayer hypothesis (Fig. 1). Below 50 % Al, planar gibbsite-like local structures were observed while above 50 % Al, three-dimensionally linked octahedra appeared. The planar Al linkages may reflect monolayer formation at the HFO surface. Multiple layer sorption should favour the formation of 3D linkages as they were indeed observed with the occurrence of boehmite-like organisation above 50 % Al.

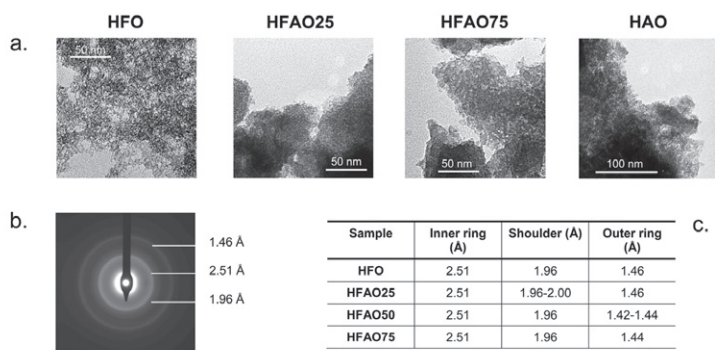
Influence of Al on HFO ordering

The presence of HFO influenced the distribution of Al-hydroxypolymers in the HFAO mixture and it influenced their ordering. Conversely, Al influenced the structural organisation in the Fe-hydroxypolymers. X-ray and electron diffraction data suggested that HFO bears the structure of a 2-line ferrihydrite whatever the concentration of Al (Fig. 2). However, subtle changes occurred with increasing Al. The EXAFS traces reflecting the local environment around an iron centre indicated improved symmetry

in the octahedral arrangement of the oxygen ions around Fe. Fitting in k and R space revealed that the number of Fe-Fe linkages decreased as Al increases in the system, indicative of a lesser degree of polymerisation of the HFO nuclei, or of a relative increase of surface Fe with disrupted octahedra linkages. Finally Raman spectra revealed vibration bands arising in the HFAO spectra with increasing Al, not assigned to either of the end-members, faintly resembling akaganeite.



1 Normalised Al K-edge XANES of (a) the samples (thick lines) and the corresponding linear combination fits (thin lines), (b) the references.



2 Bright field TEM micrographs of Fe-Al co-precipitates with 0, 25, 75 and 100 % Al. (b) The ED pattern of HFO is representative of 2-line ferrihydrite. (c) Lattice parameters d obtained from ED pattern for the HFAO series.

LUCIA & SAMBA beamlines

ASSOCIATED PUBLICATION

Interaction of Fe(III) and Al(III) during hydroxylation by forced hydrolysis: the nature of Al-Fe oxyhydroxy co-precipitates

A. Hofmann*, D. Vantelon,
E. Montarges-Pelletier, F. Villain, O. Gardoll,
A. Razafitianamaharavo and J. Ghanbaja

Journal of Colloid and Interface Science
407 (2013), 76

CORRESPONDING AUTHOR

* Géosystèmes, Université Lille 1, CNRS,
UMR 8217, 59655-Villeneuve d'Ascq, France
annette.hofmann@univ-lille1.fr

REFERENCES

- [1] R.M. Cornell, U. Schwertmann, 2003 The iron oxides. Structure, properties, reactions, occurrences and uses, Wiley-VCH ed., Weinheim
- [2] A. C. Cismasu AC et al. Geochim. Cosmochim. Acta 92 (2012), 275
- [3] Y.T. Liu & D. Hesterberg, Environ. Sci. Technol. 45 (2011), 6283

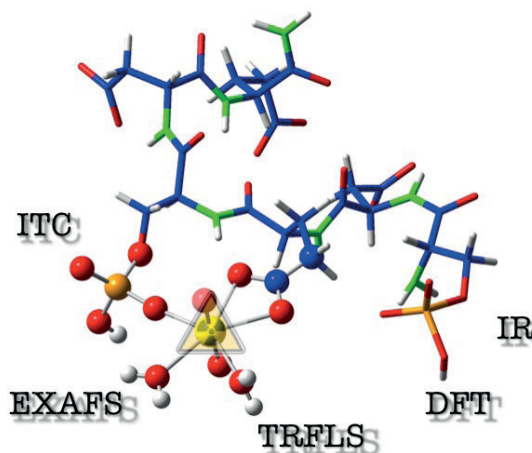
Bone growth regulation: how does osteopontin bind uranium?

The impact of radioelements on living organisms and human has been studied since the nineteen fifties and their chemical toxicity is thought to resemble heavy metal toxicity by replacement of essential metals of the organism such as iron or calcium. In the case of uranium, one challenge to better appraise its toxicity and develop countermeasures in case of exposure of living organisms is to better assess pathways of contamination. Among others, the skeleton is a targeted deposition site of this element whatever the oxidation states that have been administered to animals.

Introduction

Radioelements in general are chemical and radiological contaminants. It is known that chemical toxicity prevails in the case of uranium and thorium, while both radio- and chemical toxicity are important for plutonium. In the case of chronic and very low level exposure, the clinical consequences are still largely undefined [1]. Whatever the exposure pathway (inhalation, ingestion or wound), the soluble fractions of radioelement are absorbed and transported by blood and are either evacuated through renal excretion, or fixed in target organs. Liver is the most important soft tissue deposition site for all of them except uranium, for which it is the kidneys [2]. On internal contamination, uranium enters the blood stream in the form of soluble uranyl (the dioxo cationic form $U(VI)O_2^{2+}$) salts and protein-bound complexes and is then mainly deposited in kidney and

bone tissues. It was recently suggested that chronic mechanisms of uranyl toxicity might include phosphate interactions which could explain its *in-vivo* targets [3]. Recently, Quémeneur *et al.* suggested the use of osteopontin (OPN) as a possible uranyl exposure biomarker observing the reduced concentration of OPN in urine upon exposure [4]. Screening several peptides present in its sequence led to the identification of a phosphorylated hexapeptide pSDEpSDE as the most potent calcium growth inhibitor and thus as one possible OPN active site. We have investigated the structural aspects of the uranyl complexes formed with the pSDEpSDE peptide and the protein by a combination of techniques (calorimetric titration, vibrational spectroscopy, X-ray Absorption Spectroscopy) and quantum chemical calculations as schematized in Figure 1.

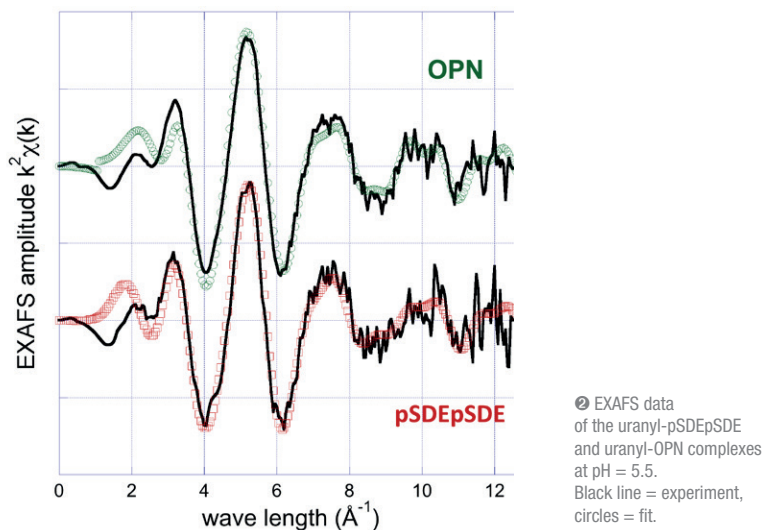


1 Molecular simulation model of the uranyl-pSDEpSDE complex.

Structure of the uranyl-pSDEpSDE peptide

Lacking crystallographic data for the peptide and protein complex, the only indications about the coordination scheme come from knowledge of the peptide amino acidic sequence and the preliminary IR data. We therefore tested *in silico* various geometrical combinations around the uranyl that were in agreement with IR, ITC and TRLS. It consisted of defining plausible geometries for a first coarse-grain refinement, using initial interatomic distances obtained from our previous work conducted on small phosphorylated biomolecules resulting in a bidentate carboxylate and a monodentate phosphate environment. The next step consisted of refining all the interatomic distances in the presence of the peptidic sequence strain and steric effects using DFT calculations. Finally, further structural investigation to probe the uranium coordination environment was done using EXAFS spectroscopy. These experiments were

performed at the MARS beamline, dedicated to the study of radioactive materials. The pSDEpSDE and OPN uranyl complexes at pH 5.5 exhibit similar EXAFS pattern as shown in Figure 2. Satisfactory fits obtained for both samples with very comparable metrical parameters have been provided. For the two complexes, axial U-O bond lengths of 1.76 Å were determined which is typical of a uranyl aquo ion. The presence of two distinct equatorial shells at ≈ 2.26 Å and 2.32-2.33 Å is in agreement with literature data for phosphate and carboxylate bidentate bonds respectively. The U-C distance at 2.91-2.93 Å was most consistent with a four-membered ring chelate resulting from a bidentate complex with a carboxylate group. Furthermore the present U-P bond length (3.83-3.84 Å) is similar to previously reported for a protonated monodentate phosphate moiety.



Conclusion

This study has described the uptake of the uranyl ion by one of the phosphorylated sites of the OPN protein involved in bond regeneration. The combination of several techniques, in particular EXAFS

with synchrotron radiation, has allowed us to characterize the structural and thermodynamic factors of uranyl binding to the OPN site responsible for mineralization control.

MARS beamline

ASSOCIATED PUBLICATION

Osteopontin: a Uranium phosphorylated binding-site characterization

S. Safi, G. Creff, A. Jeanson, L. Qi, C. Basset, J. Roques, P. L. Solari, E. Simoni, C. Vidaud and C. Den Auwer*

Chem. Eur. J. ; 19(34) (2013) 11261

CORRESPONDING AUTHOR

*Institut de Chimie de Nice, Université Nice Sophia Antipolis, UMR 7272, 06108 Nice, France

christophe.denauger@unice.fr

REFERENCES

- [1] Report of the United Nations Scientific Committee on the Effects of Atomic Radiation, ISBN 978-92-1-642010-9, 2011
- [2] P. W. Durbin, Actinides in animals and man in *The chemistry of the actinide and transactinide elements*, 3rd edition (Eds.: L. R. Morss, N. M. Edelstein, J. Fuger) Springer 2006
- [3] J. D. Van Horn & H. Huang, *Coord. Chem. Rev.* 250 (2006), 765
- [4] O. Prat et al. *Environ. Int.* 37 (2011), 657

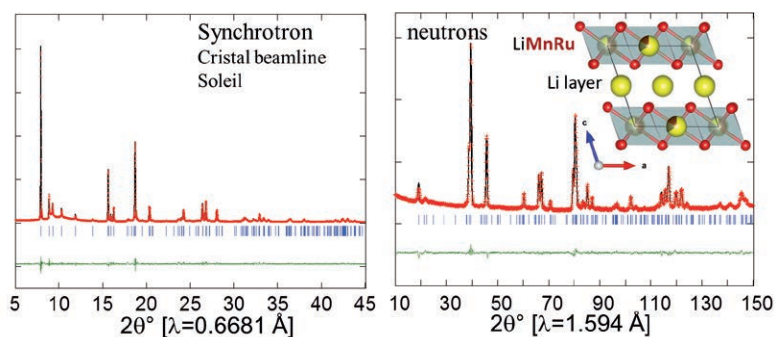
High capacity Li-rich layered compounds for Li-ion batteries

The large capacities displayed by the Li-rich layered electrodes for Li-ion batteries have been explored via a thorough study of the $\text{Li}_2(\text{Mn,Ru})\text{O}_3$ system. Such materials are based on a stacking of Li layers and honeycomb LiMnRu layers, all cations being octahedrally coordinated with oxygen atoms. We could unravel a redox activity linked to the anionic $\text{O}^{2-}/\text{O}_2^{2-}$ couple which comes in addition to the well-known cationic redox activity. This fundamental study opens the path for obtaining batteries lasting much longer than today's ones.

Lithium-ion batteries have been recognized as attractive energy storage systems not only for portable electronics but also for powering electric vehicles. Manganese containing layered compounds such as $\text{LiNi}_{1-y}\text{Co}_y\text{Mn}_{1/2}\text{O}_2$ are progressively replacing LiCoO_2 in today's Li-ion cells because of both higher voltage and capacity. Still, larger capacity values are needed to meet automobile applications.

Further attempts to improve the electrochemical properties resulted in the discovery of new series of composite cathode materials such as $(1-y)\text{Li}_2\text{MnO}_3 - y\text{LiMO}_2$ ($M = \text{Co}, \text{Ni} \dots$) which exhibit higher capacity and excellent stability [1]. Such materials show specific capacity greater than $200 \text{ mAh} \cdot \text{g}^{-1}$. However, these integrated cathodes present complex layered structures as there is still ambiguity whether they form short-range ordered domain or homogeneous solid solutions. Whatever the exact nature, it is clear that the high capacity exhibited by $\text{Li}_2\text{MnO}_3 - \text{LiMO}_2$ materials cannot be simply attributed to the presence of two phases, but is rather more complex.

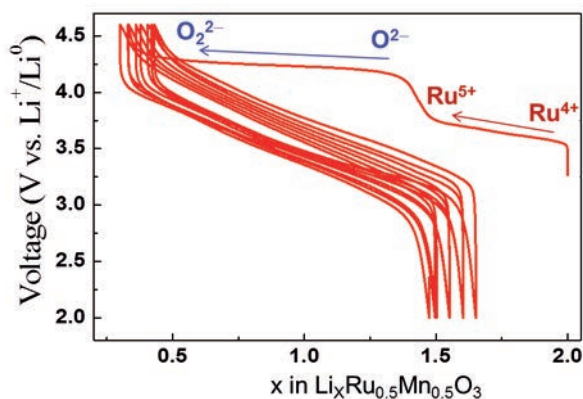
Our strategy to lift the veil on such a complexity has been to simplify the chemical nature of the problem while preserving a layered structure. We decided to study the layered $\text{Li}_2\text{Ru}_{1-y}\text{Mn}_y\text{O}_3$ system which, in addition to imparting structural stability, provides a higher electronic conductivity; then enhancing the electrode rate capability. From coupled Synchrotron and neutron powder diffraction refinements (Figure 1), we could shed light on the distribution of both light (Li, O) and heavy (Ru, Mn) atoms in the cell. The resulting analysis clearly indicates that the sample is single phase and that the large capacities can therefore be obtained without having a composite nature. $\text{Li}_2\text{Ru}_{0.5}\text{Mn}_{0.5}\text{O}_3$ is based on a face-centered cubic stacking of oxygen atoms, with cations occupying interstitial octahedral sites so as to generate pure Li layers alternating with honeycomb LiRuMn layers.



1 Rietveld refinements of neutron (D2B, Institut Laue Langevin) and Synchrotron X-Ray diffraction (CRISTAL beamline) of the $\text{Li}_2\text{Ru}_{0.5}\text{Mn}_{0.5}\text{O}_3$ compound, whose structure is shown in inset. The honeycomb LiMnRu layers alternate with pure Li layers; oxygen atoms (shown as red balls) form a close packed stacking.

Moreover, we could demonstrate, through combined *in situ* X-Ray diffraction, *ex situ* Synchrotron diffraction, X-Ray photoemission spectroscopy and DFT calculations that the 3.5 V plateau on charge (Figure 2) results from the classical cationic redox activity (Ru is oxidized from 4+ to 5+). Nevertheless the highlight of this paper remains that the origin of the 4.3 V plateau is nested in an anionic redox activity which involves the

formation of O_2^{2-} peroxy-like groups in the structure. This result has opened new research avenues for harvesting novel high capacity layered electrodes cumulating within the same structure both cationic and anionic redox processes [2]. Further work will include the understanding and the mastering of the voltage decay these materials suffer on cycling; let's bet chemists will soon provide tricks to avoid this limitation.



© Voltage versus composition curve of $Li_xRu_{0.5}Mn_{0.5}O_3$. The redox couple associated with each plateau is indicated.

CRISTAL beamline

ASSOCIATED PUBLICATION

High performance $Li_2Ru_{1-y}Mn_yO_3$ ($0.2 \leq y \leq 0.8$) cathode materials for rechargeable Lithium-ion batteries: their understanding

M. Sathiya, K. Ramesha, G. Rousse*, D. Foix, D. Gonbeau, A. S. Prakash, M. L. Doublet, K. Hemalatha and J. M. Tarascon

Chemistry of Materials 25 (2013), 1121

CORRESPONDING AUTHOR

*Chimie du Solide et Energie,
Collège de France, 11 place Marcelin-Berthelot,
75005 Paris, France

gwenaelle.rousse@college-de-france.fr

REFERENCES

- [1] M. Thackeray et al. Journal of Materials Chemistry 15 (2005), 2257
- [2] M. Sathiya et al. Nature Materials 12 (2013), 827

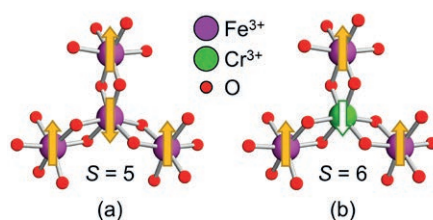
Probing spin-spin interactions in surface-supported single-molecule magnets

The ability of X-ray Magnetic Circular Dichroism (XMCD) to detect magnetism in an element-specific manner was exploited for a temperature-dependent study of Fe_3Cr single-molecule magnets deposited on a $\text{Au}(111)$ surface. The dichroic signals recorded at Fe and Cr L_3 edges over a broad temperature range provided the Fe-Cr superexchange-coupling constant, which conforms to the bulk-phase value in both sign *and* magnitude. Our data indicate that interaction with the surface has no significant influence on intramolecular spin-spin coupling.

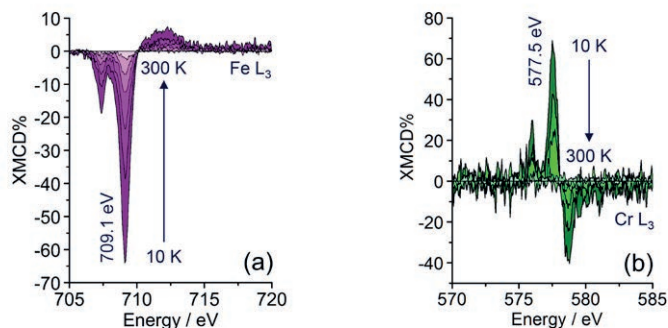
Introduction

Single-molecule magnets (SMMs) are metal-ion based molecules of special importance in the emerging field of molecular scale electronics. In these systems, an anisotropy barrier slows down the reorientation of magnetic moment, so that magnetic blocking is observed at low temperature (T) [1]. According to recent theoretical predictions, spin detection and manipulation are possible by driving a spin-polarized electric current through an individual SMM in a STM experiment [2]. It is thus important to deposit SMMs on conducting substrates in such a way that they remain structurally

and functionally intact. After years of unfruitful work on Mn_{12} SMMs, in 2009 an XMCD experiment finally revealed magnetic blocking in surface-wired tetrairon(III) (Fe_4) complexes [3]. In these small SMMs, superexchange interactions between the nearest-neighboring iron(III) ions ($s = 5/2$) are antiferromagnetic (AF) and afford a $S = 5$ ground state (Figure 1a). A proper design of molecular structure further allowed the preparation of partially-oriented monolayers which displayed spectacular waist-restricted hysteresis loops and clear signatures of resonant quantum tunneling effects [4].



1 Metal-oxygen core in Fe_4 (a) and Fe_3Cr (b) SMMs. Arrows depict the spin arrangement in the ground state with total spin S . The core is surrounded by organic ligands that provide terminal coordination to Fe ions and Fe-Cr bridging.

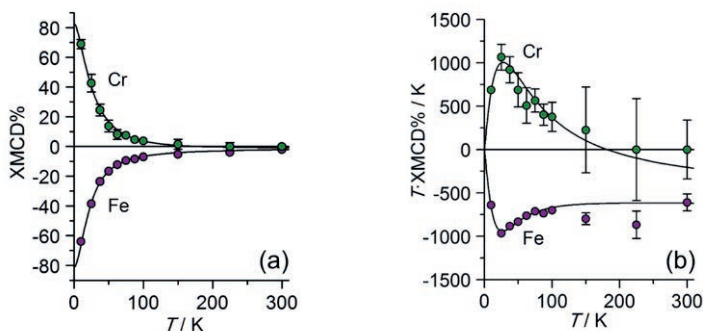


2 T -dependent XMCD spectra at the $\text{Fe } L_3$ (a) and $\text{Cr } L_3$ (b) edges measured on a monolayer of Fe_3Cr on $\text{Au}(111)$. Spectra have been recorded at 50 kOe and normalized with respect to the L_3 maximum in the corresponding isotropic XAS spectrum.

ON-SURFACE TEMPERATURE-DEPENDENT XMCD MAGNETOMETRY

We have now evidence that tetrametallic SMMs deposited on Au(111) retain a bulk-like electronic structure over the energy scale defined by superexchange interactions. To separately probe the magnetism of the central and peripheral ions, the central iron(III) was selectively replaced by a chromium(III) ion ($s = 3/2$) (Figure 1b). The Fe_3Cr complex so obtained is otherwise structurally identical to the corresponding Fe_4 species and still entails an AF Fe-Cr coupling ($J_{\text{Fe-Cr}}$). Bulk-phase samples and monolayers on Au(111) were analyzed by XMCD at Fe and Cr L_3 edges. Signals of expectedly opposite sign were observed at T values (10 K) where the ground state is predominantly populated (Figure 2). With increasing T , the XMCD% signals were found to undergo a rapid decrease in amplitude while maintaining the same profile (Figures 2 and 3a). The T dependence of magnetic polarization was however best appreciated by plotting $\text{XMCD}\% \cdot T$ vs. T data, as commonplace in

traditional magnetometry. As shown in Figure 3b, pronounced deviations from Curie law were detected below 100 K. Data analysis was based on a Heisenberg plus Zeeman hamiltonian (JS_1-S_2 convention), since in the explored T range magnetic anisotropy has no effect on magnetic behaviour. Simultaneous fitting of the two curves gave $J_{\text{Fe-Cr}} = 14.7(7) \text{ cm}^{-1}$, in excellent agreement with the value found in the bulk phase by the same method as well as by SQUID magnetometry. It is noteworthy that magnetic polarizations at Fe and Cr centers exhibit different T dependences, in full agreement with a Cr-centered Fe_3Cr topology. In fact, in Fe_3Cr systems the magnetic polarization at Fe sites is always parallel to the applied field. By contrast, polarization at the Cr site must switch from field antiparallel to field parallel around 180 K, as thermal energy overcomes AF interactions. At this T , however, the XMCD signal at the Cr L_3 edge is already zero within experimental error.



© T -dependent XMCD signal at 709.1 eV (Fe) and 577.5 eV (Cr) recorded on a monolayer of Fe_3Cr on Au(111) in a 50 kOe applied field (normalization carried out as described in the caption to Figure 2). Error bars have been omitted when smaller than the symbol size. Solid lines represent best-fit calculated curves with $J_{\text{Fe-Cr}} = 14.7 \text{ cm}^{-1}$.

CONCLUSIONS

Our findings show that the interaction with a gold surface fully preserves the spin structure of Fe_3Cr complexes. Superexchange interactions, as

determined by variable- T XMCD, compare well with bulk-phase values in both sign and strength, a rare situation for surface-supported polynuclear architectures [5].

DEIMOS beamline

ASSOCIATED PUBLICATION

On-surface magnetometry: the evaluation of superexchange coupling constants in surface-wired single-molecule magnets

E. Tancini, M. Mannini, Ph. Sainctavit, E. Otero, R. Sessoli, and A. Cornia*

Chemistry - A European Journal 19(50) (2013), 16902

CORRESPONDING AUTHOR

*Dipartimento di Scienze Chimiche e Geologiche & UdR INSTM, Università di Modena e Reggio Emilia, via G. Campi 183, 41125 Modena, Italy

acornia@unimore.it

REFERENCES

- [1] J. D. Rinehart et al. *J. Am. Chem. Soc.* 133 (2011), 14236
- [2] M. Misiorny et al. *Phys. Rev. Lett.* 111 (2013), 046603
- [3] M. Mannini et al. *Nat. Mater.* 8 (2009), 194
- [4] M. Mannini et al. *Nature* 468 (2010), 417.
- [5] V. Corradini et al. *Adv. Mater.* 25 (2013), 2816

Fluorescent nanoplatelets pile-up

Quantum nanoplatelets have recently been discovered and are under the scrutiny of a growing number of researchers due to their exceptional optical properties. We show that these colloidal nanoparticles stack one on top of each other upon addition of a polar solvent. A collective effect emerges from this self-assembly and a new optical line appears in the emission spectrum.

Bright nanoparticles

Quantum dots are semi-conducting nanoparticles which, due to quantum confinement, emit light at a tunable wavelength in the visible range. Discovered 25 years ago, these fascinating objects have drawn the attention of numerous research groups since they present significant enhanced properties as compared to classical

molecular fluorophores such as reduced photobleaching, finely tunable emission wavelength or the possibility to excite simultaneously quantum dots of different sizes. Meanwhile, applications taking advantage of these properties have come to reality and TV displays containing quantum dots will be sold to consumers next year.

Quantum platelets: shape matters

The first discovered quantum dots were spherical and the quantum confinement occurs in 3 dimensions. In 2008, CdSe nanoplatelets were discovered [1] and, since then, a growing interest has been dedicated to the solution synthesis of these two-dimensional nanoparticles. After purification, the nanoplatelets are coated with a layer of surfactant and can be dispersed in apolar organic solvents.

Importantly, their thickness can be controlled at the atomic level and it is possible to obtain a sample containing only platelets being 4, 5, 6 or 7 CdSe monolayers thick. These nanoplatelets exhibit original optical properties including narrow fluorescence emission, high fluorescence quantum yield, and ultrafast fluorescence lifetime [2].

Collective properties ahead?

If a single nanoparticle has a given physical property, bringing one or several other particles in close contact can lead to a coupling between them through various physical effects. Eventually, a new or enhanced property can emerge.

Hence, one has to take into account superstructures which can appear in solution or upon drying to assess correctly the relevant optical features of nano-objects.

Stacking

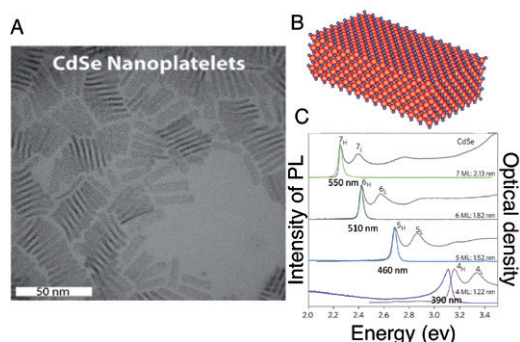
In the case of quantum platelets, we have shown using Small Angle X-ray Scattering (SAXS) performed on the SWING beamline that under certain experimental conditions, they stack one on top of each other to yield long nanoplatelet ribbons (figure 2). When dispersed in an organic solvent (such as hexane or toluene), solutions of CdSe nanoplatelets exhibit a monotonously decaying SAXS pattern characteristic of well-separated nano-objects. In contrast, when we add a more polar solvent to the dispersion (such as ethanol for example), intense Bragg peaks appear in the SAXS patterns. These peaks appear at scattering

vectors (q) values evenly spaced of q^* , $2q^*$, $3q^*$ where $q^*=1.233 \text{ nm}^{-1}$. This is characteristic of one dimension columnar assemblies of nanoparticles with an inter particle spacing of 5.1 nm. When a polar solvent is added, the increase in polarity favors the self-assembly of the platelets in such a way that the contact of the ligand with the solvent is minimal. Upon addition of ethanol the polymer chain of the ligand passes from good to bad solvent conditions and ligand/ligand interactions become energetically favored over ligand/solvent interactions.

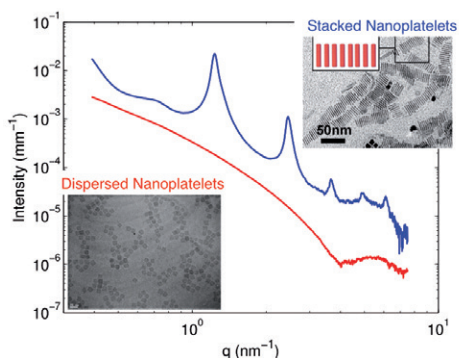
Phonon line emission revealed

This stacking has important consequences on the emission properties of the nanoplatelets (figure 3). While a unique peak is visible in the emission spectra of pure hexane dispersion, a low energy line emerges when an anti-solvent is added. A similar line is also visible when solutions are dried on a substrate. In order to unravel the physical mechanism at play for the emergence of this low-energy peak, advanced spectroscopy experiments have been performed. They

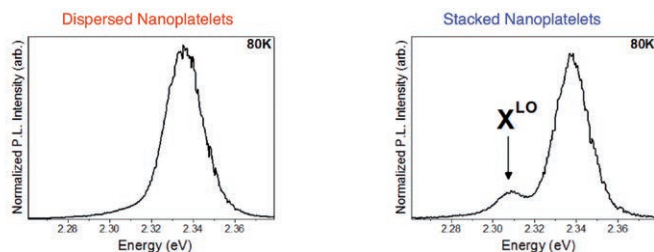
showed that this band could be attributed to the longitudinal optical (LO) phonon replica of the band-edge exciton. The appearance of the band in self-assembled nanoplatelets is explained using a model based on an efficient photon reabsorption between neighboring nanoplatelets. These findings could have potential applications in optoelectronics devices such as lasers based on the confined mode of this phonon replica.



1 A) TEM image of CdSe nanoplatelets. B) Schematic representation. C) Thickness dependent optical properties of nanoplatelets.



2 SAXS patterns of dispersed and stacked nanoplatelets acquired on the SWING beam line.



3 Emission spectra at 80K of dispersed and stacked nanoplatelets in solution.

SWING beamline

ASSOCIATED PUBLICATION

Phonon Line Emission Revealed by Self-Assembly of Colloidal Nanoplatelets

M.D. Tessier, L. Biadala, C. Bouet, S. Ithurria, B. Abecassis, and B. Dubertret

ACS Nano 7(4) (2013) 3332

CORRESPONDING AUTHOR

Laboratoire de Physique des Solides, Bât 510, Université Paris-Sud, 91405 Orsay, France

benjamin.abecassis@u-psud.fr

REFERENCES

- [1] S. Ithurria & B. Dubertret, J. Am. Chem. Soc. 130 (2008), 16504
- [2] S. Ithurria et al. Nat. Mater. 10 (2011), 936

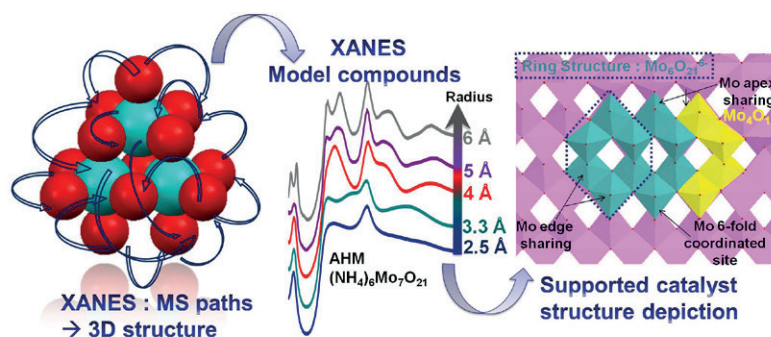
Coupling XANES and DFT calculations to unravel the structure of heterogeneous catalysts

Supported molybdenum catalysts are widely used in their sulfide state in the treatment petroleum fractions, which are important economic and environmental issues. In their oxide states they can be used in the partial oxidation of ethanol and methanol. We have used X-ray absorption spectroscopy on SAMBA coupled with DFT calculations to better understand, on a molecular level, the structure of the active phase of these catalysts and how it interacts with the support. The long-term aim is to improve the catalytic performance of this type of material.

Introduction

Catalysis is one of the fundamental pillars of our modern industry since the products manufactured through catalysis processes account for 10-15% of the gross national products of industrialized countries. The large majority of this production (up to 80%) is obtained through the heterogeneous catalysis. Improving heterogeneous catalysts is thus the heart of numerous academic and industrial research centers. Supported molybdenum oxides are widely used in heterogeneous catalysis field for numerous purposes [1]. However, a molecular-scale understanding of active phase structure of supported oxomolybdate species formed on the activated catalyst is still lacking even though it has been extensively characterized by various spectroscopies (XAS, RAMAN, XPS, NMR). This identification is a challenge which will permit a rational design of this class of catalysts. Among possible techniques, XAS [2] is very well suited to characterize

catalysts at a molecular level as it is an element-selective spectroscopy, probing both the electronic state of the absorbing element and its local environment. Although EXAFS is often used, XANES is also known to be very sensitive to the environment around the absorber atom. In addition, as the amplitude of XANES spectra is proportional to the density of unoccupied states, it can be regarded as a true probe of the electronic structure around the absorber atom. XANES being highly dependent of electronic parameters as the oxidation state or the hybridization between atomic orbitals, its interpretation is not as straightforward as EXAFS. Nevertheless, it is possible to get more relevant interpretation of spectra by calculation of XANES transitions within the multiple scattering (MS) theory [3]. Its use for simulation of XANES spectra of supported catalyst, allow us a molecular-scale identification of the structure of the active phase.



1 Illustration of the multiple scattering process (left) together with evolution of the calculated spectra of a reference compound as a function of the radius of calculation (center). Finally, the obtained supported phase is presented (right).

Results

Our approach has consisted first in the simulation of the XANES of models compounds (MoO_3 , $(\text{NH}_4)_6[\text{Mo}_7\text{O}_{24}]$, $(\text{NH}_4)_6[\text{Al}(\text{OH})_6\text{Mo}_6\text{O}_{18}]$, $(\text{NH}_4)_4[\text{Mo}_8\text{O}_{26}]$, Na_2MoO_4 , ...) in order to assign every spectroscopic fingerprint to a given structural property. We identify then the same spectroscopic fingerprints for the references compounds on a supported catalyst which allows us to formulate appropriate hypotheses on the active phase structure that will then be optimized by DFT calculations.

The preliminary investigation of XANES spectra of models compounds shows that XANES spectrum of catalyst exhibits similar characteristics of polyoxoanions compounds which indicate that the supported catalyst phase contains polymeric octahedral Mo. Furthermore, the use of XANES, allows us to probe oxygen atoms located in the second coordination shell. This feature clearly could not be possible using EXAFS, accounting on the low atomic number of oxygen. Based on these findings

Conclusion

Coupling XANES and DFT simulations for the heterogeneous catalyst characterization can be very powerful and that simulation of the XANES spectra allows a better relationship between the spectral features and the structure of the absorbing element.

and the characteristics of the catalyst's experimental spectrum, rational structures of Mo species adsorbed on (101) TiO_2 surface were generated by DFT calculations and their corresponding XANES spectra were calculated by XANES modeling. Comparison of experimental and calculated spectra (Figure 1) provide us unprecedented insights into the adsorption modes of Mo species on the titanium surface which finally bring to the light that the active site structure is derived from the Anderson one : $\{[\text{Mo}_{14}\text{O}_{45}, \text{n}, \text{Mo}_4\text{O}_{12}]^{6-}, 6, (\text{HO}-\text{TiO}_2)^+\}$, (Figure 1right). The structure of the active site established during this work favorably interacts with the surface of the support on account of the correspondence between the surface structure of the support and the adsorbed ion. This result thus showed the important role played by the oxide support in the genesis of the oxomolybdate phase, where the speciation of molybdenum depends strongly on the structure of the oxide surface, which directly controls the way the MoO_6 octahedral are arranged.

SAMBA beamline

ASSOCIATED PUBLICATION

Synergy between XANES spectroscopy and DFT calculation to reveal molecular-scale structure of heterogeneous catalysts: TiO_2 -Supported Molybdenum Oxide catalysts case

A. Tougeri, E. Berrier, A.S. Mamede, C. La Fontaine, V. Briois, Y. Joly, E. Payen, J-F. Paul, and S. Cristol*

Angewandte Chemie International Edition 52(25) (2013) 6440

CORRESPONDING AUTHOR

*Unité de Catalyse et de Chimie du Solide, Université Lille 1, UMR CNRS 8181, Cité Scientifique, 59655 Villeneuve d'Ascq Cedex, France

sylvain.cristol@univ-lille1.fr

REFERENCES

- [1] J. L. G. Fierro & J. C. Mol, in Metal Oxides: Chemistry and Applications; (Eds: Fierro, J. L. G.), TAYLOR & FRANCIS, Boca Raton. 2006 517; H. Thoulhoat & P. Raybaud in Catalysis by transitions metal sulfides, IFP Energies nouvelles publications TECHNIP 2013
- [2] V. Briois et al. Proceedings of UVX 2010, EDP Science 41 (2011)
- [3] Y. Joly, Phys. Rev. B . 63 (2001), 125120



BIOLOGY AND HEALTH SCIENCES

- 54** Polymorphic and amyloid natures of neuronal inclusions of Huntington's disease brain revealed by IR microspectroscopy
- 56** Characterization of hydrophobic peptides by photoionization Mass Spectrometry
- 58** MAN1 at the nuclear envelope blocks TGF- β signaling by stimulating dephosphorylation of the Smad transcription factors
- 60** Synchrotron radiation - tandem mass spectrometry for proteomic and structural biology
- 62** Atomic structure of 14-subunit RNA polymerase I: insight into ribosomal RNA synthesis
- 64** The novel RNase P in action
- 66** The function of translation initiation factor IF2 analyzed by an integrated structural biology approach
- 68** Crystal structure of the crystallographer MamP

BIOLOGY AND HEALTH SCIENCES

One of SOLEIL's objectives in biology and health is to continue joint development projects between the beamlines, to offer increasingly integrated approaches and covering issues relevant to users' needs.

A first "molecular" approach, integrates high-resolution macromolecular crystallography data with data obtained at lower resolution using SAXS, SRCD and MS on dynamic systems. The increasing number of publications with data acquired on several beamlines shows the success of this approach (for example Siponen et al., Bourgeois et al., Gobert et al.).

A second "organism-orientated" approach links all multimodal imaging available at SOLEIL from chemical imaging with a resolution of a few microns in the infrared (André et al.) to X-ray elemental imaging on a nanoscale, via resolutions of about 100 nm in the far UV. This "correlative imaging" approach is strongly supported by internal developments guaranteeing the localization of samples from one microscope to the next and the combination and analysis of varying multi-scale data.

Following on from PROXIMA 1, automatic sample changing equipment has now come into operation on PROXIMA 2 for crystal samples, and on the DISCO and SWING beamlines for biomolecular solutions. These systems make experimentation much more convenient in the case where significant sample to sample variation is observed. In addition the provision of automatic sample changers couple with the increased reliability of sources and beamlines, each one now having a dedicated engineer, has led to a rise in the number of industrial projects carried out on the biology beamlines.

Unique developments at SOLEIL now make it possible to analyze interactions between a polyproline-rich protein and its ligand, leading to molecular decryption of the sensation of astringency (Canon et al.).

Thanks to the coupling between a mass spectrometer and SOLEIL ultraviolet radiation, it was also possible to characterize the transmembrane fragments of membrane proteins in their extraction detergent (Bagag et al.).

We hope to continue in our advances with you in the coming years.

Matthieu Réfrégiers

Head of the "Biology and Health Sciences" Scientific Section

BIOLOGIE ET SCIENCES DE LA SANTÉ

L'un des objectifs de SOLEIL en biologie et santé est de continuer les développements conjoints entre les lignes, afin de proposer des approches intégratives toujours plus fournies et en résonance avec les problématiques des utilisateurs.

Une première approche, moléculaire, intègre les données à haute résolution de la cristallographie macromoléculaire avec des données obtenues à plus basse résolution en SAXS, SRCD et MS sur des systèmes dynamiques. L'augmentation du nombre de publications avec des données acquises sur plusieurs lignes démontre le succès de cette démarche (par exemple Siponen et al., Bourgeois et al., Gobert et al.).

Une deuxième approche, orientée « organisme », relie toutes les imageries multimodales disponibles à SOLEIL, depuis l'imagerie chimique avec une résolution de quelques microns dans l'infrarouge (André et al.), à l'imagerie élémentaire à une résolution nanométrique dans les rayons X, en passant par une résolution d'environ 100 nm dans l'UV lointain. Cette approche d'« imagerie corrélative » est fortement soutenue par les développements internes permettant de garantir la localisation d'échantillons d'un microscope à l'autre et la combinaison et l'analyse des données variées et multi-échelles.

Après PROXIMA 1, l'automatisation du passage d'échantillon démarre sur la ligne PROXIMA 2 pour les cristaux, et les lignes DISCO et SWING, pour les solutions de biomolécules. Ces systèmes facilitent beaucoup l'expérimentation lorsque des variations significatives sont observées entre échantillons. De plus, la mise à disposition de tels automates couplée à la fiabilité croissante des sources et des lignes de lumière, ainsi que l'accompagnement des lignes par un ingénieur dédié, a conduit à une montée en puissance du nombre de projets industriels accueillis sur les lignes de biologie.

Des développements uniques à SOLEIL ont par ailleurs permis d'analyser les interactions entre une protéine riche en polyprolines et son ligand, conduisant au décryptage moléculaire de la sensation d'astringence (Canon et al.).

Grâce au couplage entre un spectromètre de masse et les ultraviolets de SOLEIL, il a également été possible de caractériser les fragments transmembranaires de protéines membranaires dans leur détergent d'extraction (Bagag et al.).

Nous espérons poursuivre, avec vous, ces efforts dans les années qui viennent.

Matthieu Réfrégiers

Responsable de la Section Scientifique « Biologie et Sciences de la Santé »

Polymorphic and amyloid natures of neuronal inclusions of Huntington's disease brain revealed by IR microspectroscopy

Huntington's disease (HD) is a neurodegenerative disease characterized by the formation of protein aggregates in certain regions of the brain; some of these aggregates can reach microscopic size (inclusions). Studies in cells and animals have shown that aggregates are polymorphic and that their secondary structure is likely to condition their toxicity [1]. However, the secondary structure of proteins in the inclusions found in the brain of patients is still unknown. We show by using synchrotron Fourier-transform infrared microspectroscopy (sFTIR), that the brain of HD patients contains structurally different inclusions, some of which are amyloid. As one category of amyloid inclusions is characteristic of severely affected brain regions, it may be particularly toxic to neurons.

Introduction

HD results from a mutation in a gene encoding a protein called huntingtin [2]. Huntingtin contains a chain of 20-35 consecutive glutamines in healthy individuals, whereas this chain is expanded from 36 to 65 glutamines in patients with the adult form of HD and exceeds 65 residues in those with the much rarer and more severe juvenile form. The disease is mainly characterized by a progressive destruction of the striatum and also to a lesser extent of the cortex [3], and by the formation, in these regions,

of inclusions [4] (Fig. 1). Inclusions are located mostly in the cell cytoplasm (Cis) in adult cases and in the cell nuclei (Nis) in juvenile cases. Thanks to the high-sensitivity and the high-resolution provided by the synchrotron source, we have analyzed by sFTIR the structural nature of inclusions *in situ* in post-mortem brain of patients affected by HD. We have investigated the protein secondary structure of Cis and Nis present in the cortex and the striatum of adult as well as of juvenile HD cases.

Cytoplasmic inclusions in adult HD cases have different amyloid structures in cortex and striatum

We acquired IR spectra from Cis and from inclusion-free cytoplasm (as controls) of five adult HD cases. Differences between spectra were then studied by average second derivative spectra and principal component analysis. We found that cortical and striatal Cis display increased contributions of peaks at 1627, 1681 and 1693 cm^{-1} , all indicating β -sheet enrichment (Fig. 2). The 1627 cm^{-1} peak is also a signature of the amyloid nature

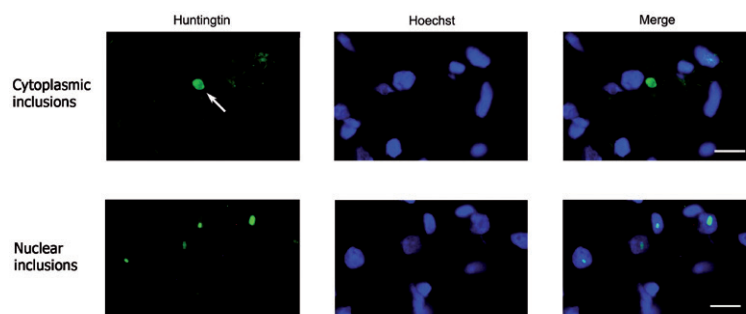
of these inclusions [3]. We showed that striatal Cis differ from cortical Cis by the presence of an additional component at 1639 cm^{-1} , assigned to " β -sheet/unordered" structures.

We photographed areas encompassing fluorescently labeled Cis and generated chemical maps representing the β -sheet/ β -helix ratio. The immunolabeled area and the area with the highest β -sheet/ α -helix ratio were clearly superimposable (Fig. 3).

Cytoplasmic inclusions in juvenile HD cases constitute amorphous aggregates

We discovered that Cis in juvenile HD cases did not differ appreciably from the surrounding cytoplasm, whether

in the cortex or the striatum (Fig. 2). Therefore, they constitute amorphous, non-amyloid protein aggregates.



1 Images of fluorescently labeled inclusions in HD brain showing one cytoplasmic inclusion (upper panels) and numerous smaller nuclear inclusions (lower panels).

Nuclear inclusions in juvenile HD cases possess an amyloid structure resembling that of striatal cytoplasmic inclusions in adult cases

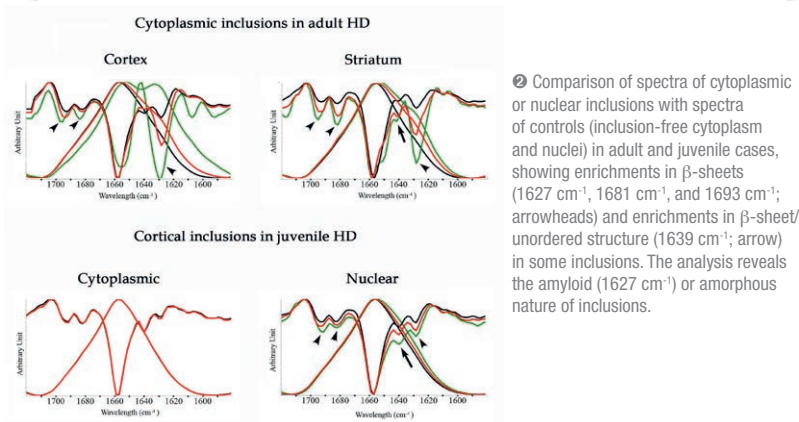
We collected spectra centered on Nis and nuclei without inclusions (as controls) in the cortex and striatum of three juvenile HD cases. We demonstrated enrichment in β -sheets (1627, 1681 and 1693 cm^{-1}) in this category of inclusions (Fig. 2). Because

one of the main contributions was at 1627 cm^{-1} , we conclude that juvenile Nis are amyloid. We also observed that they shared with adult Cis of striatum, but not those of cortex, the β -sheet/unordered enrichment in the component at 1639 cm^{-1} .

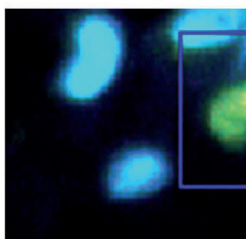
Conclusion

Our results show the structural polymorphism of inclusions in HD brain. We propose that the inclusions lacking any structural rearrangement constitute nontoxic amorphous aggregates, whereas the amyloid inclusions enriched in both

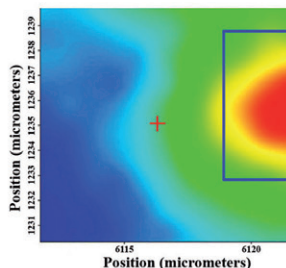
β -sheet and β -sheet/unordered are highly neurotoxic, as they are always associated with the most severe form of the disease and found in the most affected brain regions.



Immunofluorescence labeling



Chemical map showing β -sheet/ α -helix content



Comparison of the immunofluorescence labeling and the chemical mapping of an area containing an amyloid inclusion, showing the correspondence between the inclusion (green, left panel) and the area with the highest β -sheet content (red, right panel).

SMIS beamline

ASSOCIATED PUBLICATION

Structure of inclusions of Huntington's disease brain revealed by synchrotron infrared microspectroscopy : polymorphism and relevance to cytotoxicity

W. André, C. Sandt, P. Dumas, P. Djian and G. Hoffner*

Analytical Chemistry 85(7) (2013), 3765

CORRESPONDING AUTHOR

* Laboratoire de Physiologie Cérébrale, UMR 8118, Université Paris Descartes, 45 rue des Saints-Pères, 75006 Paris, France.

guylaine.hoffner@parisdescartes.fr

REFERENCES

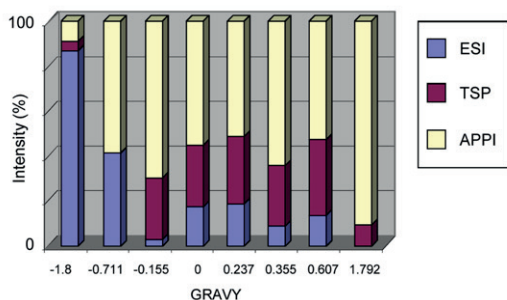
- [1] Nekooki-Machida et al. Proc Natl Acad Sci U S A 106 (2009), 9679
- [2] The Huntington's Disease Collaborative Research Group. Cell 72 (1993), 971
- [3] J. Vonsattel et al. J Neuropathol Exp Neurol. 44 (1985), 559
- [4] M. DiFiglia et al. Science. 277 (1997), 1990
- [5] Nilsson, MR. Methods, 34 (2004), 151

Characterization of hydrophobic peptides by photoionization Mass Spectrometry

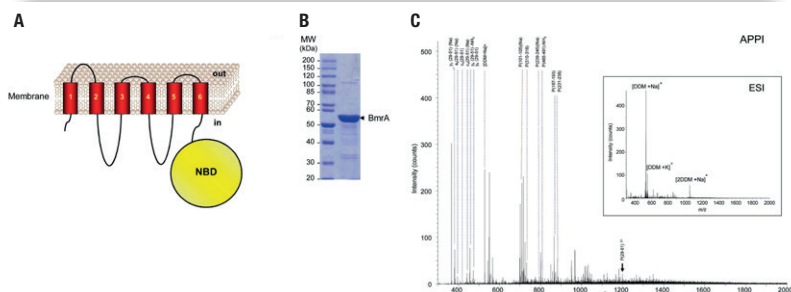
Characterization of membrane proteins is a challenging task owing to the presence of detergent necessary to extract them. These compounds are poorly compatible with classical ionization methods used in mass spectrometry. Here, the potential of atmospheric pressure photoionization (APPI) for mass spectrometric analysis of membrane peptide and proteins has been investigated and compared to classical ionization methods. APPI allowed many peptides distributed along the sequence of the protein to be detected, in contrast to electrospray ionization, which suffered greatly from the presence of detergents.

Membrane proteins, which represent about one-third of the genome [1], possess a key role in cellular functions such as cell adhesion, signal transduction, molecular transport, endocytosis and trafficking. Thus, this class of protein exhibits a high potential for characterizing new biological markers or targets for therapeutics [2]. In spite of its importance, the membrane proteome has not been explored in depth yet, owing to important challenges pertaining to the characterization of membrane proteins. The major issue in studies on membrane proteins resides in their high hydrophobicity, which requires use of detergent and surfactant for their extraction and solubilization. The intrinsic hydrophobicity of membrane proteins added with the presence of detergents in membrane preparations remains important limitations in further proteomic and mass spectrometry analysis. In the present work, potential of an alternative ionization method, based on photoionization has been investigated. Atmospheric pressure photoionization (APPI) has been coupled with synchrotron radiation on the DISCO beamline [3, 4]. We focused on the tetraspanin CD9 and the multidrug transporter BmrA. A set of peptides from CD9, exhibiting a broad range of hydrophobicity, was investigated using APPI and compared to electrospray ionization (ESI)

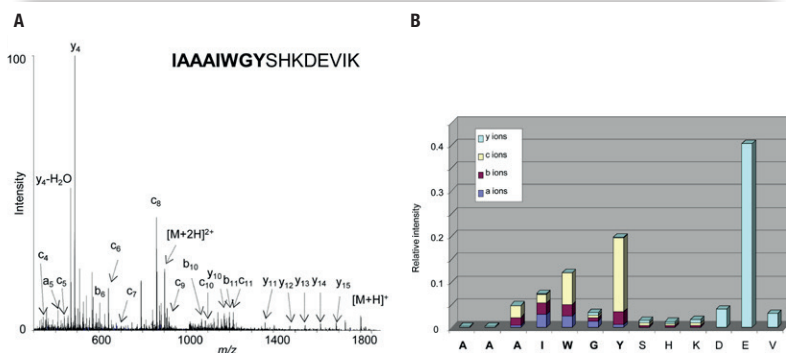
It appeared, see figure 1, that most hydrophobic peptides were hardly ionized by ESI whereas all peptides, including the highly hydrophobic one that corresponds to the full sequence of the first transmembrane domain of CD9, were easily ionized by APPI. The native protein BmrA purified in the presence of the non-ionic detergent beta-D-dodecyl maltoside (DDM) was digested in-solution using trypsin. The resulting peptides were investigated by flow injection analysis of the mixture followed by mass spectrometry. As seen in figure 2, upon ESI, only detergent ions were detected and the ionic signals from the peptides were totally suppressed. In contrast, APPI allowed many peptides distributed along the sequence of the protein to be detected. Furthermore, the parent ion corresponding to the first transmembrane domain of the protein BmrA was detected under APPI conditions. Careful examination of the APPI mass spectrum revealed a-, b-, c- and y- fragment ions generated by in-source fragmentation, see figure 3. Those fragment ions allowed unambiguous structural characterization of the juxtamembrane peptide. In conclusion, APPI-MS appears as a versatile method allowing the ionization and fragmentation of hydrophobic peptides in the presence of detergent.



① Ionization efficiency of peptides as a function of their hydrophobicity (as indicated by their GRAVY index) using three different ionization techniques: Electrospray (ESI), thermospray (TSP) and atmospheric pressure photoionization (APPI).



② (A) Topology of the protein BmrA exhibiting six transmembrane domains and a nucleotide binding domain (NBD). (B) The purified protein was loaded on a gel and stained using Coomassie blue. (C) Mass spectrometry analysis after in-solution digestion of the protein BmrA under ESI or APPI conditions. The precursor ion m/z 1198.75 corresponding to the first transmembrane domain is labelled with a black arrow.



③ (A) In-source fragmentation of a juxtamembrane peptide under APPI. (B) The abundances of each a-, b-, c- and y- sequence ions were plotted as a function of the peptide sequence.

DISCO beamline

ASSOCIATED PUBLICATION

A. Bagag, J.-M. Jault, N. Sidahmed-Adrar, M. Réfrégiers, Alexandre Giuliani* and F. Le Naour

PLoS ONE 8 (2013) e79033

CORRESPONDING AUTHOR

*Synchrotron SOLEIL, l'Orme des Merisiers, St Aubin BP48, 91192 Gif sur Yvette Cedex, France & INRA, UAR 1008 CEPIA, Nantes, France

alexandre.giuliani@synchrotron-soleil.fr

REFERENCES

- [1] T.J. Stevens & I.T. Arkin, *Proteins* 39 (2000), 417
- [2] S. Tan S et al. *Proteomics* 2008 8: 3924
- [3] A. Giuliani et al. *Nucl. Instrum. Methods Phys. Res. B* 279 (2012), 114
- [4] A. Giuliani et al. *J Synchrotron Radiat.* 16 (2009), 835

MAN1 at the nuclear envelope blocks TGF- β signaling by stimulating dephosphorylation of the Smad transcription factors

Stopping the signal at the inner nuclear envelope. Activation of cell-surface receptors for transforming growth factor β (TGF- β) results in changes in gene expression mediated by the transcription factors Smad2 and Smad3. Bourgeois et al. examined how the nuclear membrane protein MAN1 inhibits TGF- β signaling. Modeling from NMR and SAXS data, biochemical assays, and cellular assays revealed that MAN1 prevented Smad2 and Smad3 from binding to purified and cellular transcription factor FAST1 and to cellular Smad4, the latter of which promotes transcription regulation by Smad2 and Smad3. In addition, *in vitro* assays indicated that MAN1 could facilitate the dephosphorylation and inactivation of Smad2 and Smad3 by the phosphatase PPM1A. These results contribute to explain why individuals deficient in the gene encoding MAN1 have developmental defects suggestive of aberrant TGF- β signaling.

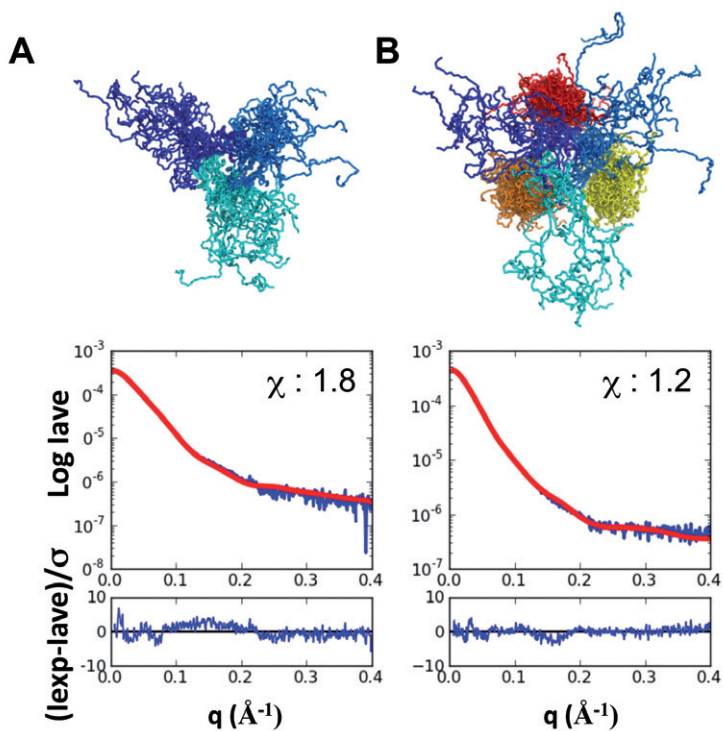


In the metazoan cell, the genome is protected by a double membrane rich in proteins called the nuclear envelope. Increasing evidences indicate that the inner nuclear envelope modulates gene expression by recruiting histone modifying enzymes and sequestering transcription factors (1). This essential functional role is supported by the large number of mutations causing diseases found in inner nuclear membrane proteins that impact cell differentiation, tissue development and aging (2,3).

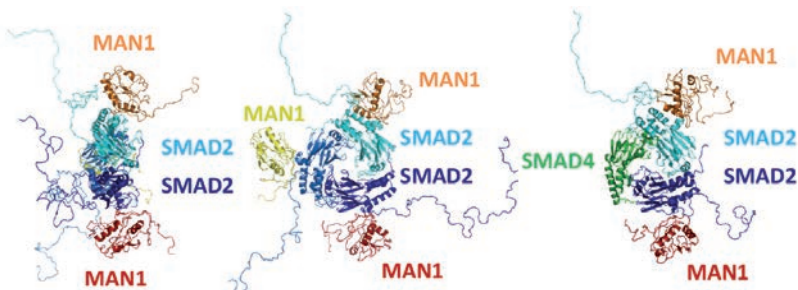
The Laboratory of Structural Biology and Radiobiology at CEA Saclay has used Nuclear Magnetic Resonance (NMR), Small Angle X-ray Scattering (SAXS) and Molecular Modeling to describe the 3D structure of several inner nuclear envelope protein fragments, often composed of globular domains linked by poorly structured polypeptide chains (see for example (4,5,6)). However, very few 3D structures of complexes involving inner nuclear protein regions are yet available.

Here, we report a model of the complex between the C-terminal region of the inner nuclear envelope protein MAN1 and the MH2 domain of the Smad2 transcription regulator. In order to calculate this model, the 3D structure of the MH2

domain of Smad2 was obtained by X-ray crystallography, the 3D structure of the Smad2 binding domain from MAN1 was calculated from NMR and SAXS data, and the relative position of the two domains in the complex was derived from biochemical identification of the residues at the interface and SAXS data on the global shape of the complex. From this model, we proposed mechanisms for the inhibition of the TGF- β signaling pathway by MAN1. In particular, our model suggested that when Smad2 is bound to MAN1, it can still bind to its essential coactivator Smad4. Interaction of MAN1 with the Smad2/Smad4 complex was confirmed *in vitro*. However, overexpression of MAN1 clearly inhibited the formation of the Smad2/Smad4 complex in cell. We showed that MAN1 overexpression led to dephosphorylation of Smad2 in cell, and it is known that dephosphorylated Smad2 cannot bind to Smad4. Finally, we showed *in vitro* that MAN1 binds to PPM1A, a phosphatase that dephosphorylates Smad2. Thus we propose that in cell, MAN1 recruits PPM1A, favors Smad2 dephosphorylation and inhibits the TGF- β signaling pathway. These results explain why patients showing genetic bone diseases due to a deletion of the Smad2 binding domain of MAN1 present aberrant TGF- β signaling.



● Models of the phosphomimetic Smad2 fragment either free (A) or in complex (B) with the MAN1 fragment obtained from SAXS data. In each panel, 20 models of the trimeric Smad2 fragment are superimposed (each monomer colored in a different shade of blue). In (B), a MAN1 fragment is bound to each Smad2 fragment (each MAN1 fragment colored in yellow, orange and red, respectively). Curves show the corresponding fit between the calculated SAXS intensity averaged on the 20 models (*I*_{ave}; red) and the experimental SAXS intensity (*I*_{exp}; blue). The chi values confirm that the deviations between the calculated and experimental intensities are close to the experimental error. The difference between the two intensities divided by the experimental error is also plotted as a function of the diffusion vector amplitude. In both panels, this difference is regularly distributed around 0 on the whole *q* interval, as expected for a random noise-like signal.



● Smad2 can simultaneously bind to MAN1 and Smad4. Two orthogonal views of a typical MAN1-Smad2 complex, and a view in which one of the Smad2 MH2 monomers was replaced by a Smad4 MH2 monomer.

SWING beamline

ASSOCIATED PUBLICATION

Inhibition of TGF- β signaling at the nuclear envelope: characterization of interactions between MAN1, Smad2 and 3, and PPM1A

B. Bourgeois, B. Gilquin, C. Tellier-Lebègue, C. Östlund, W. Wu, J. Pérez, P. El Hage, F. Lallemand, H. J. Worman and S. Zinn-Justin*
Sci Signal. 6(280):ra49 (2013)

CORRESPONDING AUTHOR

* Laboratoire de Biologie Structurale et Radiobiologie, CEA IBITECS & Université Paris Sud / CNRS UMR 8221, CEA Saclay Bât 144, 91190 Gif-sur-Yvette, France

sophie.zinn@cea.fr

REFERENCES

- [1] Arib & Akhtar, *Curr Opin Cell Biol* 23 (2011), 346
- [2] Towbin et al., *Trends Biochem Sci* 38 (2013), 356
- [3] Worman & Bonne, *Exp Cell Res* 313 (2007), 2121
- [4] Krimm et al., *Structure* 10 (2002), 811
- [5] Caputo et al., *J Biol Chem* 2006 281, 18208
- [6] Kondé et al., *Biochemistry* 49 (2010), 8020

Synchrotron radiation - tandem mass spectrometry for proteomic and structural biology

We introduce a method based upon the coupling of mass spectrometry and VUV-synchrotron radiation for biological investigations. This new approach provides information both on the primary structure of full proteins and on the localization of their noncovalent binding sites. This new methodology has been developed through the study of a human intrinsically disordered protein, namely IB5, and its noncovalent interactions with the tannin procyanidin B2 3'OG.



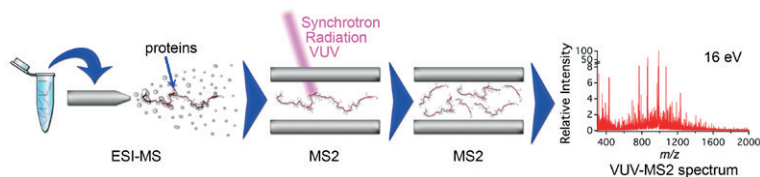
An important part of the proteome is composed of functional proteins that lack ordered structure, under physiological conditions [1]. The peculiar structures and conformations of these proteins, referred to as intrinsically disordered protein (IDP), enable them to fulfill an important repertoire of vital biological functions. Some IDPs have the ability to bind to different and/or several partners, thus producing protein-ligand complexes with distributions of stoichiometries and conformations [2]. Investigations on such systems by classical high-resolution structural methods remain extremely challenging if not intractable, owing the flexibility and the heterogeneity of the coexisting objects. In contrast, the unique ability offered by mass spectrometry to manipulate *m/z* resolved species reveals a clear advantage when dealing with such biological objects [2]. Tandem mass spectrometry (MS2) is a widely used method in structural biology in order to determine the sequence of biopolymers, such as proteins, DNAs, oligosaccharides... In MS2, an ion of interest is isolated, activated, and brought to dissociation. The analysis of the generated fragments provides structural information on the precursor ion. Recently, synchrotron radiation (SR) has been introduced as a new activation technique for MS2 [3].

In the present work, the potential of VUV-SR to provide structural information is probed through the study of a human IDP, namely IB5 [4]. The only described function of this salivary proline-rich protein (PRP) is to bind and scavenge tannins. However, the binding site of tannins on IB5 has never been precisely determined.

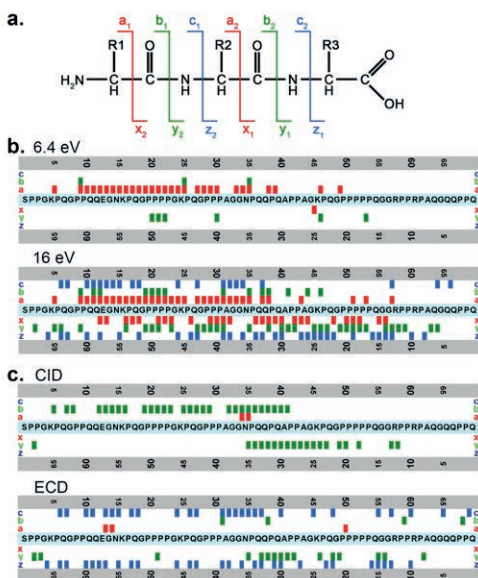
The coupling of an ion trap with the DESIRS beamline shows that SR provides an easy access to a wide variety of photon activations regimes, ranging from photodissociation (PD) to dissociative photoionization (DPI) (figure 1).

The sequence coverage of IB5, obtained in DPI regime, was higher than with classical activation techniques (figure 2). It makes SR-MS2 an efficient sequencing method. Moreover, DPI has allowed for the first time to determine the binding site of the tannin, B2 3'OG, on IB5 (figure 3). The comparison between the IB5⁷⁺ and IB5•B2 3'OG⁷⁺ MS2 spectra obtained at 16 eV has allowed to identify and interpret more than fifty peaks as fragments of IB5 noncovalently bound to B2 3'OG. It appears that all these fragments from both N- and C-terminal series contain the KPQGPPPPQGG segment of the sequence, indicating a strong interaction between B2 3'OG and this part of the protein. This sequence with a cluster of five prolines very likely adopts a PPI or a PPII helix conformation in solution. Such structural elements are thought to be crucial for IDPs in the binding with their partner, as this stable segment might provide an initial contact point. The role of the proline clusters in PRPs sequence, which were thought to be the tannin-binding site on PRP, is thus unequivocally confirmed.

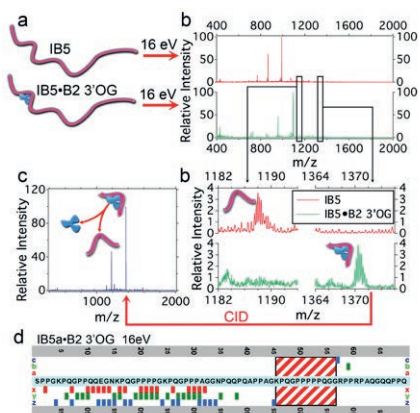
Therefore, this new method should open new perspectives in the growing and challenging fields of proteomics, structural biology and IDPs studies.



1 Diagram of the MS/MS technique based on activation by VUV synchrotron radiation.



2 Nomenclature for MS/MS peptide fragmentation (a). Patterns of IB5⁷⁺ protein fragmentation after activation at 6.4 and 16 eV (b), by CID and ECD (c).



3 Localization of the B2 3'OG binding site on IB5. The objects IB5⁷⁺ and IB5•B2 3'OG⁷⁺ were selected and irradiated with 16 eV photons (a). Comparison of the MS/MS 16 eV VUV spectra identified specific fragments in the IB5•B2 3'OG⁷⁺ fragmentation spectrum in which the m/z ratio had a mass difference corresponding to that of B2 3'OG⁷⁺ compared with fragments from the fragmentation spectrum of IB5⁷⁺ (b). CID activation of identified fragments confirmed the presence of the ligand (c). The map of B2 3'OG-carrying fragments identified the 'KPQGP PPPPGG' sequence as a B2 3'OG binding site on IB5.

DESIRS & DISCO beamlines

ASSOCIATED PUBLICATION

Photodissociation and dissociative photoionization mass spectrometry of proteins and noncovalent protein–ligand complexes

F. Canon*, A. R. Milosavljević, G. van der Rest, M. Réfrégiers, L. Nahon, P. Sarni-Manchado, V. Cheynier, and A. Giuliani

Angewandte Chemie International Edition 52(32) (2013) 8377

CORRESPONDING AUTHOR

* INRA, UMR1324 Centre des Sciences du Goût et de l'Alimentation, 21000 Dijon, France

francis.canon@dijon.inra.fr

REFERENCES

- [1] A. K. Dunker et al. *Curr. Opin. Struct. Biol.* 18 (2008), 756
- [2] F. Canon et al. *Am. Chem. Soc.* 133 (2011), 7847
- [3] A. R. Milosavljevic et al. *J. Sync. Rad.* 19 (2012), 174
- [4] F. Canon et al. *A. Angew. Chem. Int. Ed.* 52 (2013), 8377

Atomic structure of 14-subunit RNA polymerase I: insight into ribosomal RNA synthesis

We have determined the first crystallographic structure of RNA polymerase I, a large and complex enzyme responsible for one of the fundamental mechanisms of all eukaryotic cells. This work was conducted in a collaboration between Christoph Müller's team at the European Molecular Biology Laboratory (EMBL) in Heidelberg, Carlos Fernández-Tornero's lab at the Centro de Investigaciones Biológicas in Madrid, and researchers from the University of Göttingen and SOLEIL synchrotron, where some of the structural data was obtained. Structural data was also obtained at the Petra III ring at EMBL Hamburg.



Although first life forms are thought to have been initiated exclusively by RNA molecules, all known living organisms on earth are now relying on three specialized molecule types to build up their core machinery: DNA, RNA and proteins. RNA molecules are synthesized from DNA templates by RNA polymerases. There are three different RNA polymerases in eukaryotes (such as animals, plants, fungi) nucleus that are each specifically regulated and devoted to synthesize dedicated RNA molecules. All are multisubunit complexes. RNA polymerase II (Pol II) makes a precursor of messenger RNA that carries genome information to ribosomes to make proteins. RNA polymerases I (Pol I) and III make parts of the machinery which reads that messenger RNA: Pol I builds the RNA that will eventually be built into the ribosome (rRNA), while Pol III makes the transfer RNA (tRNA) that carries the protein building blocks to the ribosome. While the crystallographic structure of Pol II – the most studied type – is known since 2001 [1], obtaining detailed information on the structures of Pol I has proven extremely difficult. Part of the difficulty is that Pol I is bigger (590 versus 550 kDa) and contains more subunits (14 versus 12) than Pol II.

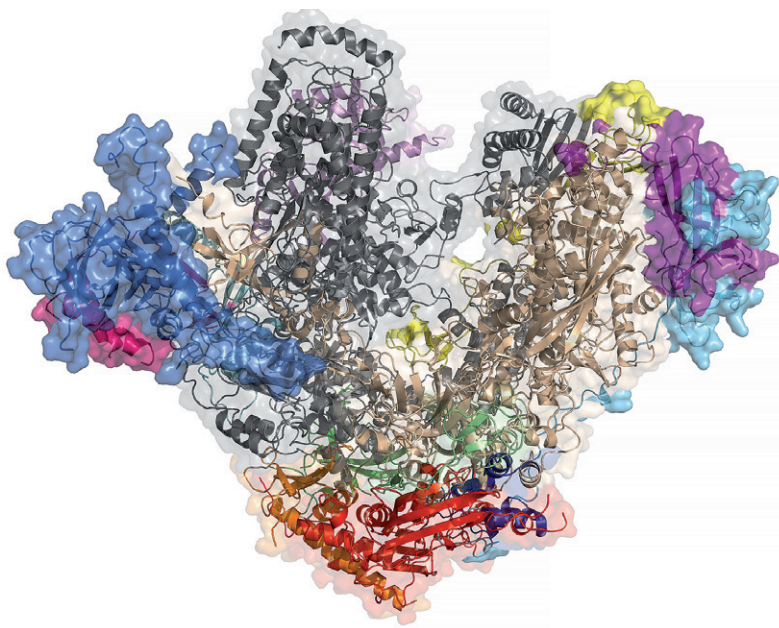
While the overall architecture and horseshoe shape of Pol I is similar to that of Pol II, this new structure reveals some important insight that helps to understand some of its specific features, like its high productivity: its product, rRNA, being the most abundant RNA in eukaryotic cells.

To achieve this high synthesis rates, we have found that the Pol I A12.2 subunit contains a domain that is remarkably similar to TFIIIS, a separate protein that Pol II transiently recruits in case of transcription pauses or to cleave wrongly

synthesized RNA. Achieving the same function through a permanently integrated factor allows Pol I to avoid long arrests and thus to achieve higher transcription rates. In another part of the molecule, a simple pivoting of the A43-A14 subcomplex could be sufficient to switch between active or inactive conformation of Pol I, whereas in the Pol II case the functional equivalent subcomplex (Rpb4-Rpb7) forms a more detachable element. Two other specific subunits (A49-A34.5, equivalent to TFIIIF) form a tight complex anchored onto Pol I by what looks like two extended arms, one contributed by each supplementary subunit (see figure 1). The interaction of this subcomplex with part of A12.2 explains its positive effect on A12.2 dependent RNA cleavage.

All these differences suggest that eukaryotic cells have fewer ways of controlling Pol I's activity, since they cannot influence it by regulating the availability of helper proteins as it is the case for RNA polymerase II. This is where another finding becomes interesting: One specific feature of Pol I discovered in this structure is what we have called the "DNA-mimicking loop", an extended conserved loop that occupies the position of transcribed DNA in the enzyme's cleft, close to the active site. This could be a built-in regulatory mechanism: its positioning could promote or inhibit the enzymatic activity.

Together, these findings can help to explain why this enzyme works faster than its Pol II counterpart: rather than relying on certain external components or rearrangements, Pol I has them already integrated, which also explains why it is bigger, and less regulated, but at the same time more efficient.



Structure of the 14 subunits, 590-kilodalton RNA polymerase I. Submodule A12.2 is represented in yellow, A49-A34.5 in purple-light blue and A43-A14 in marine-pink.

PROXIMA1 beamline

ASSOCIATED PUBLICATION

Crystal structure of the 14-subunit RNA polymerase I

C. Fernández-Tornero*, M. Moreno-Morcillo, U.J. Rashid, N.M.I. Taylor, F.M. Ruiz, T. Gruene, P. Legrand, U. Steuerwald and C.W. Müller

Nature, 502(7473) (2013), 644

CORRESPONDING AUTHOR

* Centro de Investigaciones Biológicas, Consejo Superior de Investigaciones Científicas, Ramiro de Maeztu 9, 28040 Madrid, Spain.

cftornero@cib.csic.es

REFERENCE

[1] P. Cramer et al. Science 292 (2001), 1863

The novel RNase P in action

A novel type of RNase P was recently identified which is totally deprived of catalytic RNA. This proteinaceous RNase P (or PRORP) is found in the organelles of many eukaryotes and in the nucleus of some eukaryotes including plants. In order to characterize the architecture of PRORP enzymes and to determine how they bind to pre-tRNAs to perform their 5' maturation we combined biochemical and biophysical approaches. The resulting model of a functional PRORP:substrate complex suggests a tRNA recognition mode similar to that of the ribonucleoprotein RNase P.

5' tRNA maturation in mitochondria

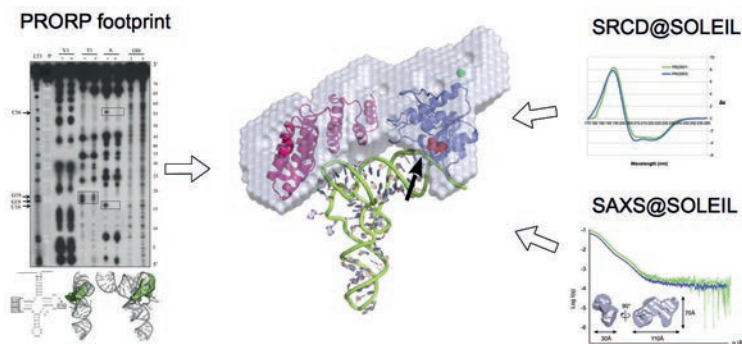
Transfer RNAs (tRNAs) are key actors of protein synthesis: they play the role of adapter molecules during the translation of messenger RNAs by the ribosome into protein sequences. They are produced as precursors with leading and trailing sequences that need to be processed. Their 5' maturation is catalyzed by a ubiquitous enzyme called RNase P. Until recently all known RNase P were ribonucleoproteins, the catalytic activity of the enzyme being held by an RNA molecule. In 2008, a new type of RNase P only composed of proteins was identified in human mitochondria [1] that corresponds to a novel family of nucleases called PRORP for "Proteinaceous RNase

P". The group of Philippe Giegé (Institut de Biologie Moléculaire des Plantes, IBMP, Strasbourg) demonstrated that the model plant *Arabidopsis thaliana* possesses three PRORP proteins. PRORP1 is localised in both mitochondria and chloroplasts whereas PRORP2 and PRORP3 are active in the nucleus [2,3]. A collaboration was initiated between two neighbouring institutes in Strasbourg (IBMP and IBMC) to examine these enzymes from *A. thaliana* and a combination of biochemical and biophysical approaches was used to gain a first structural and functional insight into tRNA recognition and maturation by PRORPs.

PRORP: an integrated structural study

PRORP sequences are characterized by the presence of pentatricopeptide repeat (PPR) motifs and a metallo-nuclease domain proposed to hold the catalytic center. Because no structure of a close homologue was known at the time we started this study, comparative modeling was carried out on separate domains. We then performed synchrotron radiation circular dichroism (SRCD) on the DISCO beamline to validate the models based on their 2D structure content and to test

the conformational stability of PRORP samples prior to further investigations. The presence of a zinc binding motif between the two main domains was demonstrated by site directed mutagenesis of putative zinc chelating residues in association with inductively coupled plasma mass spectrometry. Small angle X-ray scattering (SAXS) data collected on the SWING beamline confirmed the two domain organization of PRORPs and helped place them with respect to each other (Figure 1).

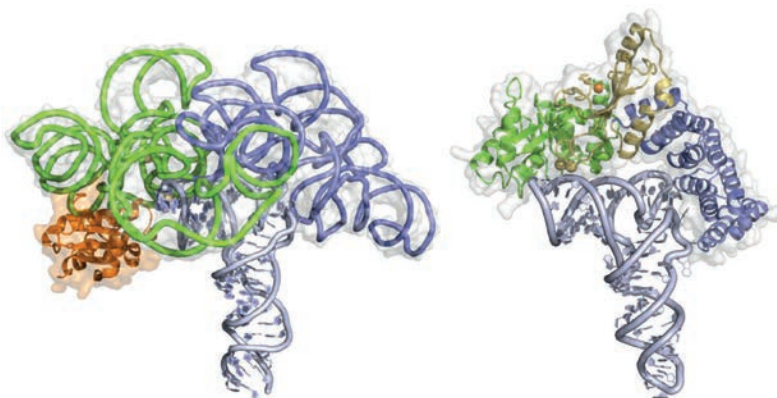


1 A first glance at a PRORP:tRNA complex. PRORP2 of *A. thaliana* was built by comparative modelling guided by SRCD and SAXS data, and the resulting model was docked onto a pre-tRNA substrate based on footprint analysis. The RNA cleavage position is indicated by an arrow.

Probing PRORP:tRNA interface

To position PRORP on its RNA substrate, the latter was subjected to RNase digestion in the presence of the enzyme. The protection footprint (Figure 1) defined the interaction interface and the PRORP enzyme was docked accordingly onto the 3D structure of a pre-tRNA. This model of the maturation complex reveals that eukaryotes have evolved PPR proteins to

recognize pre-tRNAs in a similar way as the ribonucleoproteic RNase P reminiscent from the ancient *RNA world* (Figure 2). Although the scenario of this convergent evolution remains to be established, as well as the precise catalytic mechanism of tRNA maturation, this study is a first step towards the detailed characterization of the PRORP family.



2 Classical ribonucleoprotein RNase P (left, PDB id: 3Q1R) and PRORP2 (right, model based on PDB id: 4G26) share the same pre-tRNA binding mode [4].

SWING & DISCO beamlines

ASSOCIATED PUBLICATION

Structural insights into protein-only RNase P complexed with tRNA

A. Gobert, F. Pinker, O. Fuchsbauer, B. Gutmann, R. Boutin, P. Roblin, C. Sauter* and P. Giegé.

Nature Communications 4 (2013) art.1353

CORRESPONDING AUTHOR

*Laboratoire "Architecture et Réactivité de l'ARN", UPR 9002 du CNRS, Institut de Biologie Moléculaire et Cellulaire (IBMC), Université de Strasbourg, 15 rue René Descartes, 67084 Strasbourg, France

c.sauter@ibmc-cnrs.unistra.fr

REFERENCES

- [1] Holzmam et al. Cell 135 (2008), 462
- [2] Gobert et al. Nat. Struct. Mol. Biol. 17 (2010), 740
- [3] Gutmann et al. Genes Dev. 26 (2012), 1022
- [4] Pinker et al. RNA biology 10 (2013), 1457

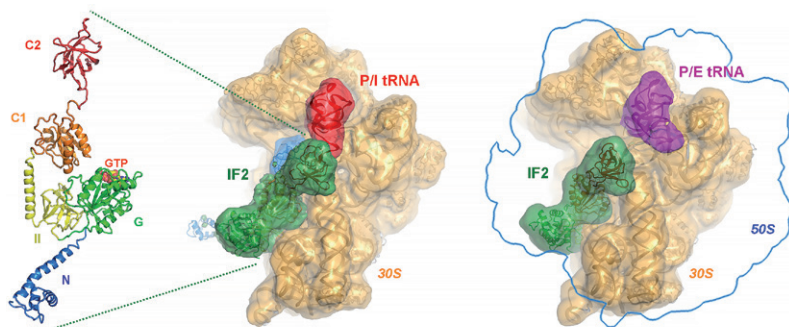
The function of translation initiation factor IF2 analyzed by an integrated structural biology approach

For many years, the group of Bruno Klaholz has been interested in the translation factor IF2 which participates in translation initiation in bacteria. Using an integrated approach to structural determination, they and their collaborators have succeeded in describing with precision this enzyme at structural and functional levels. In particular, they have brought to light a domain of its structure important for the assembly mechanisms of the ribosome subunits, unveiling a very different functioning from its eukaryote counterpart.

Decyphering IF2 structure

IF2 is a multidomain protein (see figure below). Combining results from crystallography, small-angle X-ray scattering (SAXS) and cryo electron microscopy, we have now achieved the determination of the entire 3D structure of IF2, both in solution and in its state bound to the ribosome, in which it stabilizes the initiator transfer RNA that carries the first amino acid of the future protein to be synthesized. We combined the structural studies with functional analysis of IF2 by fast kinetics and single molecule fluorescence (in collaboration with the teams of Claudio Gualerzi, Camerino, and Jody Puglisi, Stanford), analyzing dynamics of the complex in presence and absence of the N-terminal domain, and showing its crucial role in

the formation of a ribosome ready for beginning protein synthesis. Notably, we observed that its absence blocks the correct assembly of the ribosome and therefore obstructs its activity. An additional collaboration with Thomas Steitz's team from Yale University (USA) which allowed showing that the mechanism of ribosome assembly catalyzed by the N-terminal extremity of IF2 is rather different from the one known for its eukaryote counterpart, eIF5B. These results are providing key information about the molecular mechanism of translation initiation, a decisive step for the regulation of protein synthesis. Altogether, this work culminated in two articles published in Proceedings of the National Academy of Sciences.



1 Structure of the multi-domain translation initiation factor IF2 as seen in isolated form (left, crystallography and SAXS) and when bound to the 30S subunit of the ribosome (middle, cryo-EM) where it stabilizes the initiator tRNA (labelled in red). When the N-terminal domain (marked in blue in the left panel) is removed, 70S formation stalls in a non-productive state (right panel, cryo-EM) with the initiator tRNA (magenta) in a P/E-site transient position and subunit joining is affected as monitored by fast kinetics and single molecule fluorescence analysis.

The multi-approach technique showcased in this study was possible by the access to the SOLEIL synchrotron facilities and to the FRISBI infrastructure www.frisbi.eu and its Strasbourg node Instruct France Centre 1 which is also available to all Instruct member countries in Europe.

SWING beamlines

ASSOCIATED PUBLICATION

Involvement of protein IF2 N domain in ribosomal subunit joining revealed from architecture and function of the full-length initiation factor

A. Simonetti, S. Marzi, I.M. Billas, A. Tsai, A. Fabbretti, A.G. Myasnikov, P. Roblin, A.C. Vaiana, I. Hazemann, D. Eiler, T.A. Steitz, J.D. Puglisi, C.O. Gualerzi and B.P. Klaholz*

Proc Natl Acad Sci U S A, 110(39) (2013) 15656

CORRESPONDING AUTHOR

* Centre for Integrative Biology, IGBMC, 67404 Illkirch, France

klaholz@igbmc.fr

REFERENCES

- [1] A. Simonetti et al. *Nature* 455 (2008), 416
- [2] A. Simonetti et al. *Acta Cryst.* D69 (2013), 925
- [3] D. Eiler et al. *Proc Natl Acad Sci U S A* 110 (2013), 15662

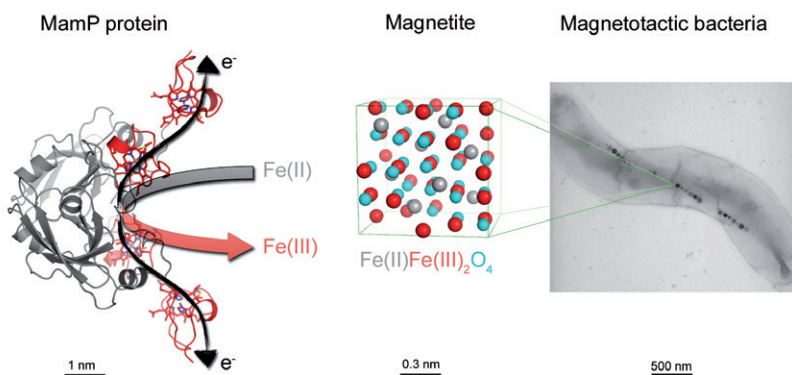
Crystal structure of the crystallographer MamP

An international consortium led by CEA researchers, in collaboration with the CNRS, has succeeded in characterizing the structure and function of a protein involved in the production of magnetite nanomagnets in magnetotactic bacteria. This protein, MamP, is crucial to the metallurgical activity of the bacterium. It is this protein that gives the magnetite its magnetic properties. This work constitutes an important advance in the understanding of these bacteria and the magnetite biomineralization process. It is expected to result in the development of additional biotechnological applications for these nanomagnets, especially in the fields of medical imaging and the decontamination of water.



Magnetotactic bacteria have the ability to synthesize nanocrystals of magnetite (Fe_3O_4) enabling them to align themselves with the terrestrial magnetic field in order to find the position in the water column that is most favorable to their survival. The alignment of the nanomagnets is similar to that of a compass needle. The magnetite crystal synthesis process is a complex one, and it is little understood at the present time. Magnetite is a compound of oxygen and iron in a mixture of two different oxidation states [Fe(II) $\text{Fe(III)}_2\text{O}_4$]. In this study, the researchers have described the mechanism by which the bacterium produces these two states, one of which, Fe(III), is essentially insoluble. The determination of the structure of the protein MamP, using PROXIMA 1 beamline, has shown for the first time that a section of this protein possesses an original folding structure known as a magnetochrome. This structure is only found in magnetotactic bacteria. The structure has a crucible-like shape capable of containing iron. Additional

experiments have shown that MamP has the ability to oxidize iron from the Fe(II) state to the Fe(III) state, and to stabilize the latter in its crucible. Mutagenesis studies and the phenotyping of magnetotactic bacteria variants have confirmed the physiological importance of this crucible. Finally, a number of *in vitro* experiments have shown that MamP is capable of producing a magnetite precursor when incubated in the presence of Fe(II) alone, proving that the Fe(III) results from the activity of this protein. This fundamental study reveals part of the process whereby iron is biomineralized and nanomagnets are synthesized in magnetotactic bacteria. The potential applications of these nanomagnets appear promising. They may, for example, be used as a contrast agent in magnetic resonance imaging. Another possible application relates to the decontamination of water supplies. Magnetotactic bacteria carrying an enzyme that breaks down a contaminant may be used to treat effluent and may then easily be removed from the water by means of a magnet.



❶ The crucible of the MamP protein (structure colored in grey, with its magnetochrome domains in red) allows transformation of Fe(II) into Fe(III), those two redox states being necessary to make magnetite nanomagnets in so-called magnetotactic bacteria.

© Pascal Arnoux/CEA

PROXIMA 1 beamline

ASSOCIATED PUBLICATION

Structural insight into magnetochrome-mediated magnetite biomineralization

M.I. Siponen, P. Legrand, M. Widdrat, S.R. Jones, W.J. Zhang, M.C.Y. Chang, D. Faivre, P. Arnoux* and D. Pignol

Nature 502(7473) (2013) 681

CORRESPONDING AUTHOR

*UMR 7265 CEA-CNRS-Aix-Marseille Université, DSV, IBEB, Laboratoire de Bioénergétique Cellulaire, 13108 Saint-Paul-lez-Durance, France
 pascal.arnoux@cea.fr



ATOMIC AND MOLECULAR PHYSICS, DILUTE MATTER, UNIVERSE SCIENCE

- 74** Advanced studies of molecular ions by resonant photoemission
- 76** Unravelling coupled electronic and nuclear angular momenta
- 78** Spectroscopy of the $^{15}\text{NH}_2$ radical
- 80** New routes to dissociation: the fourth way
- 82** Chirality reveals electronic/nuclear motion couplings
- 84** Young's double slit experiment revisited at the atomic level
- 86** Nanosolvation-induced stabilization of a protonated peptide dimer isolated in the gas phase
- 88** Photoelectron circular dichroism on gas phase alanine: a possible photophysical process at the origin of life's homochirality?

ATOMIC AND MOLECULAR PHYSICS, DILUTE MATTER, UNIVERSE SCIENCE

The gas phase offers a unique solvent-free and substrate-free environment in which isolated species can be interrogated by photons over a wide spectral range, spanning from far IR to the X-rays.

Fundamental research, often based upon a rich experiment/theory interplay, is carried out on isolated species aiming at studying their electronic and molecular structures, as well as the dynamics of the photon/matter interaction and the associated many-body couplings. Along this line, Kimberg et al. used high-resolution Resonant Photoemission coupled to high level *ab initio* calculations to unravel with an unprecedented accuracy the molecular potentials of N_2^+ , as well as the rich, associated fs nuclear wave packet motion, while Kushawaha et al. observed and modeled double-slit-like interferences in the inner-valence photoionization of small symmetric hydrocarbons, providing structural information, such as the C-C distances. Travnikova et al. pointed out a specific ultrafast dissociation mechanism in core-excited polyatomic species involving multi-mode dynamics on a barrierless potential energy surface. Electron imaging in coincidence with ions (iPEPICO) was used by O'Keefe et al. in a synchrotron+laser two-color scheme to observe an isotope-dependent complex autoionization dynamics in Xe atoms, while Garcia et al. observed by photoelectron circular dichroism (PECD) on a chiral species a striking electron/nuclear motion coupling as evidenced by a reversal of the electron angular asymmetry according to the ion vibrational excitation.

Another part of the activity concerns studies at the interface with other fields in which gas phase species are encountered (astrophysics & planetology) or are studied as model systems, i.e. elementary bricks of more complex matter (chemistry, biology). Along this line Rousselot et al. derived nitrogen isotopic ratio in amine (NH) functional group-containing molecules, by comparison between emission lines obtained from the ESO telescope and from laboratory based FT-spectroscopy, shedding light on the solar system formation. On alanine, the simplest proteic amino-acids, Tia et al. measured a clear signature of PECD, a chiroptical conformer-dependent effect, which could be an asymmetric photophysical effect linked to the origin of biomolecular asymmetry, while Milosavljevic et al. studied the effect of nano-solvation of a peptide dimer ion stored in an ion trap, and observed an unexpected stability regarding VUV irradiation attributed to the presence of water molecules in a bridging position between the two peptides.

These experiments are carried out with a large array of experimental set-ups, in constant evolution and with several major upgrades. Some of these are described in the Modeling, Methodology and Instrumentation chapter of this document.

Laurent Nahon

Head of the "Atomic and Molecular Physics, Dilute Matter, Universe Science" Scientific Section

PHYSIQUE ATOMIQUE ET MOLÉCULAIRE, MATIÈRE DILUÉE, SCIENCES DE L'UNIVERS

La phase gazeuse offre un milieu unique, sans solvants ni substrats, dans lequel des espèces isolées peuvent être étudiées sur une large gamme spectrale s'étendant de l'IR lointain aux rayons X.

Une recherche fondamentale, souvent basée sur une forte interaction entre l'expérience et la théorie, est menée sur des espèces isolées, dans le but d'étudier leurs structures électroniques et moléculaires, ainsi que la dynamique de l'interaction matière/rayonnement et les couplages à plusieurs corps qui l'accompagnent. Dans cet esprit, Kimberg et al. ont utilisé la photo-émission résonante à haute résolution couplée à des calculs ab initio de haut niveau afin d'étudier avec une précision sans précédent les potentiels moléculaires de N_2^+ , ainsi que le mouvement complexe du paquet d'onde nucléaire fs associé, alors que Kushawaha et al. ont observé et modélisé l'interférence type deux fentes dans la photoionisation en couche de valence interne de petits hydrocarbures symétriques, fournissant ainsi des informations structurales, telles que les distances C-C. Travnikova et al. ont mis en évidence un mécanisme de dissociation spécifique et ultra-rapide dans des espèces polyatomiques excitées en couche interne, impliquant une dynamique multi-mode sur une surface d'énergie potentielle sans barrière. O'Keefe et al. ont utilisé l'imagerie de photoélectron-photoion en coïncidence (iPEPICO) dans un schéma synchrotron + laser à deux-couleurs pour observer une dynamique complexe d'autoionisation dépendante de l'isotope dans les atomes de Xe, alors que Garcia et al. ont observé, par dichroïsme circulaire de photoélectrons (PECD) sur des espèces chirales, un couplage remarquable des mouvements électroniques-nucléaires, mis en évidence par l'inversion de l'asymétrie angulaire des photoélectrons en fonction de l'excitation vibrationnelle de l'ion.

Une autre partie de l'activité implique des études à l'interface avec d'autres disciplines où des espèces en phase gazeuse sont soit très présentes (astrophysique et planétologie), soit étudiées comme systèmes-modèles telles des briques élémentaires de systèmes plus complexes (chimie et biologie). Dans cet esprit, Rousselot et al. ont déduit le rapport isotopique de l'azote dans des molécules présentant un groupement fonctionnel amine (NH), en comparant les raies d'émission obtenues par le télescope ESO avec celles obtenues en laboratoire par spectroscopie TF, apportant ainsi de nouvelles informations sur la formation du système solaire. Sur l'alanine, le plus simple acide aminé protéique chiral, Tia et al. ont mesuré une signature claire du PECD, un effet chiroptique dépendant de la conformation, qui pourrait être un effet photophysique asymétrique lié à l'origine de la l'asymétrie biomoléculaire, alors que Milosavljevic et al. ont étudié l'effet de la nano-solvatation d'un dimère de peptide protoné et stocké dans un piège à ions, et ont observé une stabilité inattendue vis à vis du rayonnement VUV, due à la présence de molécules d'eau dans une position de pontage entre les deux peptides.

Toutes ces expériences ont été menées sur une grande variété de dispositifs expérimentaux en évolution constante, avec des jouvences importantes. Certaines sont présentées dans le chapitre Modélisation, Méthodologie et Instrumentation de ce document.

Laurent Nahon

Responsable de la Section Scientifique « Physique Atomique et Moléculaire, Matière Diluée, Sciences de l'Univers »

Advanced studies of molecular ions by resonant photoemission

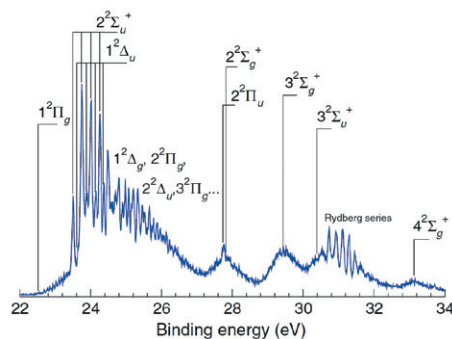
The possibility to explore excited states of molecular ions is of high interest for the investigation of the chemistry of still mysterious/unknown planetary atmospheres. The work done at the PLEIADES beamline [1] provides new information on the electronic structure of the nitrogen ions with a precision never achieved before. Synchrotron radiation with high brightness and a narrow bandwidth has allowed us to perform measurements in a sublifetime regime, exciting a selected vibrational substate of the intermediate $N\ 1s-\pi^*$ core-excited state and therefore controlling the spatial extension of the vibrational wave function. We combined the ultrahigh-resolution resonant photoemission (RPE) [2] measurements with accurate *ab initio* configuration-interaction calculations of the molecular potentials and of the nuclear wave-packet dynamics. The powerful synergy of sophisticated experimental and theoretical methods has allowed us to make a detailed analysis of molecular states, thus emphasizing the full potential of the resonant x-ray spectroscopies.

With the help of advanced theoretical modeling twelve electronic states forming the so-called “spectator” bands have been assigned and accurately characterized in N_2^+ (Fig. 1). These characterizations were not achievable in previous measurements and have only become possible in our experiment by tuning the excitation energies up to those of the highest-vibrational-quantum-number, low-cross-section vibrational substrates [3]. The use of the highly excited vibrational sublevels ($v=5,6$) was essential for the accurate potential reconstruction since - owing to the wide distribution of their wave functions - only these states allow one populating the lowest vibrational substrates in some final electronic states that were targeted in our study (Fig. 2). Using the superposition of the RPE spectra shown in Fig. 2c, the vibrational energies of few lowest vibrational sublevels of the $1^2\Pi_g$ and $1^2\Delta_g$ states were clearly identified, which allowed obtaining the most important spectroscopic constants of these potential energy curves (PECs). The $1^2\Delta_g$ state has never been observed before since its vibrational progression becomes visible only after high vibrational excitation of the intermediate state in the RPE process, and this has not been explored prior to the present measurements.

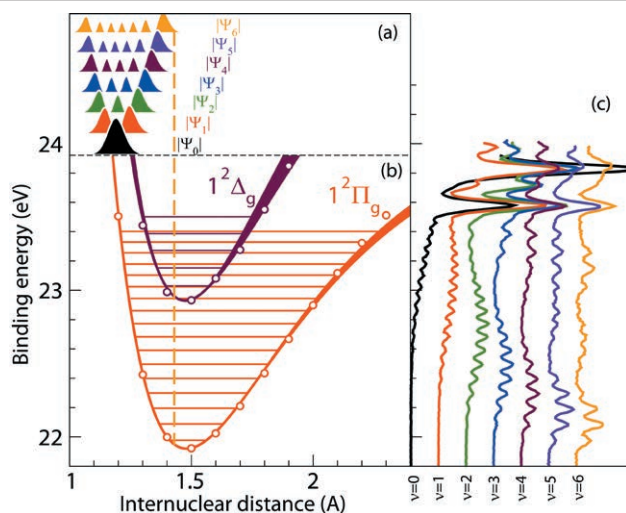
The resonant scattering cross section is known to be proportional to the square of the wave function of the vibrational sublevel involved in the scattering process. Ultrahigh spectral resolution, together with high-level theoretical simulations, has

allowed us to clearly demonstrate the phenomenon of the mapping of core-excited wave functions. Going beyond the initial prediction made for dissociative final states [5], we have shown that this mapping phenomenon is also observable for bound final states far from the equilibrium geometry (Fig. 3a). The final-state PEC shows a dissociative-like character at short bond lengths resulting in a broad feature in the RPE [1] in Fig. 3a], while the right classical turning point of the core-excited wave packet corresponds to a binding energy below the dissociation limit of the final state, resulting in a vibrational progression observable on top of the dissociative-like resonance (2) in Fig. 3a. The total envelope of the RPE profile maps the square of the vibrational wave function Ψ_1 of the core-excited state with reasonably high accuracy, which was observed experimentally for the first time. Our time-dependent numerical simulations showed that the ultrafast final-state wave-packet dynamics can be steered by controlling the excitation energy, allowing the selection of the vibrational wave functions in the core-excited state to be made (Fig. 3b).

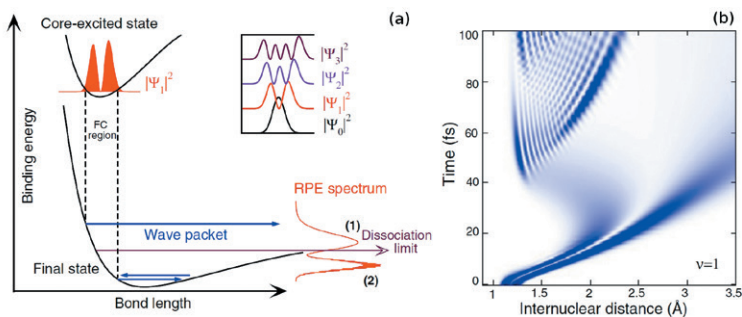
Using the textbook example provided by the nitrogen molecule, we have shown the richness of the RPE framework that combines state-of-the-art experimental and theoretical methods. The approach is general and can be extended to advanced studies of the excited ionic states of larger molecular species and easily transposed to neutral molecular states by detecting the radiative decay.



1 Experimental RPE spectra with x-ray photon energy tuned to the resonance with the ground vibrational sublevel of the $N\ 1s-\pi^*$ core-excited electronic state [3,4].



② Illustration of the PEC mapping in the framework of the high-resolution RPE spectroscopy. (a) Vibrational wave functions in the core-excited state. (b) The reconstructed molecular potentials of the $1^2\Pi_g$ and $1^2\Delta_g$ final ionic states (solid lines) and *ab initio* calculated potentials (open circles). The uncertainty in the reconstructed potential curves is represented by the thickness of the lines. (c) The experimental RPE spectra are presented in relation to the reconstructed PECs.



③ (a) Geometric interpretation of the phenomenon of mapping of the core-excited vibrational wave functions onto the $1^2\Pi_g$ bound final state based on the reflection principle. (b) The time-dependent dynamics of the correspondent final state vibrational wave packets.

PLEIADES beamline

ASSOCIATED PUBLICATION

Single-molecule X-ray interferometry: controlling coupled electron-nuclear quantum dynamics and imaging molecular potentials by ultrahigh-resolution photoemission and ab initio calculations

V. Kimberg, A. Lindblad, J. Söderström, O. Travnikova, C. Nicolas, Y. P. Sun, F. Gel'mukhanov, N. Kosugi, and C. Miron*

Physical Review X 3(1) (2013) 011017

CORRESPONDING AUTHOR

*Synchrotron SOLEIL, L'Orme des Merisiers, Saint-Aubin, BP 48, 91192 Gif-sur-Yvette Cedex, France

catalin.miron@synchrotron-soleil.fr

REFERENCES

- [1] C. Miron et al., www.synchrotron-soleil.fr/Recherche/LignesLumiere/PLEIADES
- [2] C. Miron & P. Morin, in *Handbook of High-Resolution Spectroscopy*, edited by M. Quack and F. Merkt (Wiley, Chichester, England, 2011), 1655
- [3] C. Miron et al., *Nature Phys.* 8 (2012), 135
- [4] P. Baltzer et al., *Phys. Rev. A* 46 (1992), 5545
- [5] F. Gel'mukhanov & H. Ågren, *Physics Reports* 1999 312, 87

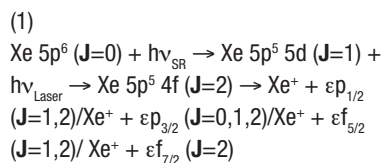
Unravelling coupled electronic and nuclear angular momenta

In this highlight we show how isotopically resolved photoelectron imaging can be used to isolate the pure electronic dynamics of a photoionization process. For atoms with nuclei possessing a magnetic moment (nonzero nuclear spin) the interaction of the nucleus with the electrons leads to a “blurring” of the photoelectron image which can cloud our view of the electron dynamics. Detecting electrons in coincidence with spin zero ions allows us to circumvent this problem which, when combined with theory, allows a greater understanding of the complex electron dynamics going on during ionization.



Measurement of Photoelectron Angular Distributions (PADs) provides information on the electron dynamics occurring during a photoionization process. One way to increase the amount of information contained in the experiment is to first prepare the target in a well-defined photoexcited state that will then be ionized with a second photon, leading to more information rich PADs than observed in single photon ionization. Comparison of these PADs to theoretical predictions provides a very stringent test of the theory used. However, for atoms with nuclei with a magnetic moment (nonzero nuclear spin, $I \neq 0$), the interaction of the nucleus with the magnetic field generated by the electrons, as illustrated in Figure 1, leads to a very significant blurring of the PAD in spite of the small size of the nucleus' magnetic moment. The result is that our picture of the electronic dynamics is obscured. Here we have applied an electron/ion coincidence scheme which allowed us to observe isotope dependent PADs for the first time. Using this method we selected only electrons emitted from atoms with no nuclear spin ($I=0$) by filtering out the other isotopes, thus allowing us to see an unclouded picture of the PADs.

The system chosen to demonstrate this technique is the two-photon ionization of the Xenon atom, which has been performed by combining synchrotron radiation ($h\nu_{SR}$) from the DESIRS beamline with the light from a visible dye laser ($h\nu_{Laser}$). The process can be described as follows:

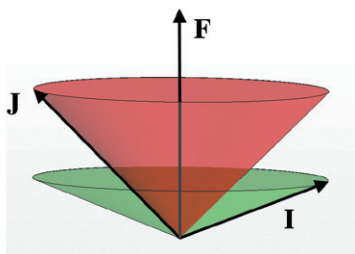


where εp and εf are possible outgoing electron waves and the subscripts are the angular momenta of outgoing electrons. The complex PADs are formed by the interplay of all of the open channels shown above. For ^{129}Xe ($I=1/2$) and ^{131}Xe ($I=3/2$), which form 26% and 21% of the natural isotope composition of Xe, the situation is further complicated by the coupling of I and J in the Xe $5p^5 5d$ ($J=1$) state, which leads to a very strong distortion of the PAD. An example of this is shown in Figure 2 where the PAD from the ^{129}Xe atom is compared with that of the $^{132,134,136}\text{Xe}$ atoms (all $I=0$ nuclei) for electrons emitted in the process described in eq. (1). It can clearly be seen that the PAD from the nonzero nuclear spin atoms is much more isotropic than the unperturbed zero spin isotopes.

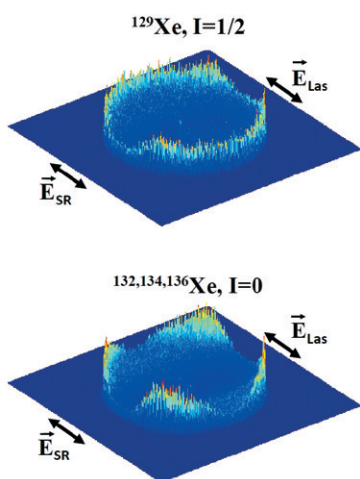
These PADs can be described quantitatively by the following formula:

$$(2) \quad I(\theta) = n (1 + \beta_2 P_2(\cos \theta) + \beta_4 P_4(\cos \theta))$$

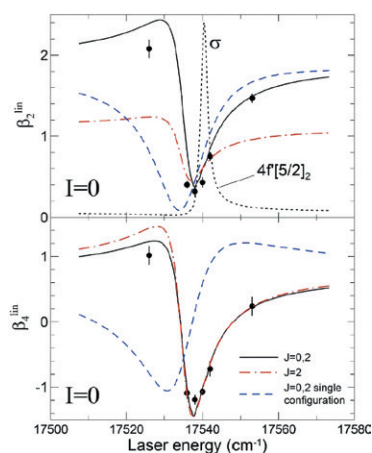
where θ is the angle between the electric field vector of the light and the direction of emission of the photoelectron and P_n are the Legendre polynomials. The measurements of β_2 and β_4 by recording photoelectron images while tuning the optical laser energy across the Xe $5p^5 5d$ ($J=1$) + $h\nu_{Laser} \rightarrow \text{Xe } 5p^5 4f$ ($J=2$) resonance are shown in Figure 3 together with the results of a number of theoretical models. Only the multiconfiguration Hartree Fock (MCHF) model including $J=0$ and 2 channels are able to describe the experimental data while simpler models fail.



❶ Coupling of the J (electronic angular momentum) and I (nuclear angular momentum). Precession of J around F leads to a decrease in the alignment of the intermediate state, and thus to a blurring of the PADs.



❷ The raw photoelectron images for parallel linear polarizations of both SR and optical laser light of the photoelectrons taken in coincidence with the non-zero and zero nuclear spin isotopes of Xe. Copyright: American Physical Society.



❸ The panels show the β_2 (top) and β_4 (bottom) parameters for Xe ions with nuclear spin $I=0$ at different laser wavelengths across the Xe $5p^5 5d (J=1) + h\nu_{\text{laser}} \rightarrow \text{Xe } 5p^5 4f (J=2)$ resonance. The experimental data (black circles) are compared to the theoretical results obtained using different approximations: MCHF (solid); MCHF only with $J=2$ dominating channels (chain); single configuration (dashed). Copyright: American Physical Society.

DESIRS beamline

ASSOCIATED PUBLICATION

Isotopically resolved photoelectron imaging unravels complex atomic Autoionization dynamics by two-color resonant ionization

P. O’Keeffe*, E.V. Gryzlova, D. Cubaynes, G.A. Garcia, L. Nahon, A.N. Grum-Grzhimailo, and M. Meyer

Physical Review Letters, **111** (2013) 243002

CORRESPONDING AUTHOR

*CNR-IMIP, CP10, I-00016 Monterotondo Scalo, Italy

patrick.okeeffe@imip.cnr.it

Spectroscopy of the $^{15}\text{NH}_2$ radical

Determination of the nitrogen isotopic ratios in different bodies of the solar system provides important information regarding the solar system's origin. For comets such a ratio can now be measured for ammonia with NH_2 emission lines thanks to new laboratory spectra obtained at the AILES beamline. These spectra have permitted to measure accurately the $^{15}\text{NH}_2$ line wavelengths. This radical is produced by the photodissociation of $^{15}\text{NH}_3$ in comets. Thanks to a large dataset of high-resolution spectra obtained with the 8-m Very Large Telescope on different comets it has been possible to identify for the first time 7 different lines of $^{15}\text{NH}_2$. Our data analysis has permitted to measure the $^{14}\text{N}/^{15}\text{N}$ isotopic ratio in comets for a molecule carrying the amine (-NH) functional group. This ratio, within the error, appears similar to that measured in comets in the HCN molecule and the CN radical, and lower than the protosolar value, suggesting that N_2 and NH_3 result from the separation of nitrogen into two distinct reservoirs in the solar nebula. This ratio also appears similar to that measured in Titan's atmospheric N_2 , supporting the hypothesis that, if the latter is representative of its primordial value in NH_3 , these bodies were assembled from building blocks sharing a common formation location.



The determination of nitrogen isotopic ratios in solar system objects is of primary importance for a good understanding of their origin. The measurements of $^{14}\text{N}/^{15}\text{N}$ isotopic ratio done so far in different solar system objects and molecules have revealed a great diversity. This ratio ranges from 441 for the present-day Sun, considered as representative of the protosolar nebula, to 50 in some organic materials of chondrite and Interplanetary Dust Particles (IDPs). Any object of the solar system (except Jupiter) is actually enriched in ^{15}N compared to the protosolar nebula.

Different explanations have been proposed to explain this enrichment that depends of the type of molecules considered. Some authors suggest, for example, that the molecules carrying the nitrile- (-CN) functional group would be more enriched in ^{15}N than the molecules carrying the amine (-NH) functional group.

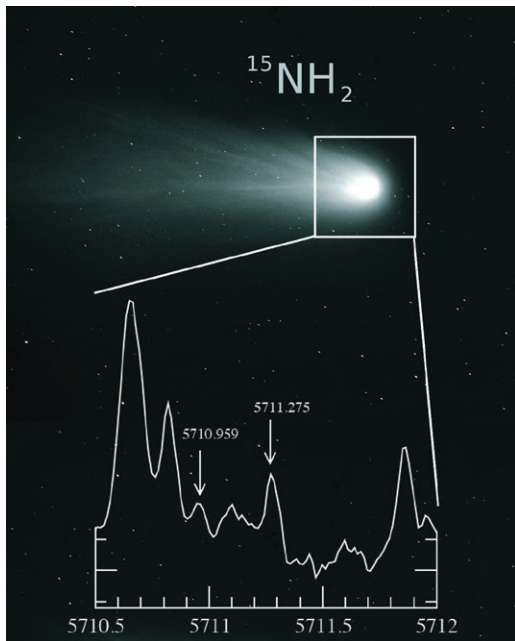
Comets are interesting targets to test this theory because they contain both HCN and NH_3 molecules (leading to CN and NH_2 radicals after photodissociation by the solar radiations). Up to recently the $^{14}\text{N}/^{15}\text{N}$ ratio had only been measured from HCN and CN in comets. This ratio had been measured in bright comets through optical observations of the CN radical [1] and millimeter observations of HCN [2]. These measurements give for both species the same non-terrestrial isotopic composition ($^{14}\text{N}/^{15}\text{N} \approx 150$ in comets versus 272 in the Earth atmosphere).

The difficulty for measuring $^{14}\text{N}/^{15}\text{N}$ in cometary ammonia was to identify unambiguously $^{15}\text{NH}_2$ emission lines. This identification implies accurate knowledge of their wavelengths, poorly known so far. An experiment conducted with the AILES beamline spectrometer

has permitted to determine the $^{15}\text{NH}_2$ wavelengths by Fourier transform spectroscopy. The analysis of this spectrum, recorded at the NH_2 Doppler width resolution (0.05 cm^{-1} , 0.017 \AA), had permitted to extract the $^{15}\text{NH}_2$ emission lines wavelengths from the mixture of $^{15}\text{N}_2$, H_2 and $^{15}\text{NH}_2$ emission lines. From this list of wavelengths it had been possible to search for $^{15}\text{NH}_2$ cometary emission lines not blended with any other bright emission lines.

Thanks to a unique collection of cometary high-resolution spectra collected on 12 different comets from 2002 to 2011 with the UVES spectrometer at the VLT ESO 8-m telescope it has been possible to search for $^{15}\text{NH}_2$ emission lines with a high sensitivity. Based on a single averaged cometary spectrum it was possible to identify seven different $^{15}\text{NH}_2$ emission lines belonging to the (0,10,0)-(0,0,0) band around 5700 \AA . These lines have permitted to compute an average $^{14}\text{N}/^{15}\text{N}$ ratio for NH_2 (and, consequently, cometary ammonia) similar to the one already measured with CN/HCN, i.e. lower than the protosolar nebula.

This scientific result, when compared to other $^{14}\text{N}/^{15}\text{N}$ measurements in solar system objects, suggests that N_2 and NH_3 result from the separation of nitrogen into two distinct reservoirs in the protosolar nebula: one with a high $^{14}\text{N}/^{15}\text{N}$ ratio in N_2 (e.g. Jupiter) and another one with a lower ratio in ammonia (Titan, comets...). The ratio measured in comets also appears similar to that measured in Titan's atmospheric N_2 (assumed to come from ammonia), supporting the hypothesis that, if the latter is representative of its primordial value in NH_3 , these bodies were assembled from building blocks sharing a common formation location.



Cometary ices create gas in the coma that can be analyzed thanks to the spectroscopic analysis. This figure presents two among the seven $^{15}\text{NH}_2$ emission lines identified thanks to this work. Credits : ESO/D. Cordier/P. Rousselot

AILES beamline

ASSOCIATED PUBLICATION

Toward a unique Nitrogen isotopic ratio in cometary ices

P. Rousselot*, O. Pirali, E. Jehin, M. Vervloet, D. Hutsemékers, J. Manfroid, D. Cordier, M.-A. Martin-Drumel, S. Gruet, C. Arpigny, A. Decock, and O. Mousis

The Astrophysical Journal Letters
(published 2013 December 16)
doi:10.1088/2041-8205/780/2/L17

CORRESPONDING AUTHOR

*Institut UTINAM-UMR CNRS 6213,
Observatoire des Sciences de l'Univers THETA,
Université de Franche-Comté, BP 1615,
F-25010 Besançon Cedex, France

rousselot@obs-besancon.fr

REFERENCES

- [1] Manfroid et al. A&A 503 (2009), 613
- [2] Bockelée-Morvan et al. ApJ 679 (2008), L49-L52

New routes to dissociation: the fourth way

A new dissociation mechanism was elaborated from the analysis of the ultrafast nuclear dynamics in highly excited molecules produced by resonant X-ray absorption. Observation of ultrafast dissociation occurring on a femtosecond timescale was explained with the help of theoretical modeling, which show that, in the very early stages of the photodissociation, the **internal rotation** of the light carbon atoms in 1-bromo-2-chloroethane (Br-CH₂-CH₂-Cl, BCE) has a significant impact on the whole dissociation process while the halogen atoms remain nearly still.



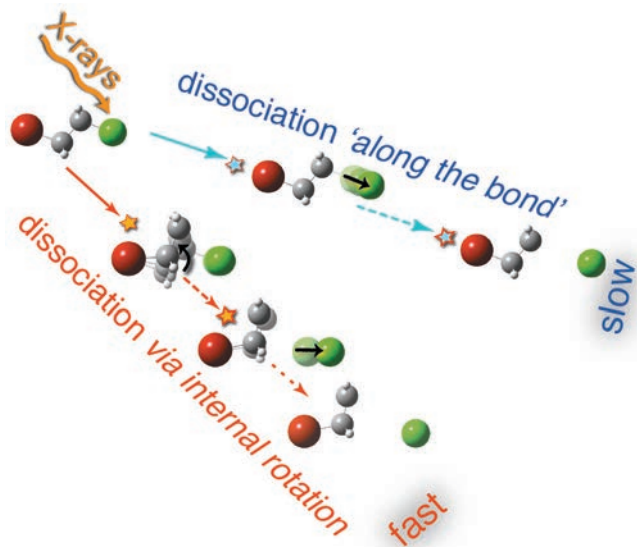
Dissociation is one of the simplest chemical reactions, where a molecule breaks apart into two or more fragments, i.e., other molecules, atoms, ions, or radicals. Understanding the mechanisms of dissociation reactions is essential as this knowledge can be the guide to the complex world of biomolecular processes. Yet dissociation pathways may remain elusive in larger systems, constituted of more than three atoms.

Until recently only two dissociation mechanisms were known: (1) stretching a bond until it breaks; (2) dissociation over a potential energy barrier through a transition state, where electrons are rearranged so that the old bonds are broken and new ones are formed. Recently a third dissociation modality was discovered – (3) the so-called ‘roaming’ reactions, which don’t follow the conventional mechanics of transition state theory. In this last type of chemical reactions, one atom wanders, or “roams”, around the molecular fragment until it finds another atomic partner to make a bond with, and leave the molecule [1].

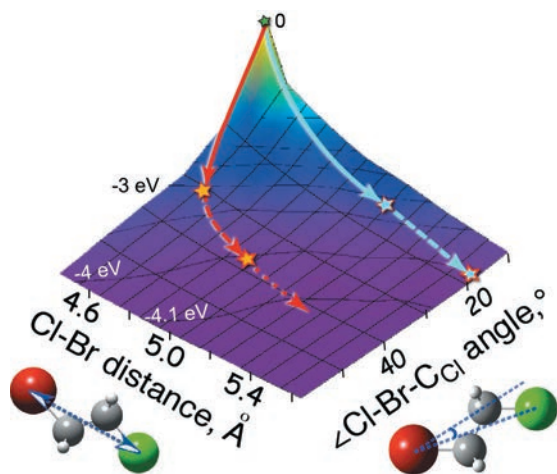
The resonant electron spectroscopy and electron-ion coincidence experiments, performed at the beamline PLEIADES and combined with theoretical modeling, revealed a new dissociation mechanism, which doesn’t fall into any of the three categories of dissociation reactions described above. In this work it is shown that in some cases stretching of the bond can be not that simple, as anticipated. The breakage of the bond can be mediated by the internal motions of other lighter atom groups of the molecule, the bond thus being broken not strictly along the bond axis. This allows yielding heavy

fragments on very short timescales, by far faster than the classical two-body dissociation would predict. It was demonstrated that in the prototypical molecular system – 1-bromo-2-chloroethane – just the rotation of the light-weight group of carbon and hydrogen atoms (-CH₂-CH₂-) around one of the halogen atoms (Br/Cl) may result in the breakage of the carbon-halogen (C-Cl/C-Br) bond (Figure 1). In reality, both the -CH₂-CH₂-rotation and the C-Cl (or C-Br) bond stretching occur simultaneously. However, due to the considerably lower masses of the carbon atoms relative to that of the halogen (Cl/Br) atom, the rotation is very fast and, therefore, extremely important in the total dissociation process. As shown in the Figure 2, which represents the potential energy surface of the neutral Cl 2p core-excited BCE molecule (lifetime $\tau \sim 7$ fs), produced by absorption of X-rays, the blue path would be followed if the molecule were to dissociate in a ‘classical way’ – the halogen atom were to separate from the residual molecular fragment by moving apart along the C-Br/C-Cl bond. However, there exists a faster (red) slope from the top of the mountain on this potential energy surface, if a third dimension, i.e. -CH₂-CH₂-rotation, is taken into account.

This new dissociation mechanism is expected to be rather general and applicable to other complex molecular systems, especially to the ones with light (-CH₂-)_x-linkages. Therefore, consideration of other reaction coordinate dimensions could be critical in modeling of dissociation reactions for prediction of proper reaction kinetics and product outcomes.



❶ Three dimensional potential energy surface for the Cl₂p core-excited BCE molecule. One coordinate represents slow stretching of the bond and another coordinate is fast internal rotation. The red arrows mark the dissociation pathway of BCE that occurs in the core-excited molecule. The blue arrows show the dissociation pathway that would be followed if the molecule were to dissociate in a “classical way” - strictly along the C-Cl bond. The red and blue stars show, where C-Cl bond is elongated by 35% and 70%, respectively.



❷ Mechanisms for the dissociation of Cl₂p core-excited BCE molecule. In blue: “classical way” - strictly along the C-Cl bond. In red: dissociation via internal rotation.

PLEIADES beamline

ASSOCIATED PUBLICATION

On routes to ultrafast dissociation of polyatomic molecules

O. Travnikova, V. Kimberg, R. Flammini, X.-J. Liu, M. Patanen, C. Nicolas, S. Svensson, and C. Miron

Journal of Physical Chemistry Letters, 4(14) (2013) 2361

CORRESPONDING AUTHOR

*Synchrotron SOLEIL, l'Orme des Merisiers, St Aubin BP48, 91192 Gif sur Yvette Cedex, France

catalin.miron@synchrotron-soleil.fr

REFERENCE

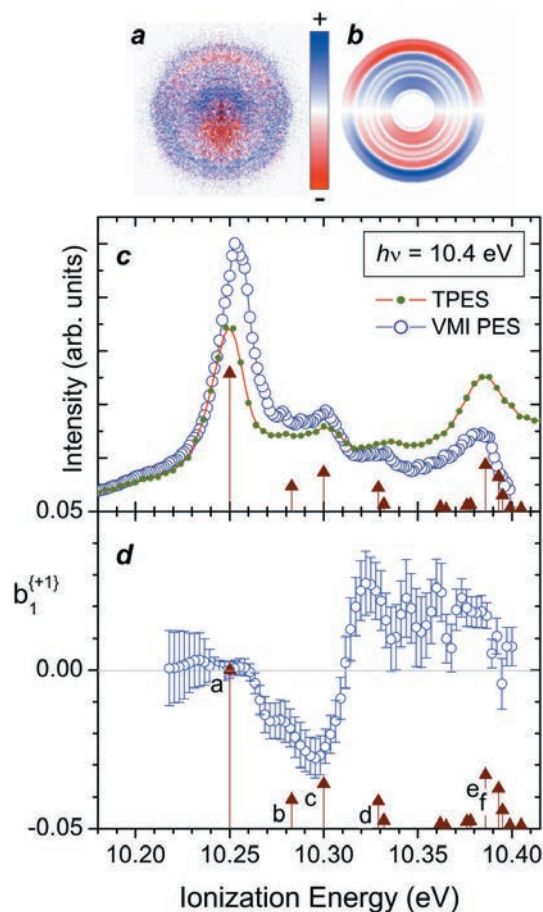
[1] J. M. Bowman & B. C. Shepler, Annu. Rev. Phys. Chem. 62 (2011), 531

Chirality reveals electronic/nuclear motion couplings

Photoelectron Circular Dichroism (PECD) is known to be very sensitive to static molecular structures of chiral systems, such as isomers or conformers. We show here that it may also probe dynamical structures, i.e. the vibrational motion sampled upon photoionization, as revealed by a spectacular inversion of the electron angular distribution asymmetry according to the final vibrational state of the resulting cation.

The coupling of electronic and nuclear motions is a striking manifestation of the complex many-particle dynamics involved in off-equilibrium systems, like excited molecules. Such a coupling may be revealed, in the case of molecular electronic transitions, by the breakdown of the so-called Franck-Condon (FC) approximation, which assumes that the probability of a given electronic transition does not depend on the nuclear geometry sampled during vibrational motion. In the case of molecular photoionization, this means that the electron continuum features should be decoupled from the vibrational energy content of the resulting ion.

In this context, chiral molecule systems can offer an enhanced opportunity for investigating molecular photoionization, including vibrational dynamics, even for randomly oriented samples. Indeed, for such chiral systems the laboratory-frame angular distribution of photoelectrons produced by photoionization with circularly-polarized light (CPL), can present a strong forward-backward asymmetry with respect to the light axis, called PhotoElectron Circular Dichroism (PECD). Quantitatively, the PECD asymmetry equals $2b_1$, where b_1 , the so-called dichroic parameter which encapsulates the chiral contribution,



PECD and dichroic parameter at 10.4 eV for the HOMO orbital of S-methyloxirane. (a) raw and (b) Abel-inverted difference images, obtained with the VMI spectrometer. The photon beam propagates from the bottom to the top of this image. (c) VMI-PES. (d) $b_1^{(+1)}$ dichroic parameter curve. The sticks correspond to the calculated vibrational spectrum.

is anti-symmetric with the swapping of either the enantiomer or the light handedness.

At DESIRS, we investigated the case of methyloxirane, recording the mass-filtered photoelectrons on a position sensitive detector via a Velocity Map Imaging (VMI) spectrometer that provides in a multiplex way the Angle-Resolved Photoelectron Spectrum (AR-PES).

From the radial distribution in the total electron image we obtain the PES, while from the ICPL-rCPL difference images the dichroic parameter, b_1 , can be obtained. The difference images (panel a and b of the figure) readily reveal a marked vibrational structure in the radial (i.e. electron energy) distribution, associated with strong forward-backward asymmetries in the angular distribution. Dramatic changes in the sign of the latter for some adjacent vibrational ring patterns can also be seen in the alternating color mapping.

The vibrational structure identified in the PES (panel c) - the origin band (peak "a") and a series of single quantum excitation of skeletal deformations (peaks "b" to "f") - exhibit very distinctive and remarkable dichroic behavior, with b_1 values (panel d) ranging from a null value for peak "a", to a negative value of -0.03 for "c", and then switching sign within a few tens of meV to a positive $\sim +0.02$ value for peaks "d" and "e". Phenomenologically, this sign change in b_1 means that the forward/backward asymmetry reverses direction for adjacent vibrational modes. This striking behavior

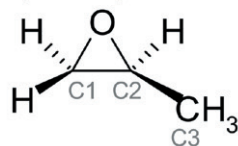
of asymmetry flipping upon vibrational (adjacent) excitation is not influenced by any continuum resonance, and has never been observed in any molecular photo-ionization experiment. Moreover, such a dependence of PECD with the vibrational energy content of the residual cation is completely unexpected within the usual FC assumptions.

This dramatic vibrational effect is probably due the known sensitivity of PECD to static geometric structures, which would be somehow replicated in dynamic structural changes occasioned by the vibrational motion sampling different regions of the nuclear configuration space.

This photoionization vibrational effect in PECD appears more remarkable than vibrational effects measured in the past on fixed-in-space molecules [1], yet it has been achieved without requiring molecular orientation because of the *intrinsically* chiral nature of the targets. In this context, PECD appears to offer a powerful, and (for chiral species) universally applicable probe of vibrational dynamics in molecular photoionization, even from randomly oriented targets. This, of course, is the "natural" situation for the ubiquitous chiral molecules in the biosphere.

Besides its fundamental interest, this finding may have important consequences for the interpretation of PECD in an analytical context, with the quickly-growing field of laser-based multi-photon PECD experiments whose outcomes may be driven by vibrational dynamics in both the intermediate and final state.

(S)-Methyloxirane



© The (S) Methyloxirane molecule

DESIRS Beamline

ASSOCIATED PUBLICATION

Vibrationally induced inversion of photoelectron forward-backward asymmetry in chiral molecule photoionization by circularly polarized light

G. Garcia, L. Nahon*, S. Daly and I. Powis

Nature Communications 4 (2013) 2132

CORRESPONDING AUTHOR

*Synchrotron SOLEIL, l'Orme des Merisiers, St Aubin BP48, 91192 Gif sur Yvette Cedex, France

laurent.nahon@synchrotron-soleil.fr

REFERENCE

[1] T. Jahnke et al., Phys. Rev. Lett. 93 (2004), 083002

Young's double slit experiment revisited at the atomic level

An international team including groups from the LCPMR (UPMC-CNRS), Paris; SOLEIL Synchrotron; the University of Trieste (Italy) and Uppsala University (Sweden), showed that it is possible to obtain very accurate information on the structure of molecules, such as the distance between the atoms that compose them. In particular, they have shown that the emission of electrons from equivalent atoms in a molecule gives rise to phenomena similar to those observed in Young's double-slit interference experiment. This famous optical experiment dating back 200 years consisted of making two beams of light issued from the same source interfere, by passing them through two close slits. A periodic pattern was observed, the distance between the fringes depending on the distance between the slits and the wavelength of the light. It is shown that the distance between two fringes (successive maxima or minima of the curves describing the relative number of electrons emitted from different equivalent atoms of the molecule) is directly correlated to the distance between the atoms from which the electrons are emitted, i.e. provides a kind of "ruler" to characterize distances on the atomic scale. The experimental and theoretical tools used in this study were relatively simple and easily accessible. This pioneering study was just a first step, as this method can be extended to complex systems.

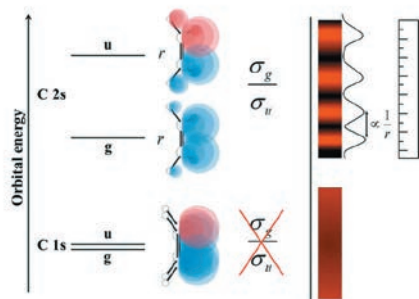


Interferences in coherent emission of photoelectrons from two equivalent atomic centers in a molecule are the microscopic analogies of the celebrated Young's double-slit experiment. While previous experiments had shown the existence of such interference phenomena in core-level ionization, this cannot be a general method, because the most effective way to detect the oscillations is to take the ratio of the symmetric and antisymmetric combinations (g/u) of core orbitals of two equivalent atoms [1,2], and this is experimentally possible for few selected systems. A schematic of the experiment is shown in Figure 1. In the present work, the novelty is the extension of the method to inner-valence orbitals, whose symmetric and antisymmetric combinations are well separated in binding energy. We obtained photoelectron spectra for the inner-valence region in the series of simple hydrocarbons C_2H_2 , C_2H_4 , and C_2H_6 , in the photon energy range of 70–700 eV, and derived the g/u cross-section ratios. The experimental and theoretical ratios are shown in Figure 2. The experimental data have been collected at the soft X-ray PLEIADES beamline at Synchrotron SOLEIL. The experimental

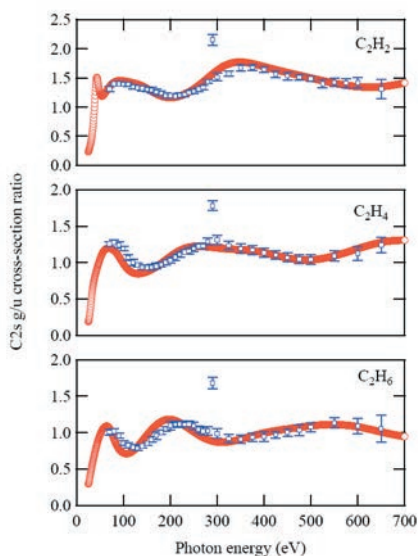
results are compared with the theoretical predictions by first-principles density functional theory (DFT) calculations [3,4]. The excellent agreement between theory and experiment is evident.

A strong dependence of the oscillation period on the C–C distance is observed, which can be used to determine bond lengths between selected pairs of equivalent atoms with an accuracy of at least 0.01 Å. The oscillation shape and period differ for each molecule. This is expected because the C–C bond length in C_2H_2 , C_2H_4 , and C_2H_6 is different. The sensitivity of the oscillations to the bond lengths is providing a new perspective for accurate estimation of those.

The present work clearly demonstrates the importance of interference phenomena in photoionization. These structures, which are easily experimentally accessible and are most evident in terms of cross-section ratios, are highly informative of geometrical structure, conformational equilibria, molecular electronic structure, etc. The present results open the way to extensive investigations of such phenomena in a wide range of systems.



❶ Schematic representation of double-slit interference in core and inner-valence photoionization of a polyatomic molecule and its relationship with the bond length. Interference cannot be observed in the C 1s core levels, where it is impossible to resolve the g/u splitting due to the large natural lifetime.



❷ Cross-section ratios between the C 2s-derived orbitals photoionization channels in C_2H_2 , C_2H_4 and C_2H_6 . The red circles are calculated points, and the blue squares with error bars are experimental results.

PLEIADES beamline

ASSOCIATED PUBLICATION

From double-slit interference to structural information in simple hydrocarbons

R. K. Kushawaha, M. Patanen, R. Guillemin, L. Journal, C. Miron, M. Simon, M. N. Piancastelli*, C. Skates and P. Decleva
PNAS 110 (38) (2013) 15201

CORRESPONDING AUTHOR

*Sorbonne Universités, UPMC Univ Paris 06, UMR 7614, Laboratoire de Chimie Physique-Matière et Rayonnement, 75005 Paris, France, and Department of Physics and Astronomy, Uppsala University, 75120 Uppsala, Sweden
maria-novella.piancastelli@physics.uu.se

REFERENCES

- [1] X.-J. Liu *et al.*, J Phys B At Mol Opt Phys 39 (2006) 4801
- [2] L. Argenti *et al.*, New J Phys 14 (2012) 033012
- [3] D. Toffoli *et al.*, Chem Phys 276 (2002) 25
- [4] M. Stener *et al.*, J Chem Phys 122(23) (2005) 234301

Nanosolvation-induced stabilization of a protonated peptide dimer isolated in the gas phase

The structure and functionality of biomolecules, as well as their susceptibility to external factors (such as ionizing radiation), are intrinsically linked with their aqueous environment. The structure-function paradigm postulates that proteins are required to adopt a specific folding to be biologically active. Weak molecular interactions have been proposed to have a major role in protein folding and in the formation of macromolecular complexes. In particular, the solvent has a key role in self-assembling processes. The recent measurements performed at DESIRS beamline, combined with theoretical study on protonated leucine–enkephalin peptide dimer ion, have shown that nanosolvation of a fragile biomolecular complex by only a few water molecules appears to have a dramatic impact on its stability.



The need to gain a deeper understanding of the effect of water solvation on the protein structure has led to an intensive investigation of gradual solvation of biomolecules – the limit of the so called microsolvation (or nanosolvation), referring to only a small and well-defined number of attached water molecules, has been conceived. However, the experimental investigation of nanosolvated species under well-defined conditions is challenging. We report a comparative experimental and theoretical study on the bare protonated leucine–enkephalin (Leu-Enk) peptide dimer ion and on the same system hydrated with three water molecules, showing already a clear nanosolvation effect. The Leu-Enk dimer is used here as a model system for peptide–peptide interactions, which is pertinent not only for non-covalent complex formation but also for the acquisition of secondary and ternary structures of proteins.

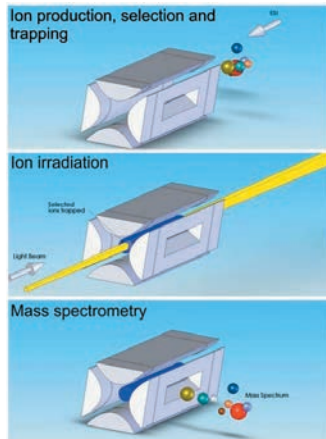
By using a recently developed experimental setup [1], in which an ion trap mass spectrometer equipped with electrospray sources is coupled to the DESIRS VUV beamline, it has been possible to isolate in the gas either the bare or the hydrated precursor, and to measure the photon-induced fragmentation intensity at different photon energies (figure 1). The results showed a drastic suppression of both the hydrated precursor dissociation into monomers (figure 2 - top) and the peptide backbone cleavage, thus clearly demonstrating a significant stabilization of the system due to the addition of only a few water molecules.

Furthermore, the solvation-induced stability was substantiated by detecting the doubly charged ion produced upon

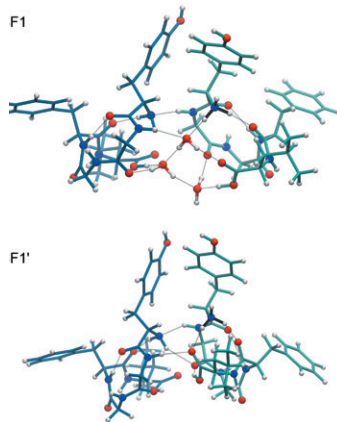
photoionization of the hydrated protonated species, which can be preserved in the gas phase, thus also allowing a precise determination of the ionization threshold (figure 2 - bottom). The apparent increased stability toward VUV irradiation of the hydrated complex with respect to the bare species is striking and questions the energy dissipation process, since the nanosolvation produces a frustrated dissociation in the dimer even for irradiation at energies below the ionization threshold.

Theoretical study, employing molecular dynamics and density functional theory (DFT) calculations, of the structure of the nanosolvated peptide dimer is consistent with the experimental findings. The calculations show that hydration with only 3 water molecules does not affect significantly the 3D structure of the dimer (figure 3), but rather stabilizes it by about 1.5 eV. Actually, the dimer is formed via non-covalent bonds (H-bonds) both in the bare and the solvated case. However, the binding is strongly enhanced upon nanosolvation, due to the flexibility of H₂O to adjust its bridging position and orientation with respect to the other molecules, thus increasing the effective number of hydrogen bonds.

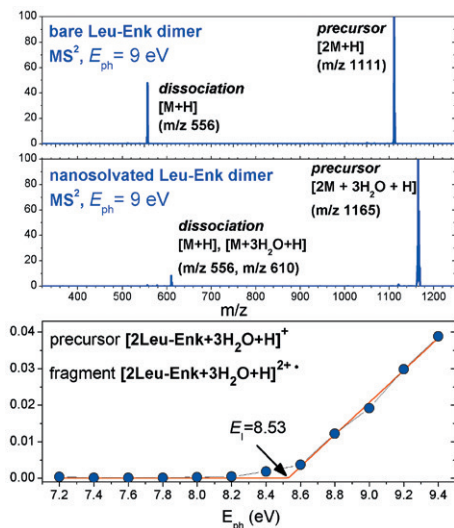
The present results are important to consider when stability of protein non-covalent complexes and protein structure is assessed for isolated non-hydrated ions, by mass spectrometry for example. Moreover, the phenomenological shielding effect of microsolvation observed here is of interest in the field of radiation damage and could help in the future to have a better understanding of these processes at the molecular level.



① Principle of the experimental method.



② B3LYP/6-31+G(d,p) optimized geometry of the lowest energy CF1 conformer found of $[2 \text{ Leu-Enk}+3\text{H}_2\text{O}+\text{H}]^+$ and the corresponding bare dimer CF1' $[2 \text{ Leu-Enk}+\text{H}]^+$. Thin gray lines represent H-bonds; black lines denote NH_3^+ group



③ Nanosolvation of a leucine–enkephalin peptide dimer by only 3 water molecules has a dramatic impact on its stability to VUV photon irradiation. A significant reduction of the fragmentation abundance of the hydrated protonated peptide dimer precursor, isolated in the gas phase, was observed. Bottom: photoionization yields of $[2\text{Leu-Enk}+3\text{H}_2\text{O}+\text{H}]^{2+}$ (m/z 582.25–584.0) fragment. The full line represents the linear Wannier fit.

DESIRS beamline

ASSOCIATED PUBLICATION

Nanosolvation-induced stabilization of a protonated peptide dimer isolated in the gas phase

A. R. Milosavljević*, V. Z. Cerovski, F. Canon, L. Nahon and A. Giuliani

Angewandte Chemie International Edition 52(28) (2013) 7286

CORRESPONDING AUTHOR

* Institute of Physics, University of Belgrade, Pregrevica 118, 11080 Belgrade, Serbia

vraz@ipb.ac.rs

REFERENCE

[1] A.R. Milosavljević et al. *Journal of synchrotron radiation* 19 (2012), 174

Photoelectron circular dichroism on gas phase alanine: a possible photophysical process at the origin of life's homochirality?

Gas phase pure enantiomers of alanine, the simplest chiral amino-acid, have been photoionized by VUV circularly-polarized light (CPL) at the Lyman α wavelength, giving rise to a measured large asymmetry (4%) of the electron angular distribution, and because of momentum conservation, of the corresponding parent alanine ion. This asymmetric photophysical process could be linked to the origin of life's homochirality, the fact that only L-amino acids, the chiral building blocks of proteins, are found in the biosphere.



Within a bottom/up approach of biomolecular complexity, the gas phase study of elementary sub-units of key macro-biomolecules allows one to probe, in a solvent-free environment, electronic and structural characteristics that will be involved in the formation of larger molecular structures. Amino acids, the building blocks of proteins, which are also chiral may provide a clear dichroic signature when probed, here for the first time, via PhotoElectron Circular Dichroism (PECD), a chiroptical, orbital-specific and conformer-sensitive effect giving rise to large forward/backward asymmetries in the photoelectron angular distribution upon photoionization by circularly polarized light (CPL).

Two complementary vaporization techniques (resistive heating followed by supersonic expansion and aerosol thermodesorption) were used in order to produce gas phase pure enantiomers of alanine, a fragile thermolabile biomolecule (Figure 1). They were then photoionized by the VUV CPL from DESIRS and the corresponding electrons and ions detected by the DELICIOUS3 double imaging e^-/ion coincidence spectrometer.

Electron imaging measurements made at the Lyman α radiation photon energy (10.2 eV), the most intense radiation in the interstellar medium, revealed a strong overall asymmetry for the outermost orbital (Figure 2), of 4 % as obtained by filtering on the alanine parent ion. Despite the presence of different conformers, this electron angular distribution asymmetry appears independent of sample temperature (and hence of conformer population) and may have some link with the origin of life's asymmetry.

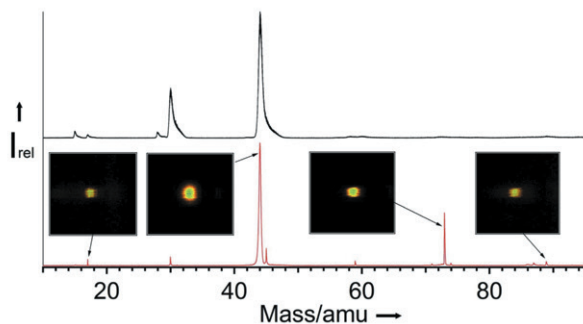
Indeed, since its discovery by Pasteur more than 150 years ago, the origin of biomolecular asymmetry remains a puzzling mystery, which traces back

probably to the origin of life itself. Amino acids were discovered in carbonaceous meteorites, with enantiomeric excesses (e.e) and isotopic composition indicating an extra-terrestrial origin. Were there to be an interstellar origin of elementary building blocks of life, one should look for an asymmetric bias applied before this organic matter was delivered on our planet, inducing a significant e.e, which was probably a necessary condition for the development of life on Earth.

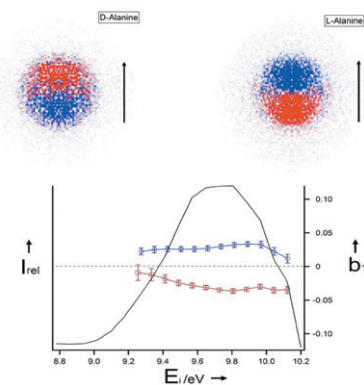
Among the deterministic scenarios are those based upon asymmetric photon-induced processes involving CPL, for which astronomical sources have indeed been reported. Several asymmetric *photochemical* processes were proposed and simulated in the condensed matter, by using UV CPL, leading to significant e.e, in the few % range.

Our findings on alanine asymmetric electron emission suggest that PECD could be an alternative *photophysical* asymmetric process, acting on gas phase amino-acids in the interstellar medium. Indeed, because of momentum conservation, the recoil motion of the corresponding produced chiral ions should exhibit an opposite asymmetric flux, leading to a significant and spatially resolved e.e (up to 4 % for alanine) in a given line of sight.

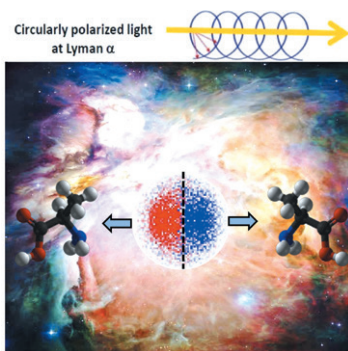
PECD could therefore produce an enantio-enriched gas phase ion cloud of a given handedness, separating from its counterpart (Figure 3), which would then be captured, neutralized and embedded into comets and meteorites seeding Earth with an exogenous organic matter presenting an initial e.e. It might therefore, in combination with other processes, have triggered the appearance of biomolecular asymmetry and consequently could have assisted the emergence of life.



❶ Time-of-Flight (TOF) spectra of alanine photoionized at 10.2 eV, with neutral species produced by aerosol thermodesorption (black line) or resistive heating associated to an adiabatic expansion (red line). Inserts correspond to ion images showing the Kinetic Energy Release for a few ion masses indicating for instance that m/z 73 corresponds to a spurious decomposition product.



❷ PECD and PES measurement recorded at 10.2 eV on oven-produced D- and L-alanine. (a) Raw difference images, filtered on all alanine-related ions, showing a PECD-induced forward-backward asymmetry with respect to the light propagation axis (depicted by the arrow). (b) The corresponding PES and b_1 dichroic parameter distribution over the HOMO band. The blue (resp. red) data correspond to the D- (resp. L-) enantiomer. The filtering on the parent mass (m/z 89) gives an asymmetry ($2b_1$) of 4%.



❸ Artist view of two enantio-enriched alanine ion clouds separating one from the other in interstellar space.

DESIRS beamline

ASSOCIATED PUBLICATION

Photoelectron circular dichroism on gas phase amino acid alanine at the Lyman- α radiation

M. Tia, B. Cunha de Miranda, S. Daly, F. Gaie-Levrel, G. Garcia, I. Powis and L. Nahon*

Journal of Physical Chemistry Letters, 4 (2013) 2698

CORRESPONDING AUTHOR

*Synchrotron SOLEIL, l'Orme des Merisiers, St Aubin BP48, 91192 Gif sur Yvette Cedex, France

laurent.nahon@synchrotron-soleil.fr



PHYSICS AND CHEMISTRY OF CONDENSED MATTER, EARTH SCIENCES

- 94** Synchrotron UV/visible imaging discriminates historical pigments
- 96** Programming the self-assembly of alloy nanowires: a combinatorial approach
- 98** Why do γ -Fe nanoparticles inside carbon nanotubes abnormally expand at high temperature?
- 100** Terahertz magneto-electric excitations in a chiral compound
- 102** Molecular refrigerators
- 104** Caffeine in cosmetics – optimizing its release into the body by means of "MOFs"
- 106** Resonant magnetic x-ray scattering on artificial spin ice
- 108** $\text{LuFe}_2\text{O}_{4+x}$: from multi-ferroicity to oxygen storage

PHYSICS AND CHEMISTRY OF CONDENSED MATTER, EARTH SCIENCES

When synchrotron light meets extraordinary materials, outstanding results often appear. This statement is well illustrated in the Hard-Condensed matter section of the 2013 SOLEIL Highlights that sheds light on materials with remarkable properties, often using a multimodal, multiscale approach with the synchrotron as a key ingredient.

First, Bertrand et al. have used an improved microscope setup at DISCO to study zinc oxide white pigment. If the pigment shows an apparent homogeneous photoluminescence at the macro scale, the results clearly reveal that it is highly heterogeneous at the micro- and nano-scale.

Bonilla et al on the other hand performed XAS and XRD at SAMBA and SIXS, in par with TEM and SQUID to investigate the structure of self-assembled vertical epitaxial Co-Ni alloy nanostructures grown by a combinatorial approach. The XRD data confirms the full epitaxial relationship between the nanowire and the substrate while XAS establishes the fcc structure of the alloys, hence validating the synthesis method.

At smaller scale, Corradini et al. have characterized an assembly of isolated Fe cage molecules deposited on a gold surface by STM, XPS and XMCD realized on DEIMOS. Their results demonstrate that the magnetocaloric effect is preserved in single molecules deposited on a substrate, opening the way for magnetic cooling process at the molecular level.

In functionalized materials, Cunha et al. have carried out a vast survey of the drug encapsulation and release from biocompatible porous metal-organic frameworks (MOF) while Hervieux et al. demonstrated the oxygen storage ability of a layered oxide material and its cycling possibility using XRD and other lab-based techniques. In both cases, high-resolution diffraction performed at CRISTAL helped reveal the structural changes at the nm scale during the process, a key step towards improving the uptake mechanism.

More fundamentally, Chaix et al. developed synchrotron THz experiment at AILES to study a chiral langasite compound. The results disclose a new kind of low energy excitations both magnetic and electric active, and associated to atomic vibrations. These findings demonstrate that atomic vibrations can acquire a magnetoelectric character, thus opening new routes to carry and process information.

Finally, Peron et al. used soft X-ray resonant scattering at SEXTANTS to study the magnetization of lithography produced artificial spin ice comprising a dense array of nanomagnets. The resonant scattering process when observed in a wide portion of the reciprocal space provides a direct mean to extract the number of reversed moments.

As shown here, the need to combine different techniques on the same sample is likely to become more urgent in the future. This applies to the synchrotron studies too. The vast range of techniques developed in The Hard Condensed Matter section shall be extremely useful to that aim.

Jean-Pascal Rueff

Head of the "Physics and Chemistry of Condensed Matter,
Earth Sciences" Scientific Section

PHYSIQUE ET CHIMIE DE LA MATIÈRE CONDENSÉE, SCIENCES DE LA TERRE

Lorsque la lumière synchrotron rencontre des matériaux extraordinaires, des résultats exceptionnels sont généralement produits. La section « Matière Dure » des Highlights de SOLEIL 2013 illustre parfaitement ce principe en apportant un éclairage nouveau sur les matériaux aux propriétés remarquables, le plus souvent dans une approche multimodale, multi-échelles, avec le rayonnement synchrotron comme ingrédient principal.

Tout d'abord, Bertrand et al. ont utilisé un dispositif de microscope sur la ligne de lumière DISCO pour étudier le pigment blanc d'oxyde de zinc. Si ce pigment présente une photoluminescence apparemment homogène à l'échelle macroscopique, les résultats démontrent clairement un caractère hautement hétérogène aux échelles microscopique et nanoscopique. D'autre part, Bonilla et al. ont effectué des mesures XAS et XRD sur les lignes SAMBA et SIXS, combinées à des mesures TEM et SQUID, pour des études structurales de nanostructures verticales d'alliage Co-Ni épitaxiées, dont la croissance est contrôlée par une approche combinatoire. Les données XRD confirment la relation d'épitaxie entre les nanofils et le substrat, tandis que les mesures XAS établissent la structure fcc des alliages validant ainsi la méthode de synthèse.

À une plus petite échelle, Corradini et al. ont caractérisé un assemblage de molécules-cages de Fe déposées sur une surface d'or par STM, XPS et XMCD sur la ligne DEIMOS. Leurs résultats démontrent que l'effet magnétocalorique est préservé dans des molécules uniques déposées sur un substrat, ce qui ouvre la voie vers un procédé de refroidissement magnétique au niveau moléculaire.

Dans les matériaux fonctionnalisés, Cunha et al. ont mené une vaste étude de l'encapsulation et de la libération de médicaments par des structures organométalliques (MOF) tandis que Hervieux et al. ont démontré la capacité de stockage de l'oxygène et les possibilités de cyclage dans un matériau constitué de couches d'oxydes par XRD ainsi que d'autres techniques de laboratoire. Dans les deux cas, la diffraction à haute résolution effectuée sur CRISTAL a permis de dévoiler les changements structuraux qui se produisent à l'échelle du nanomètre pendant le processus, une information essentielle pour améliorer le mécanisme de stockage.

De manière plus fondamentale, Chaix et al. ont développé une expérience synchrotron THz sur la ligne AILES pour étudier un composé de langasite chiral. Les résultats révèlent un nouveau type d'excitations à faible énergie, actives à la fois magnétiquement et électriquement, et associées à des vibrations atomiques. Cette découverte démontre que les vibrations atomiques peuvent acquérir un caractère magnétoélectrique et ouvrir ainsi de nouvelles voies pour transporter et traiter des informations.

Enfin, Peron et al. ont utilisé la diffusion de rayons X mous sur SEXTANTS pour étudier la magnétisation d'une glace de spin artificielle produite par lithographie et comprenant une grille dense de nano-aimants. Lorsqu'il est observé sur une vaste portion de l'espace réciproque, le processus de diffusion résonante fournit une méthode directe pour extraire le nombre de moments inversés.

Ces résultats montrent le besoin croissant de combiner différentes techniques expérimentales sur le même échantillon dont la demande se fera plus pressante encore dans l'avenir. Ceci s'applique aussi aux études synchrotron. Les nombreuses techniques développées par la section « Matière Dure » devraient s'avérer extrêmement utiles dans ce but.

Jean-Pascal Rueff

Responsable de la Section Scientifique « Physique et Chimie de la Matière Condensée,
Sciences de la Terre »

Synchrotron UV/visible imaging discriminates historical pigments

Careful chemical and physical characterization of pigments used by artists can tell us about artistic intent, trade in source materials, historic technology and more. We looked at the pigment zinc white, ZnO — used in the antique world as a medicine and cosmetic, and in the Western world as a pigment from the late eighteenth century on. ZnO is a class II-IV semiconductor having a wide band gap of c. 3.37 eV and, in general, an intense emission at c. 380 nm. However, we found that historic samples of the pigment have very distinct and diverse photoemission behaviour, inhomogeneous at the nanoscale, which can be used to discriminate among different sources, perhaps even different batches of the material.

ZnO, a semiconductor pigment whose emission is sensitive to production method and source

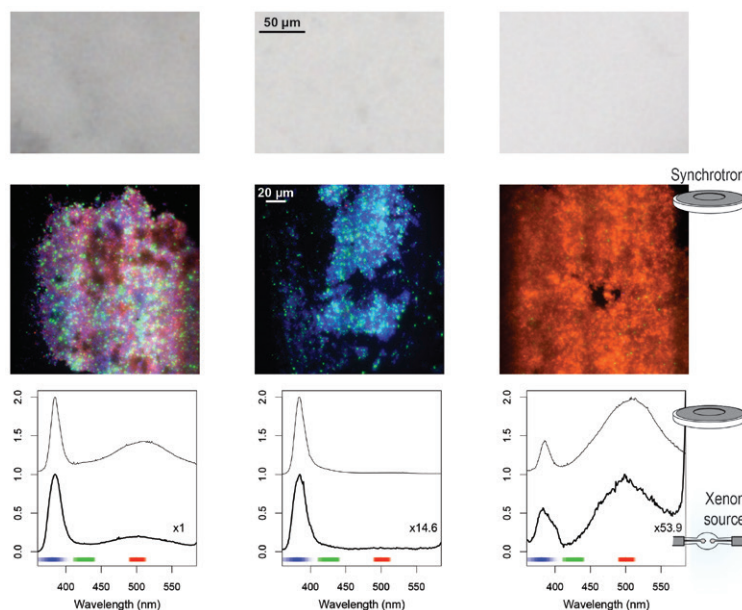
ZnO photoluminescence (PL) spectrum is very sensitive to defects created by impurities and vacancies in the crystal structure. Historical preparations of ZnO include the indirect process from molten metal, the direct process from an ore, and wet (precipitation) methods [1]. These methods give products that can be highly pure and apparently homogeneous. However, even among

one manufacturing process, variations in the photoluminescence behavior of the product occur, and at the microscopic level different crystallites can have different emission behavior. Within this work, a novel methodology is developed to acquire quantitative data on the heterogeneity of PL properties of semiconductors pigments at the scale of individual grains.

Accessing the luminescence of individual pigment grains

We gathered examples of historical ZnO pigments collected from international institutions. The sample preparation consisted of dispersing pigment in powder form onto indium foil allowing preservation of the distribution of the grains while minimizing mechanical stress and sample contamination,

and preventing interference on PL properties from embedding materials. The approach relies on the stability of the synchrotron UV source and its tunability in the 180–1000 nm excitation range, two critical parameters for ancient materials studies [2,3].



1 Study of three distinct historical zinc white pigments. From top to bottom: light microscopy images, synchrotron full-field PL images on a common intensity scale (40 \times objective), spectra from raster-scan synchrotron PL (thin lines) and laboratory macroscopic measurements (thick lines).

A new synchrotron approach to study ancient materials

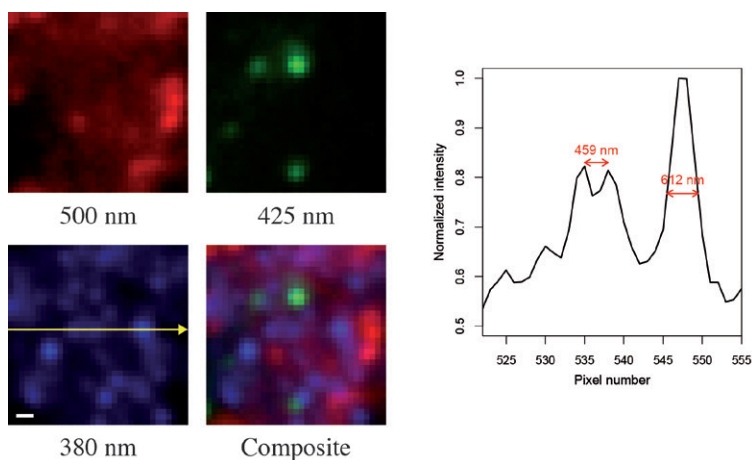
The use of the two deep UV-optimized microscopes at the DISCO beamline [4] provided unprecedented coupling of submicrometric spatial resolution and 3 orders of magnitude in spatial dynamics, with synergistic spectral and spatial characterization of samples. Radiometric calibration of spectra from raster scan microspectroscopy

measurements was implemented using self-written procedures and the SpectroMicro Package developed at IPANEMA. RGB false colors images of the historical ZnO pigments shown were constructed using correction to provide identical intensity scaling thereby allowing visual intercomparison of the main associated emissions.

Differentiating pigments at the grain level

We have performed careful measurements at high spatial and spectral resolution to obtain the distribution of the emission spectra in different powder samples, and have shown that we can discriminate among them. Historical zinc white powders that appear homogeneous at the macroscale are highly heterogeneous at the micro- and nanoscales, and are markedly distinct from one another in that the relative intensities of the band-edge and the two defect-associated emissions observed at the submicrometer scale are very different (Fig. 1). Access to this resolution, thus far inaccessible with conventional PL in the DUV, allowed

straightforward visualization, comparison, and study of the luminescence from individual mineral grains (Fig. 2). Having established that we can identify and measure the diverse PL behavior of different batches of ZnO, we are interested in how it compares to particle shapes and size, and how it corresponds to known variation in chemistry, demonstrated by the variability in long-term stability of different paints. This research shows that we can compare ZnO in various artworks, and in different layers within one work to help determine the relationships between them, such if they were painted using the same batch of paint.



2 Synchrotron full-field PL images of a zinc white powder under DUV excitation (280 nm, 100 × objective, 153 nm projected pixel size; scale bar: 500 nm).

DISCO beamline & IPANEMA

ASSOCIATED PUBLICATION

A multiscale photoluminescence approach to discriminate among semiconducting historical zinc white pigments

L. Bertrand*, M. Réfrégiers, B. Berrie, J.-P. Echard, and M. Thoury

Analyst 138(16) (2013), 4463

CORRESPONDING AUTHOR

* IPANEMA, CNRS, Ministère de la Culture et de la Communication, USR 3461, BP48 Saint-Aubin, 91192 Gif sur Yvette cedex, France; Synchrotron SOLEIL

loic.bertrand@synchrotron-soleil.fr

REFERENCES

- [1] H. Kühn, in *Artists' Pigments: A Handbook of their History and Characteristics* vol. 1, ed. R. L. Feller, National Gallery of Art, Washington, DC, USA, 1986, 169
- [2] M. Thoury et al. *Anal. Chem.* 83 (2011), 1737
- [3] L. Bertrand et al. *Phys. Rep.* 519 (2012), 51
- [4] F. Jamme et al. *Microsc. Microanal.* 16 (2010), 507

Programming the self-assembly of alloy nanowires: a combinatorial approach

Ferromagnetic nanowires are interesting objects for fundamental studies in nanomagnetism. Finding ways to obtain wires with reduced diameters and controlled composition and structure is thus an important task. This work reports on a new approach, relying on self-assembly, for growing epitaxial alloy nanowires assemblies in a matrix. It allows one to obtain epitaxial wires, with 4 nm diameters, and controlled composition and magnetic anisotropy.

Introduction

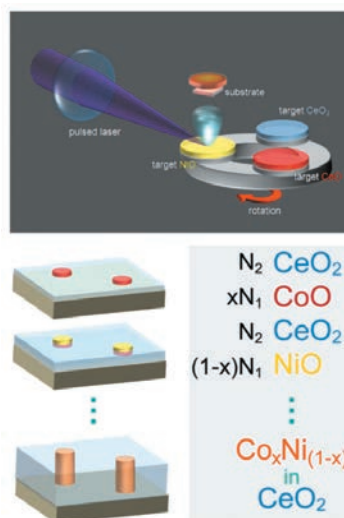
Heteroepitaxy of horizontal structures is a well-established way of obtaining coherent stacking of different materials and thus developing systems with new properties of interest in many areas of physics, including optoelectronics, magnetism and spin electronics. In recent years new types of vertical

epitaxial heterostructures have emerged, where a material grows epitaxially in the form of nano-pillars or nanowires in the matrix of another material. This geometry might lead to progress in the field of multi-functional nano-composites or even to strain-engineering by controlling deformations along the wire axis.

A new technique for obtaining alloy nanowires

The method used in this study is based on a combinatorial approach to pulsed laser ablation, illustrated in Figure 1. Controlled amounts of Co, Ni and cerium oxide are deposited sequentially, in a sub-monolayer regime, on a $\text{SrTiO}_3(001)$ substrate.

This results in the self-assembly of $\text{Co}_x\text{Ni}_{1-x}$ alloy nanowires embedded in a monocrystalline $\text{CeO}_2/\text{SrTiO}_3(001)$ matrix. The diameter of the wires is very small (4 nm) and their density can exceed $1 \text{ Tb}/\text{inch}^2$.



1 Diagram explaining the combinatorial method used for the epitaxial growth of cobalt-nickel alloy nanowires in $\text{CeO}_2/\text{SrTiO}_3(001)$. By adjusting the sequence of laser shots on the target to deposit the cobalt, nickel and matrix in controlled quantities in sub-monolayers, it is possible to obtain self-assembled cobalt-nickel alloy vertical nanowires embedded in the matrix.

Proofs of alloy nanowires formation

The metallic character of these wires has been shown by X-ray absorption measurements at the Ni and Co K-edges, carried out on the SAMBA beamline. Chemical mapping of the samples, by energy-filtered transmission electron microscopy at the Ni and Co L-edges, has shown nanowire growth within the matrix and confirmed the formation of an alloy: Co and Ni are clearly present simultaneously in the nanowire. These results are backed-up by X-ray absorption measurements at the K-edge: the structure

around the atoms of nickel and cobalt has been modified at the same time and depending on the ratio between the two species.

The resulting system is epitaxial: $\text{Co}_x\text{Ni}_{1-x}$ is in cube-on-cube epitaxy with the matrix, which grows itself epitaxially on the substrate. This could be established by high resolution transmission electron microscopy and X-ray diffraction measurements performed on the SIXS beamline.

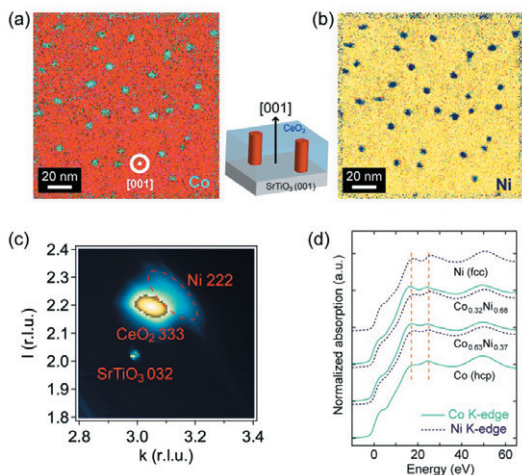
Programming the composition of the alloy...

The ability to control the composition by the sequence used for growth has been checked: the Co/Ni ratio in the wire is indeed as programmed. This allows the magnetic anisotropy of the nanowires to be adjusted: an enhancement of the magnetic anisotropy is observed when the proportion of cobalt increases, starting from pure nickel.

In principle, this method can be applied to other compounds and thus control a physical property that depends on the composition of the epitaxial nanowires

or nanopillars. In the case of cobalt-nickel alloys, it will be possible to optimize the Co/Ni ratio while maintaining a cubic crystal structure. This is not possible in bulk systems for percentages of Co higher than 65%: the system then transits to the hcp phase. The situation may be different for very small diameter nanowires in vertical epitaxy.

This study was funded by C'nano IdF and ANR (ANR-2011-BS04-007).



(a-b) Planar views using electron microscopy, filtered at the cobalt and nickel L-edges. The discs are the signature of the presence of alloy wires seen in the direction of growth [001]. (c) Reciprocal space map of arrays of epitaxial nickel wires in $\text{CeO}_2/\text{SrTiO}_3(001)$. (d) X-ray absorption spectra at the nickel and cobalt K-edges showing the metallic character of the wire and the nickel-cobalt alloy formation. In the wire alloy spectra, the intensity of the two peaks represented by the vertical dashed lines is characteristic of a face-centered cubic (fcc) structure

SAMBA & SIXS beamlines

ASSOCIATED PUBLICATION

Combinatorial growth and anisotropy control of self-assembled epitaxial ultrathin alloy nanowires

F.J. Bonilla, A. Novikova, F. Vidal*, Y. Zheng, E. Fonda, D. Demaille, V. Schuler, A. Coati, A. Vlad, Y. Garreau, M. Sauvage-Simkin, Y. Dumont, S. Hidki, and V.H. Etgens

ACS Nano 7 (5) (2013), 4022–4029

CORRESPONDING AUTHOR

* Institut des Nanosciences de Paris, UMR7588 CNRS / Sorbonne Universités UPMC, Campus Jussieu, Case courrier 840, 4 place Jussieu 75252 Paris Cedex 5, France

franck.vidal@insp.jussieu.fr

Why do γ -Fe nanoparticles inside carbon nanotubes abnormally expand at high temperature?

The thermal expansion of γ -Fe (austenite) nano-crystals confined inside multiwalled carbon nanotubes (MWCNTs) is studied in situ, using synchrotron x-ray diffraction, as a function of temperature. A peculiar behaviour is evidenced for these nano-crystals: the thermal expansion becomes abnormally high above $\sim 450^\circ\text{C}$. A scenario involving progressive carbon uptake into γ -Fe gives a satisfactory understanding of the phenomenon, and allows one to propose a value of the carbon solubilization rate in γ -Fe particles confined in MWCNTs.

Introduction

Carbon nanotubes can be viewed as nano-containers, where confined matter can exhibit unusual properties. Iron nano-crystals inside CNTs are formed during the synthesis of MWCNT samples by aerosol-assisted CCVD [1]. In this study,

we focused on the thermal expansion behaviour of γ -Fe particles contained in the inner core of MWCNTs (Figure 1) by means of an in situ x-ray scattering experiment as a function of temperature conducted on the Diffabs beamline.

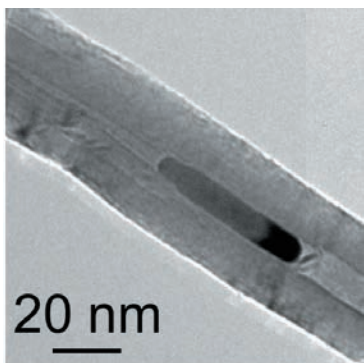
Results and Discussion

The existence of γ -Fe crystals under ambient conditions may appear surprising as this crystalline phase is not supposed to be stable. It has already been discussed that after formation at high temperature, where γ -Fe is stable, the narrow space available in the CNT does not allow the structural phase transition from the γ phase to the low temperature stable α -Fe phase (ferrite) to take place. The γ -Fe structure would consequently be conserved at low temperature [2]. Figure 2 shows the relative thermal expansion of γ -Fe deduced from the 200 peak position. The thermal expansion coefficient, A , is defined by:

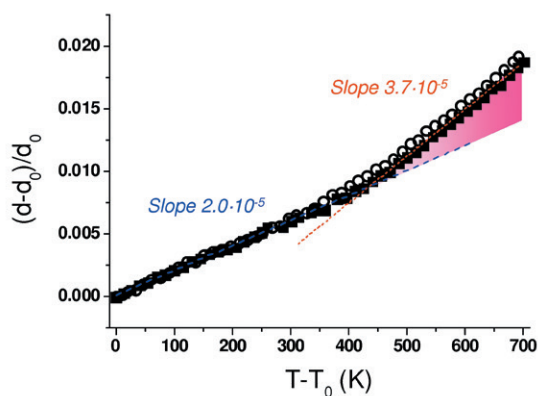
$$\frac{d - d_0}{d_0} = A \cdot (T - T_0)$$

where d is the reticular distance at temperature T and d_0 is the reference reticular distance at temperature T_0 (T_0 is equal to 50°C in our experiment). The thermal evolution of γ -Fe nano-crystals exhibits a peculiar behaviour, featuring two thermal regions in which the thermal expansion is different. For temperatures lower than 450°C , the thermal expansion coefficient is equal to $2.0 \cdot 10^{-5} \text{ K}^{-1}$. It is similar to that measured for γ -Fe nano-inclusions in

FeCu crystals [3]. However, the large value of $3.7 \cdot 10^{-5} \text{ K}^{-1}$ measured at temperatures above 450°C is very unusual. We propose that the increased thermal expansion could originate from the gradual intercalation of carbon atoms in the fcc lattice of γ -Fe as interstitial atoms. Such a phenomenon is likely, considering the large quantity of carbon available in the vicinity of iron-based particles. Based on the work by Onik et al. [4] dedicated to the intercalation of carbon atoms in austenite, it is possible to derive the solubilization rate of carbon into γ -Fe nanoparticles from the measured excess of lattice expansion. A maximum solubilization of 2.1 Carbon atoms / 100 Fe atoms is deduced from our data at 750°C . We therefore determine a carbon thermal solubilization rate of $8.4 \cdot 10^{-3} \text{ Carbon at.K}^{-1}$ in the $500\text{--}750^\circ\text{C}$ temperature range. Moreover, it is worth noting that the same slope change in the variation of lattice parameter with temperature appears both during heating and cooling. The phenomenon of carbon uptake is thus reversible. The possibility of tuning the carbon contents in the crystalline lattice of γ -Fe nanoparticles could open interesting perspectives for applications in the field of magnetism.



① Transmission electron microscopy image of a particle of γ -Fe inside a MWCNT.



② Thermal expansion of the 200 inter reticular distance of γ -Fe. Squares and circles represent experimental points obtained during the temperature increase and decrease, respectively. Lines represent linear fits of the data and the corresponding slopes are given.

DIFFABS beamlines

ASSOCIATED PUBLICATION

Anomalous thermal expansion of γ -iron nanocrystals inside multiwalled carbon nanotubes

J. Cambedouzou*, P. Landois, S. Rouzière, M. Pinault, C. Mocuta, L. Hennet, D. Thiaudière, M. Mayne-L'Hermite, and P. Launois

Physical Review B 88 (2013), 081402(R)

CORRESPONDING AUTHOR

* Laboratoire de Physique des Solides, UMR CNRS 8502, Université Paris Sud, F-91405 Orsay, France; Institut de Chimie Séparative de Marcoule, UMR 5257 CEA/CNRS/UM2/ENSCM, F-30207 Bagnols sur Cèze, France.

julien.cambedouzou@enscm.fr

REFERENCES

- [1] M. Pinault et al. Nano Letters 5 (2005), 2394
- [2] H. Kim et al. J. Mater. Res. 18 (2003), 1104
- [3] P. Gorria et al. Phys. Rev. B 72 (2005), 014401
- [4] M. Onink et al. Scr. Metall. Mater. 29 (1993), 1011

Terahertz magneto-electric excitations in a chiral compound

We have determined the terahertz spectrum of the chiral langasite $\text{Ba}_3\text{NbFe}_3\text{Si}_2\text{O}_{14}$ using the AILES beamline. Two excitations are revealed that are shown to have a different nature. The first one, purely magnetic, is observed at low temperature in the magnetically ordered phase and is assigned to a magnon. The second one persists far into the paramagnetic phase and exhibits both an electric and a magnetic activity at slightly different energies. This magneto-electric excitation is interpreted in terms of atomic rotations and requires a helical electric polarization.

Introduction

The electric-field control of spins and the converse magnetic-field control of electric dipoles inspire a number of hybrid technologies and motivate fundamental research on multiferroics and magneto-electric materials [1]. These magneto-electric couplings can also have signatures on the elementary excitations emerging from the ordered states that prevail in these compounds. Magnons or phonons, for instance, correspond to coherent deviations of the spins or of the atomic positions out of their equilibrium. Recently

a novel type of excitations was discovered in multiferroics, the so-called electromagnons [2]. It is now perceived as an electric-charge dressing of magnons. This dressing enables the electric-field control of magnons and is thus foreseen to be used in magnonics. Here we report experimental evidence of the dual phenomenon, which are atomic vibrations dressed with currents, hence magnetically active, that we observe in the terahertz (THz) spectrum of the chiral compound $\text{Ba}_3\text{NbFe}_3\text{Si}_2\text{O}_{14}$.

THz spectroscopy

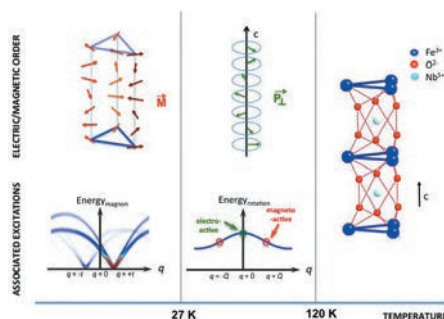
THz spectroscopy is particularly well suited to investigate magneto-electric excitations since (i) the THz energy range coincides with that of magnons and phonons and (ii) the THz wave delivered by the synchrotron radiation (98% polarised at SOLEIL) carries both an electric (e) and a magnetic field (h), so that rotating the sample with respect to the wave polarization allows

the unambiguous determination of the activating field. Probing THz excitations is not an easy task since no intense sources exist. This region of the spectrum has only begun to be explored. One recent way is the use of synchrotron sources. The AILES beamline at SOLEIL has been designed with that purpose.

$\text{Ba}_3\text{NbFe}_3\text{Si}_2\text{O}_{14}$ a chiral magnetic compound

When chirality meets magnetic order, unusual magnetic and electric properties often appear, encouraging the search for novel multiferroic and magneto-electric phenomena [3]. $\text{Ba}_3\text{NbFe}_3\text{Si}_2\text{O}_{14}$ crystallizes within the $P321$ space group thus displaying structural chirality (Figure 1).

Its remarkable magnetic properties are due to the Fe^{3+} ions [4] arranged in triangles. Below the Néel temperature $T_N=27$ K, the system develops a chiral magnetic order with a 120° spin structure within the Fe triangles that rotates along the c axis and forms magnetic helices.

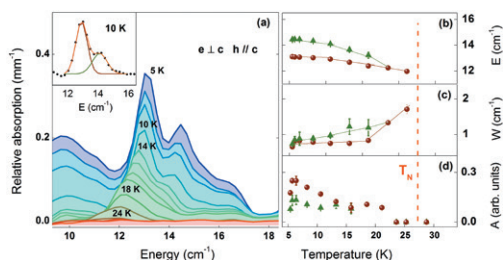


1 Suggested phase diagram for the Fe langasite due to the chiral, tubular structure of the compound. Below 27 K, a helical magnetic order occurs and magnons can be excited. Below 120K, a helical polarisation sets in which is responsible for the E1-E2 magneto-electric excitation.

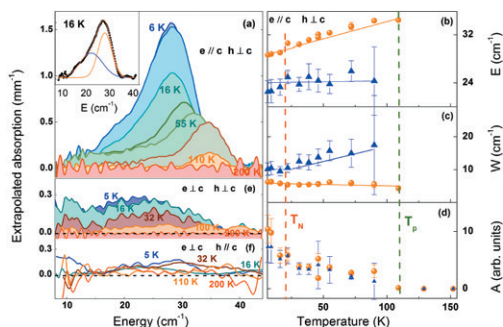
Magnetic and magneto-electric properties

THz spectra have been measured in the temperature range 6 K - 200 K (Figure 2-3). Around 13 cm^{-1} magnons are present at low temperatures and disappear when approaching T_N . These magnetic excitations are in agreement with the neutron inelastic measurements and spin wave calculations on this compound [5]. More surprisingly, other broader excitations are observed, centered at 23 cm^{-1} (E1) and 29 cm^{-1} (E2) at low temperatures that disappear only above $T_p \approx 100 \text{ K}$. Using different THz polarization, we have determined that E1 is magneto active with $h \perp c$, while E2 is electric active with $e // c$. Both excitations cannot be associated to the magnetic order since they persist up to T_p which is almost 4 times T_N ; they are also absent in the spin wave neutron measurements at the equivalent zone center. These excitations are more likely related to the lattice. Based on symmetry analysis in the P321 space group, we propose a model depicted in

Figure 1. We suggest that there exists a lattice excitation (E2) associated to atomic rotations around the c -axis that can be excited by $e // c$ similarly to conventional optical phonons. Its magneto active counterpart E1 is more subtle: it required a static polarization P_{\perp} perpendicular to the c -axis. The shift in energy between E1 and E2 reflects the dispersion curve of these excitations: while E1 is excited at $q=0$ as for an optical phonon seen in optical spectroscopy, E2 is excited for a wave vector Q corresponding to the periodicity of P_{\perp} along the c -axis. We have then foreseen the existence, below T_p , of a polar helicoidal state. It is formed by an helical arrangement of electric dipoles which, due to the chirality of the compound, must itself have a definite sense of rotation. Our findings widen the type of magneto-electric excitations that could be used for magnonics applications.



2 THz excitations probed with a $125 \mu\text{m}$ beam splitter. (a) Absorption spectra relative to the one at 45 K. Insert: Gaussian fits. (b) (c) (d) temperature dependence of the fits position, width and area.



3 THz excitations probed with the $6 \mu\text{m}$ beam splitter. (a) Absorption spectra obtained for $e // c$ and $h \perp c$. Insert: Gaussian fits. (b) (c) (d) Temperature dependence of the fits position, width and area. (e) (f) Same as (a) for the other THz polarizations.

AILES beamline

ASSOCIATED PUBLICATION

THz magnetoelectric atomic rotations in the chiral compound $\text{Ba}_3\text{NbFe}_3\text{Si}_2\text{O}_{14}$

L. Chaix, S. de Brion*, F. Lévy-Bertrand, V. Simonet, R. Ballou, B. Canals, P. Lejay, J.B. Brubach, G. Creff, F. Willaert, P. Roy and A. Cano

Physical Review Letters 110 (2013) 157208

CORRESPONDING AUTHOR

* Institut Néel, CNRS - Université Joseph Fourier, BP166, 38042 Grenoble Cedex 9, France

sophie.debrion@neel.cnrs.fr

REFERENCES

- [1] N.A. Spaldin & M. Fiebig, Science 309 (2005), 391
- [2] A. Pimenov et al. Nat. Phys. 2 (2006), 97
- [3] R. D. Johnson et al. Phys. Rev. Lett. 108 (2012), 067201
- [4] K. Marty et al. Phys. Rev. Lett. 101 (2008), 247201
- [5] M. Loire et al. Phys. Rev. Lett. 106 (2011), 207201

Molecular refrigerators

Experiments performed at DEIMOS beamline by a team of researchers of the Italian National Research Councils (CNR), the University of Manchester and French CNRS found that a single molecule may well work as magnetic refrigerator on its own. This is possible by exploiting the magnetic properties of special class of molecules, i.e. paramagnetic organometallic compounds that show a particular behavior, known as magnetocaloric effect (MCE), which makes them excellent refrigerants at cryogenic temperatures. “besides the curiosity” - explains the researcher - “this opens the way to miniaturize devices –such as highly sensitive detectors of electromagnetic waves- on one chip where a thin layer of such a molecule can be used to cool down the whole chip.” Their results are published in *Advanced Materials*.

Introduction

Research in nanotechnology aims at scaling down the size of systems and devices while maintaining interesting performances down to few nanometers,

that is approx. 10000 times smaller than a human hair. Along this line, researchers are currently investigating how small a refrigerator can be.

The magnetocaloric effect

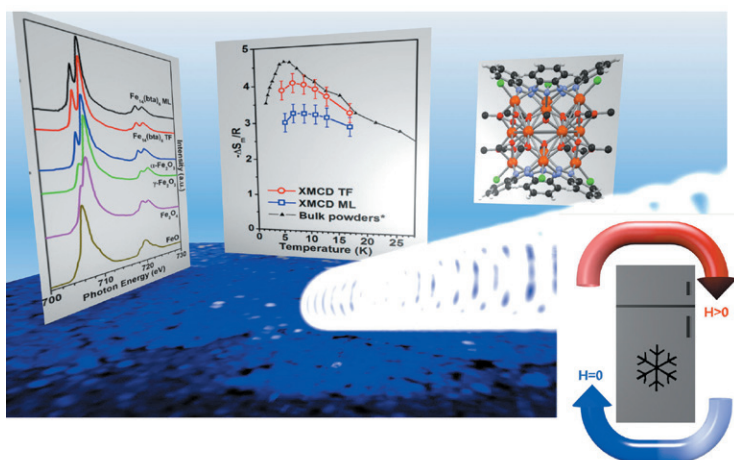
The magnetocaloric effect occurs by performing a particular thermodynamic cycle, called adiabatic demagnetization, which exploits the variation of entropy due to the application and subsequent adiabatic removal of an external magnetic field that induces a temperature decrease. The magnetocaloric effect is quantified by the change in entropy per unit mass: although this effect occurs in many magnetic materials, only in a few cases the entropy change is large enough to make magnetic materials usable as refrigerants

in practice. Molecular nanomagnets, to exhibit a strong magnetocaloric effect, must be characterized by a ground state with high spin and low entropy, should have a low magnetic anisotropy, which facilitates the polarization in the presence of a magnetic field, these facts give rise to an excess of entropy resulting from the presence of low-lying excited spin states. Finally, to optimize cooling performances in working conditions, the molecular mass should be small for a given change in magnetic entropy.

A layer of molecular iron clusters

In the experiments performed at SOLEIL, a sub-monolayer of molecular iron clusters, namely $\text{Fe}_{14}(\text{bta})_6$, have been deposited on substrates and its magnetic cycle has been studied by using polarized X-ray radiation. The substrates used were gold and graphite (HOPG, Highly Ordered Pyrolytic Graphite). The samples were produced from liquid solutions with dichloromethane (DCM) as solvents. For the analysis other surface techniques

have been employed, including STM, XPS, AFM, FTIR. However, the use of synchrotron radiation allowed, for the first time, to directly observe huge magnetocaloric effect at the level of a single molecule and to establish that cooperative effects, like long range order which is dominant in conventional magnetic refrigerants, play only a minor role in this case.



❶ A sub-monolayer distribution of isolated molecular $\text{Fe}_4(\text{bta})_6$ nanomagnets is deposited intact on a Au(111) surface and investigated by X-ray magnetic circular dichroism spectroscopy. The entropy variation with respect to the applied magnetic field is extracted from the magnetization curves and evidences high magnetocaloric values at the single molecule level.

DEIMOS beamline

ASSOCIATED PUBLICATION

Magnetic cooling at a single molecule level: a spectroscopic investigation of isolated molecules on a surface

V. Corradini, A. Ghirri, A. Candini, R. Biagi, U. del Pennino, G. Dotti, E. Otero, F. Choueikani, R. J. Blagg, E. L. J. McInnes and M. Affronte*

Advanced Materials 25(20) (2013) 2816

CORRESPONDING AUTHOR

*S3 Centre, Institute Nanoscience - CNR, via G. Campi 213/A, 41125 Modena, Italy
marco.affronte@unimore.it

Caffeine in cosmetics – optimizing its release into the body by means of “MOFs”

Hybrid metal-organic frameworks or MOFs are very promising candidates for societally relevant applications in catalysis, separation or, more recently, biomedicine. A group from Institut Lavoisier de Versailles, pioneer in the MOF biomedical field, has studied, notably on the CRISTAL beamline, the encapsulation and release of caffeine, which is of great interest to the cosmetics industry due to its lipolytic action.

Introduction

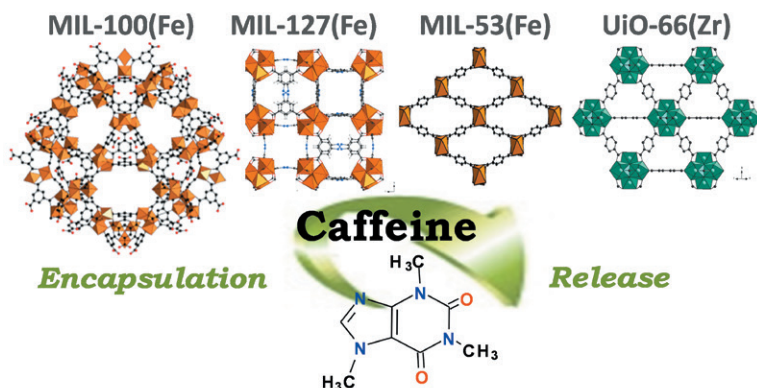
MOFs or (metal-organic-frameworks) typically consist of a regular assembly of inorganic entities (clusters, chains, planes...) and organic ligands combining polycomplexing functions (carboxylates, phosphonates...) [1]. These crystalline solids possess a network of regular micro- or meso-porous cavities and channels. The versatility of their structures (porosity/ connectivity, topology, etc.) and their chemical compositions (metal, ligand) make MOFs very promising candidates for applications in strategic areas such as catalysis, separation [1] or, more recently, biomedicine [2]. In particular, their high and regular porosity, as well as the presence of an amphiphilic environment (having both hydrophilic and hydrophobic parts, metal cation and organic ligand), well-adapted to the adsorption of different drugs, have led to remarkable encapsulation capabilities and progressive releases under physiological conditions [3]. A thorough microscopic understanding of both the encapsulation and release

of the active ingredient from MOF-type carriers is however crucial for a better control of these processes. This has motivated the recent studies of the group of Institut Lavoisier, pioneer in this field, which are focused on streamlining the encapsulation of therapeutic molecules within a series of porous MOFs [4]. In this context, a systematic study of the main factors governing the encapsulation of active ingredients and their release kinetics from MOFs with various topologies and chemical compositions was performed by combining experimental techniques and numerical simulations performed in collaboration with one group of Institut Charles Gerhardt Montpellier (Figure 1). The caffeine molecule, exhibiting a remarkable lipolytic action highly suitable for the cosmetics field, was selected. Indeed, the current lack of effective caffeine formulations on the market is mainly due to its strong tendency to crystallize, which leads to low capacities (< 5 wt%) and uncontrolled releases [5].

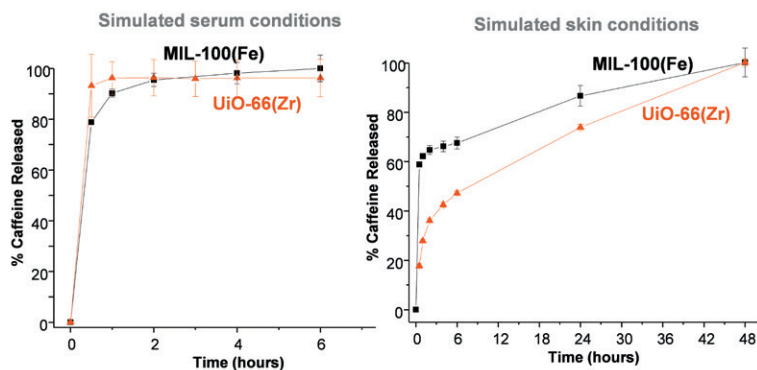
Results

MOFs have proved to be very promising candidates to overcome this technological barrier in the cosmetics industry (see related publication). In particular, an exceptional encapsulation rate of 50 wt% was achieved using biocompatible MOFs such as the mesoporous iron(III) trimesate MIL-100(Fe). In addition, the structures of flexible MOFs loaded with caffeine has been analyzed through a combination of high resolution X-ray powder diffraction data on the CRISTAL beamline, and numerical simulations (density functional theory) to better understand the conformation of caffeine and its interactions with the pore walls. For instance, the caffeine is not aligned along the direction of the tunnel of the microporous iron(III) terephthalate MIL-53 but adopts an orientation at a slight angle to the channel axis, leading to interactions through relatively strong hydrogen bonding between the oxygen of the caffeine carbonyl group and the hydroxy group

present at the MOF inner pore wall. Furthermore, the release of caffeine strongly depends on the nature of the medium (Figure 2). Under serum conditions (phosphate buffer solution pH = 7.4, 37°C), caffeine is rapidly released following on the whole the degradation of the MOF, while in a simulated skin physiological medium (distilled water pH = 6.3, 37°C), caffeine is progressively delivered, as a consequence of the degree of confinement and MOF-drug interactions. Thus, considering a typical cosmetic administration ranging between 8 and 24 h, the most promising porous MOFs for the topical administration of caffeine are the mesoporous iron(III) trimesate MIL-100(Fe) and the microporous zirconium(IV) terephthalate UiO-66(Zr), which combine record caffeine encapsulation rates and progressive releases over 24 hours.



1 Schematic representation of the selected MOFs : MIL-100(Fe), MIL-127(Fe), MIL-53(Fe) and UiO-66(Zr) structures and caffeine molecule (MIL: Materials from Institut Lavoisier; UiO: University of Oslo). Iron and zirconium polyhedra and carbon atoms are in orange, blue and black, respectively. Hydrogen atoms have been omitted for clarity.



2 Caffeine release from UiO-66(Zr) and MIL-100(Fe) under simulated serum (left) or skin conditions (right) ($T=37^{\circ}\text{C}$).

CRISTAL beamline

ASSOCIATED PUBLICATION

Rationale of drug encapsulation and release from biocompatible porous Metal–Organic Frameworks

D. Cunha, M. Ben Yahia, S. Hall, S. R. Miller, H. Chevreau, E. Elkaim, G. Maurin, P. Horcajada*, and C. Serre

Chemistry of Materials 25 (2013) 2767

CORRESPONDING AUTHOR

*Institut Lavoisier, UMR CNRS 8180, Université de Versailles Saint-Quentin-en-Yvelines, 45 avenue des Etats-Unis, 78035 Versailles cedex, France

patricia.horcajada-cortes@uvsq.fr

REFERENCES

- [1] Special issues: Chem. Soc. Rev, 2009 38, 1201; Chem. Rev., 112 (2012), 673.
- [2] P. Horcajada et al., Chem. Rev., 2012 112, 1232; J. Della Rocca et al., Acc. Chem. Res., 44 (2011), 957; I. Imaz et al., Chem. Comm., 47 (2011), 7287.
- [3] P. Horcajada et al., Angew. Chem. Int. Ed., 2006, 118, 6120; P. Horcajada et al., Nature Mater. 9 (2010), 172.
- [4] C. Gaudin et al., Micropor. Mesopor. Mater., 2012 157, 124 ; D. Cunha et al., J. Mater. Chem. B, 1(8) (2013), 1101.
- [5] E. Toutitou et al., J. Pharm. Sci., 83 (1994), 1189

Resonant magnetic x-ray scattering on artificial spin ice

We probed the magnetic signatures of an artificial spin ice with soft x-ray resonant magnetic scattering at the SEXTANTS beamline. Exploiting the extended view of reciprocal space accessible with a CCD detector, we could identify pure magnetic Bragg peaks associated with long-range ordering in the dipolar-coupled nanomagnet arrays. In addition, the evolution of the magnetization as a function of the applied field was determined from the magnetic circular dichroic contrast at the Bragg peak positions. These measurements provide an important step for the future study of frustrated nanomagnet systems with unprecedented spatial and temporal resolution.

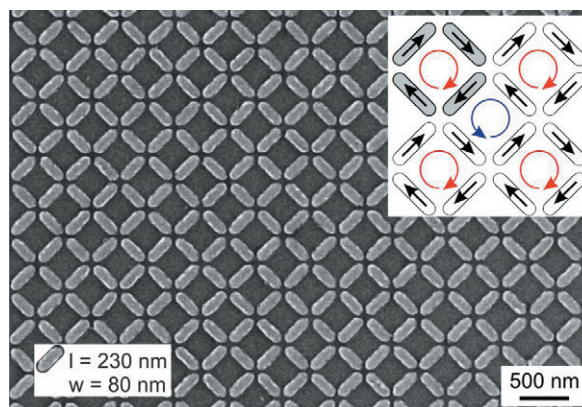
Introduction

Frustration is an important concept in physics, which arises in different systems when all interactions cannot be satisfied at the same time. Artificial spin ice, consisting of arrays of closely spaced nanomagnets placed at the sites of a square or kagome lattice [1], is an example of a magnetic system that is frustrated by the competition between the dipolar interactions.

Until now, microscopy methods have mainly been used to investigate artificial spin ice with the lateral dimensions of the nanomagnets typically of the order of hundreds of nanometres, which results in static magnetic moments [2]. By using superparamagnetic elements with smaller volumes, the magnetization dynamics in systems with magnetic fluctuations

can be accessed [3], so providing a new route to understand the mechanisms driving artificial spin ice. For studying such dynamics, scattering techniques offer an invaluable alternative to imaging, thanks to the significantly better spatial resolution and the promise of improved temporal resolution.

In this work, carried out at the SEXTANTS beamline, we studied artificial square ice (Figure 1) using soft x-ray resonant magnetic scattering (SXRMS). Using an in-vacuum CCD detector, we mapped a large fraction of the two dimensional reciprocal space at once, which allowed us to clearly distinguish all the relevant features of the scattering patterns, facilitating the interpretation of the data.

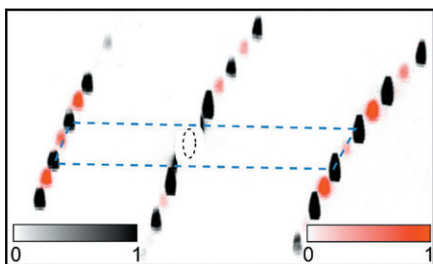


1 Scanning electron microscopy image of an artificial square ice array. The insert shows the magnetic ground-state ordering with the unit cell highlighted in grey.

Ordering revealed in as-grown artificial square ice

Artificial square ice has a magnetic ground state which can be observed in as-grown samples [4]. In this long-range ordered state, the magnetic moments form alternating vortices of opposite chirality, as depicted in the inset of Figure 1. Here the magnetic unit cell is bigger than the structural one, and the corresponding Bragg peaks in reciprocal space should appear at intermediate positions.

Tuning the photon energy to the Fe L_3 absorption edge, we measured scattering patterns sensitive to both the charge and the magnetic scattering (Figure 2), while going to off resonant photon energies gave pure charge scattering. Comparing the two measurements, we could unambiguously identify the pure magnetic peaks (shown in red) corresponding to the magnetic ground state ordering.



② Scattering pattern measured on the as-grown artificial square ice at the Fe L_3 edge. The structural Bragg peaks are coloured in black, and the magnetic peaks in red. The dashed frame highlights the first order diffraction peaks.

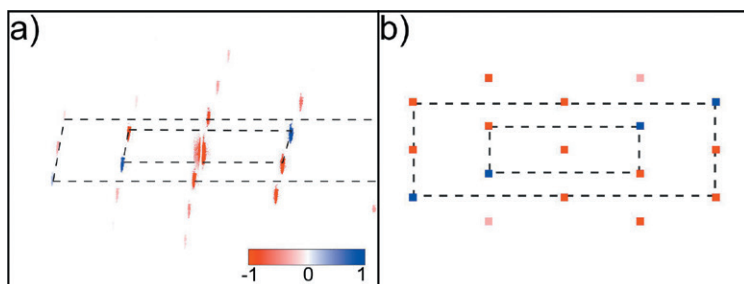
Magnetization reversal in individual sublattices

In order to follow the evolution of the magnetization in an applied magnetic field, we recorded scattering patterns of the magnetic configurations, making use of the x-ray magnetic circular dichroism (XMCD) at the Fe L_3 edge [5]. By calculating the difference between scattering patterns recorded with right and left circularly polarized x-rays, we observed a stepwise change of the XMCD contrast. An example of a dichroic pattern is shown in Figure ③a for a value of the applied magnetic field close to the coercive field.

Artificial square ice is composed of nanomagnets with two orientations, forming two distinct sublattices orthogonal to each other, which scatter the photons with different angular dependence. Therefore the dichroic patterns contain information not only on the total magnetization of the array, but also on the contributions from

the individual sublattices. To extract these contributions, we numerically simulated the scattering patterns taking into account the magnetization for each sublattice. Fitting the model to the experiment, we could quantitatively reproduce the dichroic intensity up to the second order Bragg peaks (Figure ③b), and therefore estimate the number of reversed moments in each sublattice for a given applied field.

In this work, we have demonstrated that important insights into the magnetic configuration of artificial spin ice can be obtained by SXRMS. This study opens the way to more sophisticated experiments, such as scattering with coherent x-rays, which will play an important role in the further investigation of thermally active systems and the understanding of frustration in systems with competing interactions.



③ (a) Dichroic scattering pattern measured at the Fe L_3 edge at the coercive field. (b) Numerical simulation of the scattering pattern. By matching the Bragg peak intensities, we are able to determine the number of reversed nanomagnets in each sublattice. The black dashed frames are a guide to the eyes.

SEXTANTS beamline

ASSOCIATED PUBLICATION

Extended reciprocal space observation of artificial spin ice with x-ray resonant magnetic scattering

J. Perron, L. Anghinolfi*, B. Tudu, N. Jaouen, J.M. Tonnerre, M. Sacchi, F. Nolting, J. Lüning and L.J. Heyderman

Physical Review B 88 (2013), 214424

CORRESPONDING AUTHOR

*Laboratory for Mesoscopic Systems, Department of Materials, ETH Zürich, 8093 Zürich, Switzerland; Paul Scherrer Institut, 5232 Villigen PSI, Switzerland

luca.anghinolfi@psi.ch

REFERENCES

- [1] L.J. Heyderman and R.L. Stamps. *J. Phys.: Condens. Matter.* 25 (2013), 363201
- [2] R.F. Wang et al. *Nature* 439 (2006), 303
- [3] A. Farhan et al. *Nat. Phys.* 9 (2013), 375
- [4] J.P. Morgan et al. *Nat. Phys.* 7 (2011), 75
- [5] C.T. Chen et al. *Phys. Rev. B* 42 (1990), 7262(R)

LuFe₂O_{4+x}: from multi-ferroicity to oxygen storage

A detailed investigation of multiferroic LuFe₂O₄ has shown that the layered structure of this compound is remarkably efficient in accommodating oxygen insertion or desorption, thus making rare-earth ferrites interesting candidates for applications as oxygen sensors or solid oxygen fuel cell oxides.



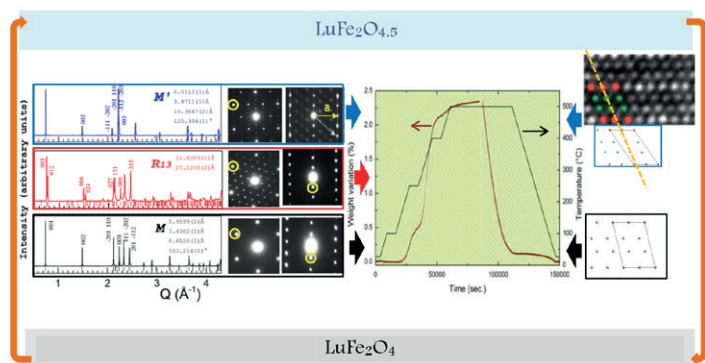
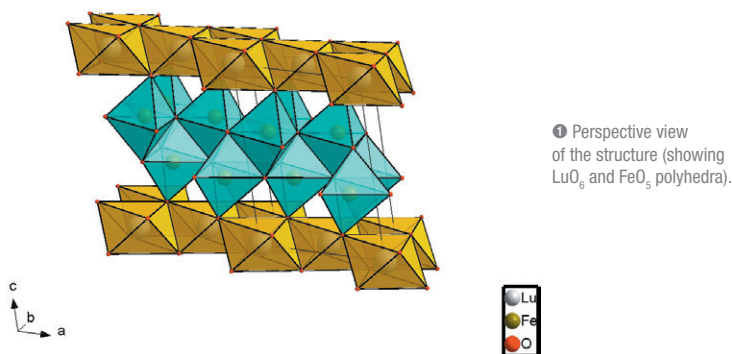
Transition metals oxides have been generating numerous studies in materials science for many years, owing to the variety of their structures and properties, some of the best-known examples being high critical temperature superconducting cuprates, or magnetoresistive manganites. Multiferroic compounds, *i.e.*, materials which exhibit two coupled ferroic properties, also occupy a privileged place, as the possibility to modify a property while playing on the other opens a large array of potential applications. The material under study, LuFe₂O₄, caught our attention because it was reported to be **ferroelectric** at room temperature - in relation with a charge ordering of iron +2 and +3 species [1], and **anti-ferromagnetic**, below 250 K [2]. In addition, the structure of this oxide is rather unique because it combines bi-dimensional and frustration characteristics, originating from the stacking of triangular [Fe₂O₄] and [LuO₂] slices (Figure 1).

Combining different complementary techniques, X-ray, neutron and electron powder diffraction (XRPD, NPD and ED, respectively), transmission electron microscopy including high resolution (TEM and HRTEM), thermal gravimetric analysis (TGA), and magnetic and electrical characterizations, we started to investigate the impact of small changes in the synthesis conditions upon the structural and magnetic behaviors of LuFe₂O₄ samples. The observation of small additional Bragg peaks, with respect to the expected structure, on the XRPD pattern, recorded at room temperature on the CRISTAL beamline, was hitherto confirmed by the existence of weak satellites in the ED patterns in some areas of the crystals [3]. The coherence between both types of results led us to attribute these satellites to an incommensurate modulation, originating from a very low oxygen excess with respect to stoichiometric LuFe₂O₄, and involving a nanoscale segregation between more and less oxygenated areas. This first indication of non-stoichiometry was at the origin of a comprehensive study of oxygen insertion - desorption in this ferrite.

TGA in controlled atmospheres, coupled with TEM and XRPD studies, have shown in the course of this subsequent study that it is possible to vary the oxygen content, **significantly**, and in a **controlled** manner, from LuFe₂O₄ to LuFe₂O_{4.5}. The characteristics of the successive steps are schematized in Figure 2. The introduction of oxygen in the matrix occurs through the progressive extension of modulated regions, followed by sliding, layer by layer, of the [Lu] and [Fe] planes against each other, until a new monoclinic structure is formed. This structure (O_{4.5}) is very stable up to 700°C and, moreover, reducing annealing (under Ar/H₂) restores the initial structure (O₄). This intercalation/de-intercalation mechanism is topotactic, as in the battery materials, and the compound quality is maintained despite the relative sliding of the layers.

The cycling ability was tested with five consecutive cycles of oxidation/ reduction, and the storage capacity was determined to be 1642 μmolOg⁻¹, in agreement with the O₄ to O_{4.5} evolution, which is accompanied by a rather uncommon increase of the cell volume. The reaction conditions at low temperatures, the high sensitivity to oxygen, the stability of the different phases (vs. the oxygen content) and the structural phenomena involved in the transitions allow one to consider the use of this material in systems such as sensors, solid oxygen fuel cell oxide (SOFC) or catalysts. Indeed, the layer sliding mechanism is known to accommodate efficiently non-stoichiometry and to prevent structural collapses. In addition, the wide range of temperature, of time and of partial oxygen pressure, in which both valences of iron (+2 and +3) can coexist, also suggests that this compound could be used as a catalyst for the degradation of pollutants and alkanes.

The interest for the LnFe₂O₄ type of compounds (Ln = Y and Ho Lu) is reinforced by this discovery, and add another degree of freedom, **oxygen content**, as a new path to multifunctionality.



② Schema of the successive steps of the process, XRD data (CRISTAL), ED patterns, TGA and drawing of the layer sliding (from left to right).

CRISTAL beamline

ASSOCIATED PUBLICATION

Oxygen storage capacity and structural flexibility of $\text{LuFe}_2\text{O}_{4+x}$ ($0 \leq x \leq 0.5$)

M. Hervieu, A. Guesdon, J. Bourgeois, E. Elkaïm, M. Poiénar, F. Damay, J. Rouquette, A. Maignan and C. Martin*

Nature Materials, published online: 24 Nov 2013, doi: 10.1038/NMAT3809

CORRESPONDING AUTHOR

*Laboratoire CRISMAT, ENSICAEN, UMR 6508 CNRS, 6 Boulevard du Maréchal Juin, 14050 Caen Cedex, France

christine.martin@ensicaen.fr

REFERENCES

- [1] N. Ikeda et al. Nature 436 (2005), 1136
- [2] J. Bourgeois et al. Phys. Rev. B 86 (2012), 024413
- [3] J. Bourgeois et al. Phys. Rev. B 85 (2012) 064102



MODELING, METHODOLOGY AND INSTRUMENTATION

- 114** SPI Boards Package a flexible multipurpose set of boards for various scientific applications
- 116** An in-house developed X-ray imaging detector for synchrotron based micro-tomography
- 118** A new double charged particle imaging spectrometer for gas phase VUV photoionization studies
- 120** Development of high performance heat transfer devices for synchrotron facilities
- 122** A new tool for greenhouse gases Infrared absorption modelling
- 124** A versatile source to make complex nanoscopic objects fly under vacuum
- 126** Simultaneous fast-scanning XRF, dark field, phase-, and absorption contrast tomography
- 128** The secondary source of NANOSCOPIUM

MODELING, METHODOLOGY AND INSTRUMENTATION

In 2013, the Modeling, Methodology and Instrumentation section at SOLEIL again presented a number of new instruments in the service of science. This year, proposals from all divisions (Experimentation, Computers & Electronics and Technical & Valorization Services) made it possible to offer diverse contributions showing, yet again, how dynamic instrumentation is at SOLEIL. Naturally, the cross-disciplinary approach of the groups is at the heart of this dynamism. On the AILES beamline, a new cryogenic cell for infrared spectroscopy, on DESIRS, a new spectrometer for gas phase studies, on PLEIADES, a new chamber for the production of nanoparticles. In supporting laboratories, the study and development of heat sinks with high heat transfer coefficients and the commissioning of a laboratory for the study of thermal phenomena. The development of new detectors used for tomography applications and a system of slits or secondary sources for the NANOSCOPIUM beamline, with its unusual mechanical and thermal constraints. Finally, new acquisition boards (SPI BOARD PACKAGE) for synchronizing multiple commands or samples with the detector.

This transition period between the beamline construction phases and the operational phase is an ideal time for the MMI section. Indeed, now we have the opportunity to restructure our activities, with the aim of pooling skills to foster the emergence of new projects. With instrumentation increasingly at the cutting edge, driven by future Diffraction Limited Storage Rings and LUNEX5, it must meet extreme analysis conditions (spatial, spectral and temporal resolutions). The success of SOLEIL's own research is equally challenging and fulfilling for the members of this section. Indirectly, we have contributed to the scientific achievements presented in this Highlights 2013, which makes us very proud!

Muriel Thomasset & Pascale Prigent

Heads of the "Modeling, Methodology and Instrumentation " Scientific Section

MODÉLISATION, MÉTHODOLOGIE ET INSTRUMENTATION

En 2013, la section Modélisation, Méthodologie et Instrumentation de SOLEIL présente, encore une fois, un nombre de nouveaux outils instrumentaux au service de la science. Cette année, des propositions émanant de toutes les divisions (Expériences, Informatique & Electronique et Service Techniques & Valorisation) permettent de présenter des contributions diverses montrant, à nouveau, le dynamisme de l'instrumentation à SOLEIL. Naturellement, la transversalité des équipes est au cœur de ce dynamisme. Sur la ligne AILES, une nouvelle cellule cryogénique pour la spectroscopie infrarouge, sur DESIRS, un nouveau spectromètre pour des études en phase gazeuse, sur PLEIADES, une nouvelle chambre pour la production de nanoparticules. Dans les laboratoires support, l'étude et le développement de dissipateurs à chaleur à fort coefficient d'échange, la mise en service d'un laboratoire pour l'étude des phénomènes thermiques. Le développement de nouveaux détecteurs pour des applications de tomographie, le dispositif de fentes pour la source secondaire de la ligne NANOSCOPIUM ayant des contraintes mécaniques et thermiques hors du commun. Et pour finir, de nouvelles cartes d'acquisition (SPI BOARD PACKAGE) pour des applications de synchronisation de commandes multiples ou d'échantillons avec le détecteur.

La transition entre la phase de construction des lignes de lumière et la phase d'opération est un moment privilégié pour la section MMI. En effet, ce moment est l'occasion de structurer nos activités autrement, avec pour objectif la mise en commun des compétences pour favoriser l'émergence de nouveaux projets. L'instrumentation, toujours plus aux limites, portée par les futurs Diffraction Limited Storage Rings et LUNEX5, devra répondre aux conditions d'analyses extrêmes (résolutions spatiales, spectrales et temporelles). La réussite de cette recherche propre à SOLEIL est également motivante et épanouissante pour les membres de la section. Indirectement, nous contribuons aux succès scientifiques présentés dans ce Highlights 2013 et nous en sommes très fiers !

Muriel Thomasset & Pascale Prigent

Responsables de la Section Scientifique « Modélisation, Méthodologie et Instrumentation »

SPI Boards Package a flexible multipurpose set of boards for various scientific applications

The machine and beamlines continually improve their performance: to be able to perform fast and complex experimental data acquisition we need to control accurately the beam parameters and to synchronize the data with the sample position or angle in order to focus only on useful data. The SPI Boards Package is a set of electronic boards developed in order to provide a simple and modular solution for the applications requiring such synchronization or embedded control tasks.

Since 2008, when the accelerators and beamlines received users, operational feedback has allowed us to identify some ways of responding to requests for rapid and synchronous data acquisition. This challenge has been met in two specific scientific domains:

- The first domain is the synchronization of multiple-commands to electromagnetic insertion devices in the storage ring, as a function of the settings of the machine and in order to improve beam stability.
- The second domain is the synchronization of detectors with motorized devices like sample stage or goniometer in order to acquire and accurately characterize the pertinent data.

The SPI BOARDS PACKAGE (SPIBP) is a set of electronic boards allowing to embed process-specific and synchronization functions at low level. It gives us a modular platform to develop solutions with simple, reliable and durable tools. In the SPIBP architecture, the boards can be connected together in a daisy chain, and communicate with a controller via a Serial Peripheral Interface (SPI) Bus. Communication with the SOLEIL software control and data acquisition system is performed via Ethernet. Each board can be connected with others as needed. The SPIBP enables us to deliver solutions for applications with either analog interface or position encoders. We can control or command directly power supplies that drive electro-magnets or process any position encoder signal in order to correlate data on photon energy or sample position.

In the first domain, a typical application is to improve the beam stability by embedding feedforward control for electromagnetic insertion devices inside a SPI platform. For instance, the ElectroMagnetic/Permanent magnets Helical Undulator (EMPHU) is made of steel poles surrounded by coils and permanent magnets fixed on two girders which are attached to a motorized carriage. In this configuration, the vertical field is generated by means of main coils powered by a DC current, and the horizontal magnetic field by permanent magnets. The vertical movement of the girders then changes the peak field values. In addition to the power supply of the main coils, 8 sets of coils locally correct the magnetic field. For the feedforward correction, lookup tables are defined to predict the value of all power supplies as function of the girder position and the current in the main coils. The changes of the polarization and parameterization with tables downloaded inside the SPI platform are requested from the supervision. In operation the SPI platform reads directly the girder position thanks to a position encoder input and generates analog signals synchronously to drive the 9 power supplies of EMPHU. The SPI platform manages both the fast switching of the EMPHU and the beam correction. This undulator is the second source for the DEIMOS beamline, dedicated to the study of magnetic and electronic properties using polarized light. During dichroism experiments the sample is scanned alternatively in right and left polarization. EMPHU fast polarization switching rate is



① The SPIController, a board of the SPIBP.

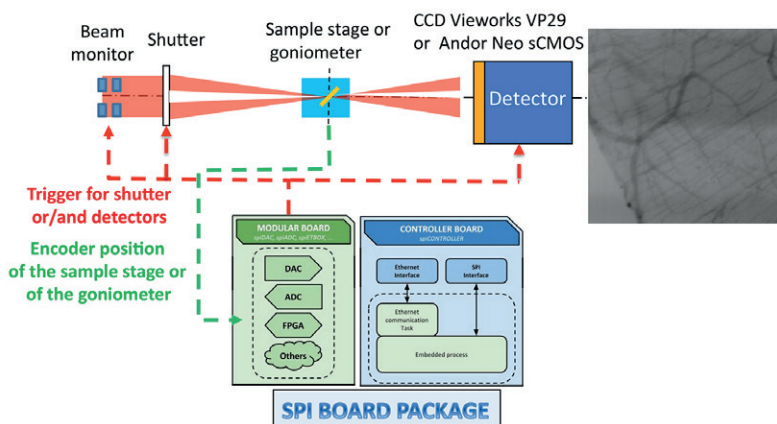
achieved in less than 200ms and enables a reduction of the noise resulting from the drift in environmental conditions (beam orbit drift, temperature, even the sample itself).

In the second domain, the aim is to allow simultaneous acquisition on one or more detectors in correlation with sample scanning.

On the PROXIMA 1 beamline which studies the 3D structure of protein molecules, a SPI platform opens a shutter and triggers the acquisition of a Pilatus pixel array detector and an X-ray beam position monitoring system once the goniometer has reached its nominal speed. In this case the SPI platform reads a position encoder and performs calculation before sending digital output to open the shutter and to trigger the detectors. Synchronized images

and corresponding beam metadata can be obtained in a rapid (10ms) timescale. On the METROLOGY beamline, the IPANEMA team has used a similar platform to trigger cameras based on the sample stage position to achieve a tomographic experiment (Figure 2). In this case the time spent for each dataset collection is between 5 to 20 min for 2500 to 7000 images collected and a total of up to 180 GB of raw data. We gain a factor of 20 in comparison to traditional step by step scanning method.

Today 18 SPI platforms are in operation in SOLEIL with different configurations and many other future uses can be imagined. The SPI Board package is developed as an open hardware development and shared under CERN OHL V1.1 license on www.ohwr.org.



2 Synchronous acquisition with the sample position or movement

Control & Data Acquisition Computing and Electronics Group

ASSOCIATED PUBLICATION

Y.M. Abiven*, P. Betinelli, J. Bisou, F. Blache, S.X. Cohen, P. Gourhant, N. Leclercq, F. Langlois, F. Marteau, P. Ohresser, and A. Thompson

CORRESPONDING AUTHOR

* Synchrotron SOLEIL, l'Orme des Merisiers, St Aubin BP48, 91192 Gif sur Yvette Cedex, France

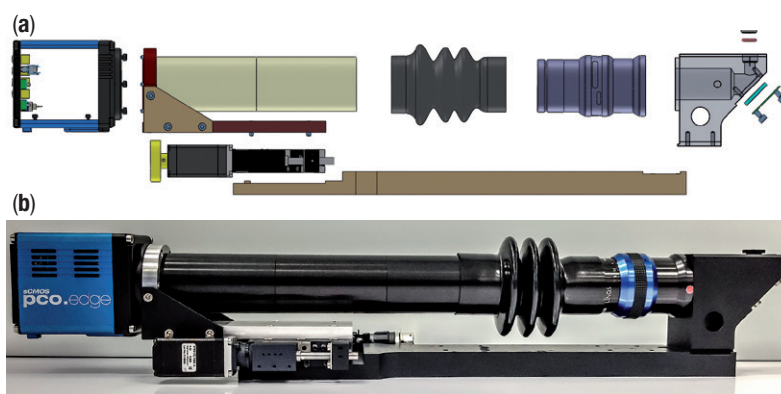
yves-marie.abiven@synchrotron-soleil.fr

An in-house developed X-ray imaging detector for synchrotron based micro-tomography

Hard X-ray micro-tomography is a powerful tool to reveal the internal structure of thick objects in a non-destructive manner. The unique characteristics of synchrotron radiation, such as high flux, monochromaticity, and partial coherence facilitate sensitive fast tomography in absorption and phase contrast modes, down to micrometer spatial resolution. For these imaging techniques, the performances of the detector are particularly important [1]. The Detectors and Design & Engineering groups at SOLEIL, in collaboration with Paris Sud Orsay University, have designed, developed, manufactured and assembled a fast, sensitive and high resolution indirect imaging X-ray detector with the goal of carrying out preliminary micro-tomography test experiments on SOLEIL beamlines, and to be used by students for practical classes. We present here the performances of the X-ray detector deduced from measurements on the METROLOGY beamline and we demonstrate the feasibility of phase contrast tomographic reconstruction with a test sample.

The detector is based on a thin single crystal scintillator screen YAG:Ce (20 μ m freestanding) coupled with a low distortion objective (QIOP TIC Inspec.xL 105mm f/4 – G3) allowing to magnify by three the image onto a new generation CMOS scientific sensor (2560 x 2160 pixels) of the low noise and high speed (100Hz) PCO edge camera [2]. The field of view is 4.7 mm x 5.5 mm with pixels of 2.3 μ m. A 45° tilted mirror, inserted between the scintillator and the objective, reflects the visible light coming from the scintillator out of the X-rays axis, to prevent any radiation damage on the sensor. The characteristics of these

components were beforehand measured in laboratory with visible light and, especially, the Numerical Aperture (NA) of the objective and the PCO Edge camera properties (dark noise, saturation capacity and electronic gain). The measurement results are summarized in Table 1. A mechanical assembly was designed in-house, with a motorized translation to focus the optics onto the scintillator screen. A particular attention was given to the parallelism between of the different plans: sensor, mirror and scintillator screen. Figure 1 gives a detailed 3D view of the mechanical concept and a picture of the X-ray detector.



1 X-ray tomography detector (a) Exploded 3D view of mechanical design (b) Final device photography

TABLE 1: X-RAY DETECTOR CHARACTERISTICS

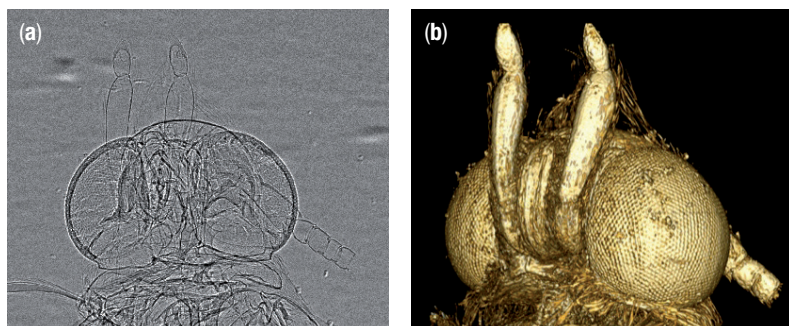
Camera	Scientific CMOS - PCO Edge
Frame rate	Max. 100 fps
Pixel format	2560 x 2160 pixel
Pixel size	6.5 μ m
Analog-to-digital resolution	16 bits
Gain e ⁻ / analog-to-digital unit	0.545 e ⁻ /ADU
Saturation capacity	29155 e ⁻
Dark current	2-6 e ⁻ /pixel/s
Temporal dark noise	1.5 e ⁻
Objective	Qioptic Inspec.xL 105 mm f/4, M = 2.86
Numerical aperture (NA)	0.125
Working distance	81.3 mm
Scintillator	YAG:Ce \varnothing 9mm x 20.2 μ m (+/-0.2 μ m)
Image size	5.55 mm x 4.17 mm
Pixel Image size	2.3 μ m

The X-ray detector performances were assessed with 17.4 keV photons at the METROLOGY beamline. The overall gain value was measured to be 0.005 ADU/X-ray, therefore in accordance with the absorption of the 20 μ m YAG:Ce scintillator and the objective collection efficiency evaluated [3]. The X-ray detector spatial resolution was deduced from the modulation transfer function (MTF) calculated by Fourier transform of the Line Spread Function obtained with a classical knife edge method [4]. The measurement is in good agreement with the analytical model with 10% modulation transfer contrast obtained around 61 cy/mm, corresponding to a detail object of 8 μ m. Finally, the Detective Quantum Efficiency (DQE) was inferred from the Noise power spectrum measurement. The calculated DQE (0 cy/mm) is only 2% and this low value is due to the poor X-ray absorption of the scintillator and the limited light collection of the optics.

The first phase-contrast tomography reconstruction of the head of a small insect (food moth) has been carried out on the METROLOGY beamline and demonstrates clearly the performance

of this X-ray imaging detector. For this tomographic acquisition, 2000 images over 180° have been taken. The tomograms were reconstructed, see in figure 2.

These results, in particular the spatial resolution, shows that the expertise gained with the development and characterization of many beam viewers or X-ray cameras enables SOLEIL to design, build and qualify to completeness more complex imaging systems. The skills of the Detector and Design and Engineering groups, the capabilities of the Mechanical workshop and the availability of the X-ray beam and of a versatile end station on the METROLOGY beamline allow to design instruments exactly tailored to the experimental requirements of the imaging applications of SOLEIL. The detector shall be used soon to produce a fast (a few minutes only) large tomography reconstruction from a few thousand images, taking advantage of a high flux white beam and of the high frame rate of the camera [5]. Furthermore, other detectors are currently designed in house for the tomography beamlines of SOLEIL.



2 Image of the head of a moth (a) In-line phase contrast. (b) Volume rendering of the Edge Enhancement Computed Tomography.

Detector & Conception Engineering Groups

ASSOCIATED PUBLICATION

MTF, NPS and DQE characterization of an in-house developed X-ray imaging detector for synchrotron based micro-tomography

K. Desjardins*, M. Bordessoule, S. Hustache, C. Meneglier, A. Carcy, S. Bonnin and K. Medjoubi

IWORID 2013 Proceeding

CORRESPONDING AUTHOR

* Synchrotron SOLEIL, l'Orme des Merisiers, St Aubin BP48, 91192 Gif sur Yvette Cedex, France

kewin.desjardins@synchrotron-soleil.fr

REFERENCES

- [1] P.-A. Douissard et al. 2012 JINST 7 P09016
- [2] PCO, <http://www.pco.de>
- [3] Lui et al, Med. Phys. 21 (1994) (7):1193
- [4] International Standard ISO 12233:2000(E)
- [5] K. Medjoubi et al. J. Synchrotron Rad. 20(2) (2013) 293

A new double charged particle imaging spectrometer for gas phase VUV photoionization studies

The electron/ion double coincidence imaging spectrometer Delicious III, is the successful continuation of our pioneering efforts to couple the velocity map imaging (VMI) technique to a synchrotron beamline, to benefit from its high collection efficiency, particle energy resolution and multiplex capabilities. The new coincidence scheme has been extended to include ion imaging and now allows high quality photoelectron images to be filtered as a function of the cation mass, translational energy and direction, which opens new avenues of research in photochemistry or cluster science.

At DESIRS, two permanent endstations are available for external users, one of which, the molecular beam chamber SAPHIRS, is dedicated to valence-shell photoionization processes in the gas phase on a large variety of systems, from bare atoms up to nanoparticles, spanning several scientific fields. Thus, the endstation must be extremely versatile while guaranteeing a certain degree of specialization for tailored individual needs, all in a user-friendly manner and reliably.

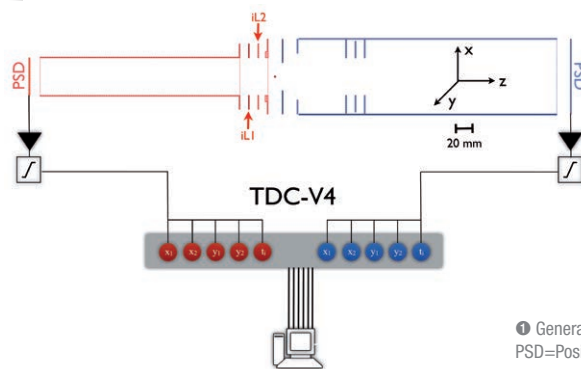
To obtain a complete picture of the photoionization event, we start by dramatically reducing the number of initial states available in the neutral through the use of a molecular beam, where the neutral's internal energy is converted into kinetic energy along the beam's direction. Then we study, with as much detail as possible, the final state consisting of a departing electron plus cation, and how the initial energy deposited into the system is shared and evolves among the different degrees of freedom (electronic and nuclear continua).

To achieve this goal in the most comprehensive way, the spectrometer, DELICIOUS III, is capable of separating the different photoionization events in time, so that an electron can be correlated to a given ion coming from *the same* photoionization event, the so-called PhotoElectron Photon COincidence scheme, or PEPICO. More precisely the spectrometer, as shown in Figure 1,

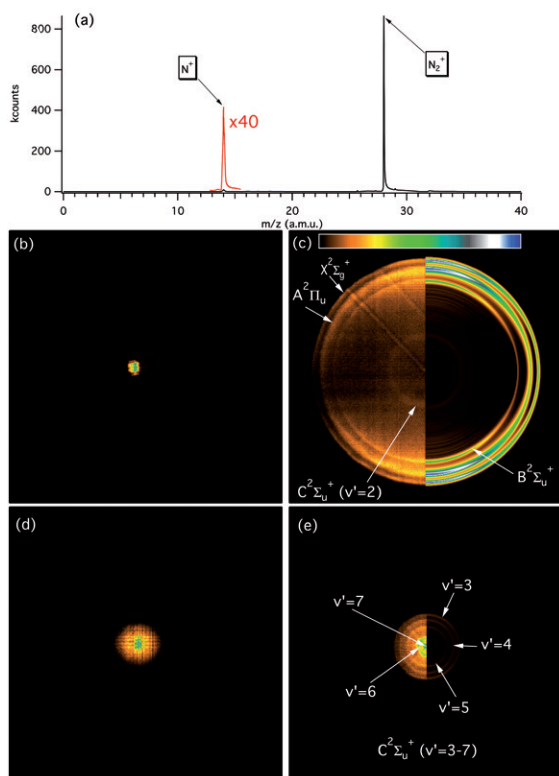
is based upon a double imaging concept, which yields the full cation velocity vector, i.e., total kinetic energy and angles of ejection, and correlates this information with the photoelectron velocity mapped images, so that the photoelectrons can be filtered in ion mass, ion direction and ion kinetic energy.

The multidimensional data delivered by DELICIOUS III can be reduced in many ways and will stimulate new experimental research on photochemistry or cluster science. As an example of the performances, let us consider the photoionization of N_2 above its dissociation threshold, i.e., at a photon energy of 25.6 eV. The absorption of the photon produces an electron and a N_2^+ cation with a wide distribution of internal energies, depending on the kinetic energy of the departing photoelectron. If the amount of internal energy is above the dissociation threshold, the parent ion will break to give $N + N^+$. Figure 2 shows the raw coincident photoelectron and photoion images for the N_2^+ and N^+ obtained after applying the mass filter. The position and arrival times of the particles are then extracted and converted to velocity distributions to yield the results displayed in Figure 3.

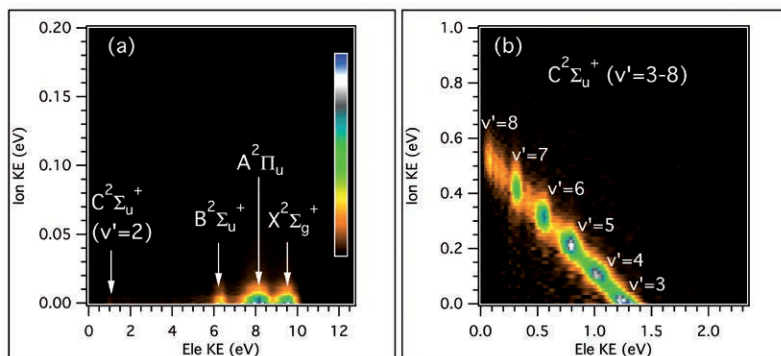
Delicious III has been conceived *in-house* at SOLEIL, from the ray-tracing simulations to the mechanical conception, and most of the electronics have been custom-made by nearby groups, perpetuating the know-how within the Orsay/Saclay area.



1 General principle of DELICIOUS III.
PSD=Position Sensitive Detectors



② (a) Mass spectrum showing the N_2^+ and N^+ ions. The left figures, (b) and (d) present the photoion images for the N_2^+ and N^+ masses respectively. The right figures (c) and (e), correspond to the photoelectrons correlated to the production of N_2^+ and N^+ , resp. In all the 2D images, the radius is proportional to the particles' kinetic energy.



③ Electron/ion kinetic energy correlation diagrams for the photoionization of molecular nitrogen above the dissociative ionization threshold for the N_2^+ and N^+ masses. The internal energy of the N_2^+ ion is given by energy conservation as: $h\nu = E_{int} + KE_{ele}$, so that very fast electrons are correlated to ions with small internal energy. Conversely, for slow photoelectrons, the parent ion will have an important energy reservoir that will be dissipated via dissociation to $N_2^+ \rightarrow N^+ + N$. Therefore, panel (a) shows that the N_2^+ ion has no translational energy (does not come from a fragmentation event), and can exist only for fast photoelectrons. Panel (b) shows that the N^+ fragment only appears for slow photoelectrons ($KE_{ele} < 1.25$ eV, correlated to the C electronic state of the N_2^+ cation), and the fact that intensity appears along a diagonal line means that only one dissociation channel is open. The figure provides a very clear picture of the spectroscopy of the parent ion, as well as its fragmentation pathways—appearance energies and barrier heights.

DESIRS beamline

ASSOCIATED PUBLICATION

DELICIOUS III: A multipurpose double imaging particle coincidence spectrometer for gas phase vacuum ultraviolet photodynamics studies

G. A. Garcia*, B. K. C. De Miranda, M. Tia, S. Daly, and L. Nahon

Review of Scientific Instruments 84(5) (2013) art. n°053112

CORRESPONDING AUTHOR

* Synchrotron SOLEIL, l'Orme des Merisiers, St Aubin BP48, 91192 Gif sur Yvette Cedex, France

gustavo.garcia@synchrotron-soleil.fr

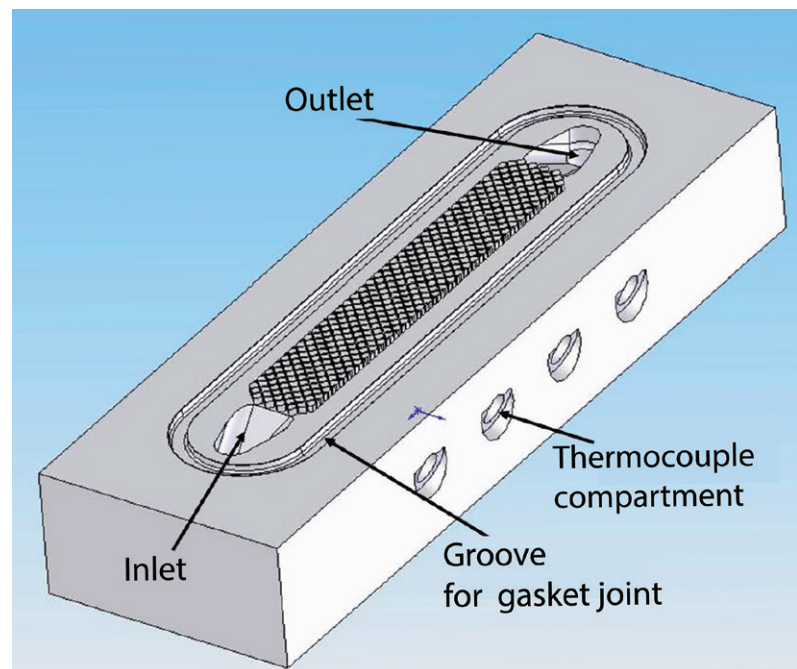
Development of high performance heat transfer devices for synchrotron facilities

Design of light beam absorbers for synchrotron facilities requires knowledge of the actual performance of heat sinks. More specifically, the key parameters are firstly the heat transfer coefficient at fluid-structure interfaces and secondly the head losses. Conventional approach is not always practical since for the more demanding situations it either results in over-design, uneconomical process, or even failure to achieve the desired performance. In order to improve knowledge of conventional heat-exchangers, and also to evaluate the benefit of introducing higher performance designs, a thermal-mechanical laboratory has been built at SOLEIL, and a Ph. D. Thesis financed (2009-2012). Three types of channels have been tested. Depending on the flow rate domain (Reynolds number), substantial differences have been evidenced, allowing for more insightful design choices. Additionally, a more efficient numerical computation technique has been developed for the resolution of the inverse heat conduction problem. Such technique will allow for fast reconstruction of the heat coefficient patterns, based on series of tests with localized heat excitation/temperature measurements.

One salient feature of synchrotron radiation facilities is their capability to deliver stable, high brilliance photon flux, as a result of the deviation of relativistic electrons. Based on first principles, the emitted photon beams are produced uniformly over a 360° span, while end-users (beamlines) can only use a small fraction of that angular aperture. Consequently, it is necessary to introduce components that are able to absorb the corresponding unused power. Such devices, generally named “absorbers”, are placed in to the storage ring in order to save space. Therefore, not only must they accommodate the high incoming thermal fluxes (in the order of a few *hundreds* of MW/m²), but also they must avoid excessive heating so that ultra-high vacuum conditions can be achieved and damages induced by thermal-mechanical induced stresses can be avoided. To meet such a result, one key aspect is the ability to introduce efficient heat-sinks.

In this particular case, it is vital to be in a position to drain the absorbed energy in a highly efficient, compact heat-exchanger. Compactness allows for placing the heat sinks closer to the heat sources and results in shorter heat-conduction paths, simultaneously reducing hot spots and thermal-mechanical stresses.

With those constraints in mind, it is evident that conventional heat exchangers might not fulfill the requirements in all cases. It is also a well-established fact that even for standard geometries, large uncertainties remain in actual values (not to mention space-wise distribution) of the heat transfer (film) coefficient. To deal with those difficulties, standard engineering practice implicitly uses lower-bound, uniform values, as available in the open literature. While efficient and appropriate in most cases, SOLEIL mechanical engineering team has found that it becomes not viable anymore for



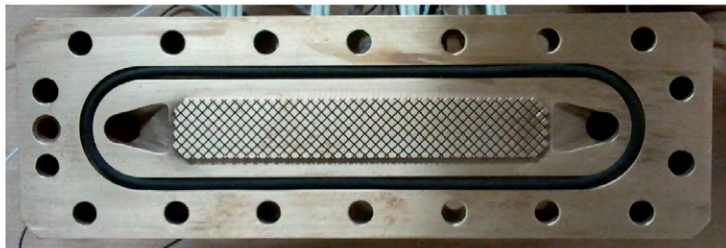
1 Isometric view of diamond shaped fins heat exchanger

the most demanding cases. Therefore, an in-house laboratory has been setup and Ph. D. thesis ([1]) kicked off in 2009, with the objective of resolving both above mentioned shortcoming, i.e. develop and validate methods for i/ obtaining correlations applicable for high performance heat sinks and ii/ determination of the *local* heat exchange coefficients, using an inverse method. Three different prototypes of the heat sinks (one with rectangular mini-channels and two with diamond shaped fins) have been manufactured and tested. Tests were conducted both at atmospheric pressure and in a vacuum chamber. For the mini-channel tests, experimental results were found to be in good correlation with those available in the literature, especially at low Reynolds (i.e. low fluid velocity) numbers. However, in the case of diamond shaped fins, poor agreement was found and new correlations have been proposed. Assuming identical external dimensions and fluid cross section, diamond shaped pins heat sinks have been shown to be much more efficient than mini-channels, the difference being greater at low Reynolds number. Not surprisingly, the induced pressure drop

is always more important for diamond shaped fins. Therefore optimal solution was demonstrated to be largely case dependent, and should inevitably take into account practical limitations (pressure drop and fluid flow rate feasibility). In the case of cooling optical devices, fluid flow rate limitation may become even more stringent due to flow-induced vibrations, so that diamond shaped fins, though more expensive, may become the solely viable option.

Measurements of the thermal contact resistance between parts of the heat sinks were also conducted, which is particularly relevant in the case of cooling of optics on their back side.

A basis for a new, more efficient technique for the resolution of the inverse heat conduction problem is also proposed. This technique has been verified to yield faster results, by reducing the number of numerical calculations necessary to achieve convergence to a solution. Robustness issues, however must be solved before this technique can be routinely used. This will require reduction of sensitivity to measurement errors.



© Diamond shaped fins heat exchanger (prototype)

Conception-Engineering

ASSOCIATED PUBLICATION

N. Jobert* and J. Dasilvacastro

CORRESPONDING AUTHOR

* Synchrotron SOLEIL, l'Orme des Merisiers, St Aubin BP48, 91192 Gif sur Yvette Cedex, France

nicolas.jobert@synchrotron-soleil.fr

REFERENCE

[1] "Development and validation of high-efficiency heat sinks for beamlines absorbers", A. Hamza Ph.D. Thesis, Université de Reims Champagne Ardennes, January 2013

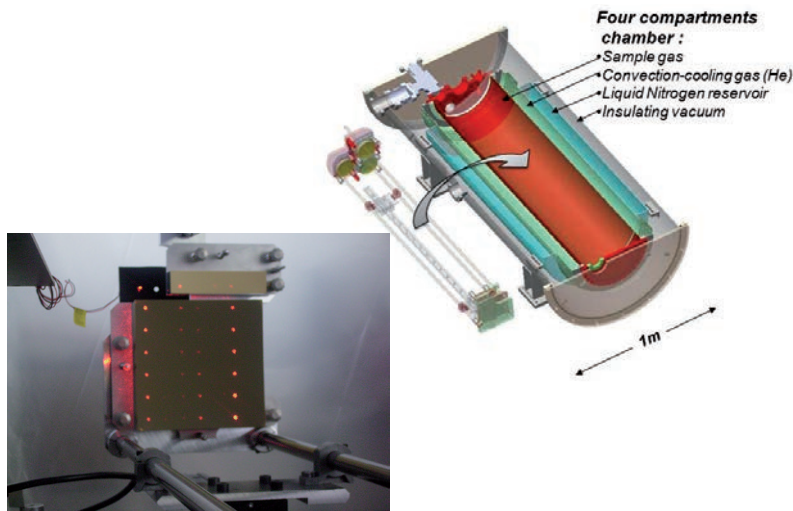
A new tool for greenhouse gases Infrared absorption modelling

Infrared (IR) spectroscopy plays a key role for the remote sensing of atmospheric or astrophysical systems, in particular for the quantification of important gases for the radiation budget of the Earth's atmosphere. This has motivated the development of a long-path cryogenic gas cell at Soleil, in collaboration with the LISA (CNRS-U. D. Diderot and Paris-Est). Measurements at different temperatures are used to study these molecules in situ conditions or to depopulate excited vibrational or rotational levels, a prerequisite for analysis and modelling of their IR absorption. A unique, specific cryogenic gas cell, homogeneously cooled or heated between -190 and $+100^{\circ}\text{C}$, compact and stable enough to be used on the AILES beamline, yet capable of generating optical paths between 3 and 145 meters long, has been developed at SOLEIL. The cell operates in both mid and far IR ranges, allowing easy switching and a rapid change of optical path.

Cryogenics and IR optics, a long pathway and stability: conflicting demands...

For our purpose, the distance light travelled in the absorbing gas can be controlled between 3 and 140 meters, but also at temperatures between -190 and $+100^{\circ}\text{C}$. The cell construction involved corrosion-resistant materials, IR optics compatible with low temperatures, ultra high vacuum and cryogenic systems that do not generate any acoustic vibration. The design was based on the 5-mirror arrangement of Chernin and Berskaya [1] recirculating the beam a number of times between two sets of mirrors (figure 1). This generates long optical path lengths, refolding the beam on itself, making up to 48 round trips in the cell. It enables optimally filling the cell volume and excellent vibrational stability characteristics. Metal mirrors with gold and hard alumina ultrathin coating were employed for their good chemical or mechanical resistance and high reflectivity (99% or better). All mirror holders are equipped with computer-controlled micrometers for optical adjustments and path changes, even at low temperature. A laser can be injected coaxially to the IR beam axis, to check the optical path without venting the interferometer for checking the alignment with visible light (figure 1, insert).

Measuring down to 30 cm^{-1} imposes here a 12 mm focus point size. All elements are thus dimensioned to have twice the focus diameter between two adjacent foci and yet up to 6 columns and 8 rows of focus spots on the field mirrors, yielding a 141 m maximum path length. For the broad spectral coverage, diamond windows were brazed on the stainless steel envelopes for letting the infrared beam in and out the sample gas cell and the outer Dewar vacuum chamber. Interferometry is very sensitive to vibrations and care was taken to minimize any source of acoustic noise. Thus, a concept with a completely static configuration was chosen (no forced circulation pump, no closed-cycle cooler) including a large cryostat around the cell body. Here, the cooling power originates from the heat of vaporization of liquid nitrogen, keeping a surrounding jacket at a constant 77 K temperature. The gas is brought at low temperature through radiative and convection cooling by filling an intermediate jacket with helium gas. The helium pressure can be varied to adapt the cooling power to the desired end temperature. A totally vibration-free operation is ensured by cryogenic trapping and the use of ion pumps.



1 Schematic viewcut of the cryogenic multi pass Infrared gas cell

A need for metrological precision

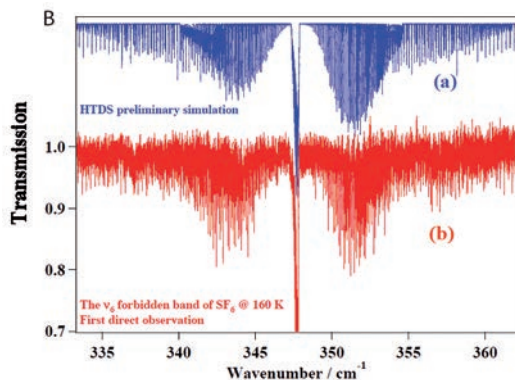
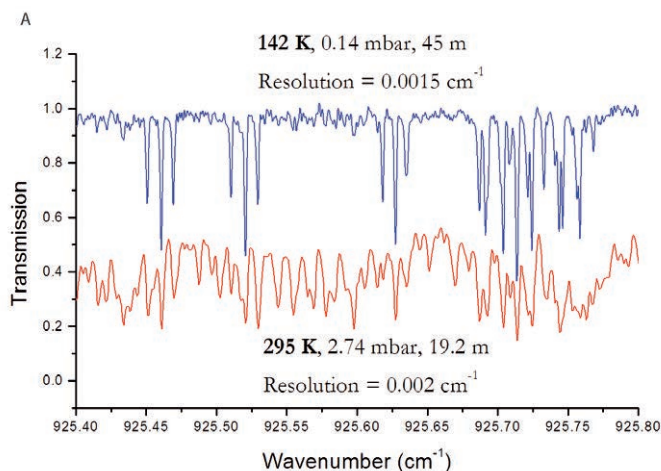
One specific requirement implied development of a cryogenic pressure sensor in the sub-millibar range, for accurately measuring the pressure of the gases for which the profiles and IR absorption cross-sections are being determined. Such a device has also been developed at SOLEIL in collaboration with the Ultra-High Vacuum Group, and enables

in situ measurements of pressure in the 40 to 0.1 mbar range, with 1% accuracy, regardless of temperature. Temperature homogeneity is another major issue and no less than fifteen sensors are dispatched inside the cell and ten regulation control loops ensure a $\pm 2^\circ\text{C}$ temperature homogeneity down to -190°C .

First results and perspectives

The first measurements were carried out in late 2012 and this unique equipment has allowed new observation of spectroscopic features for a potent greenhouse gas (SF_6)

(figure 2) [2]. Since then, the equipment is now operational on the AILES beamline, and investigating atmospheric trace gases.



Examples of greenhouse gas Infrared spectra for optical absorption modelling.
A) C_3H_8 . High Resolution measurements near $11\ \mu\text{m}$ wavelength at 142K for line by line analysis. Note the spectral simplification at low (blue) versus ambient (red) temperature.
B) SF_6 . Observation (red) of the ν_6 IR-forbidden band in the $33\ \mu\text{m}$ region at 160K for modeling IR absorptions (blue) of this high global warming power gas of anthropogenic origin.

AILES beamline

ASSOCIATED PUBLICATION

A new, low temperature long-pass cell for mid-IR to THz spectroscopy and synchrotron radiation use

F. Kwabia Tchana, F. Willaert, L. Lago, X. Landsheere, M. Chapuis, C. Herbeaux, P. Roy, and L. Manceron*

Review of Scientific Instruments, 2013, 84(9) (2013) art. n° 093101

CORRESPONDING AUTHOR

* Synchrotron SOLEIL, l'Orme des Merisiers, St Aubin BP48, 91192 Gif sur Yvette Cedex, France

laurent.manceron@synchrotron-soleil.fr

REFERENCES

- [1] S.M.Chernin & E.G. Barskaya, Appl. Optics 30 (1991), 51
- [2] V.Boudon et al. Phys. Chem. Chem. Phys. 16 (2014), 1415

A versatile source to make complex nanoscopic objects fly under vacuum

We designed a versatile source chamber capable of producing, under vacuum, beams of clusters and nanoparticles for studying their interaction with soft X rays. In its design, special care was taken to use standard components and enable rapid switching between different experimental configurations.

Introduction

Clusters and nanoparticles are important forms of matter bridging the gap between isolated atoms, molecules and the solid state. These systems are therefore of interest in diverse research fields ranging from stellar cloud chemistry, heterogeneous catalysis, to aerosol physics, for example. Studying the physical properties of these different complex systems by sophisticated spectroscopic methods requires the samples to be either generated or introduced into the high vacuum environment of the spectrometers.

Experiments on clusters or nanoparticles have already been implemented at different synchrotron facilities [1,2], but for the first time, the same synchrotron beamline proposes to these two communities the possibility to study these objects with a panel of spectroscopic

tools, such as conventional high-resolution electron spectroscopy (VG-Scienta end station), Auger electron-ion coincidence technique (EPICEA end station) or mass spectrometry. Our aim was to create a source chamber with a versatile, modular, and transportable design. Emphasis was also put on using standard, off-the-shelf products for as many components as possible, to ease experimental maintenance and flexibility. The source chamber also had to be integrated into the SOLEIL TANGO control system for computer control. This enables the recording of all actuators' positions, giving a comprehensive view of experimental settings, and automated scans of actuator positions versus different sensor values. This point is crucial for quick experimental set up, and for finding optimum source conditions.

The PLEIADES Multi Purpose Source Chamber (MPSC)

The MPSC was designed and built in the framework of the Nano-PLEIADES ANR project. It can be coupled with two permanent end stations, a reflectron mass spectrometer belonging to the consortium, or any external user experiment with a CF200 port. Mechanical design and fabrication was performed by the local company, Mecaconcept SARL.

Figure 1 depicts cuts of the MPSC chamber in the two configurations: nanoparticles and clusters. The large chamber (B) is a vertical cylinder with a plexiglass top lid (for quick inspection and servicing without disconnecting the source and experimental chamber). Attached to this chamber are two turbo pumps connected to a Root backing pump.

A differential pumping wall holding the skimmer guarantees a pressure in the experimental chamber in the 10^{-5} mbar range. The source comprises a holder tube together with either the aerodynamic lens system or the molecular/cluster beam system. The holder tube and skimmer can move (with μm accuracy) under vacuum in order to allow the source's outlet and the skimmer to be aligned to each other, and the latter to the synchrotron beam and detector axis. An optional extra differential pumping stage (D') can be used for more demanding nanoparticles. Furthermore, to decrease the time to change the source configuration, it can be isolated from the experimental chamber by retracting it and closing the vacuum tight valve (C).

Nanoparticles configuration

An atmospheric nanoparticle flow is obtained by spraying a liquid solution (nanoparticles in suspension), with an atomizer source. After passing through a diffusion dryer, the aerosol is directed to the lens system made with a calibrated limiting orifice (usually 200 μm), then a relaxation chamber (the tube holder) and ends with the aerodynamic lens itself, based on a design published by Jayne et al

Clusters configuration

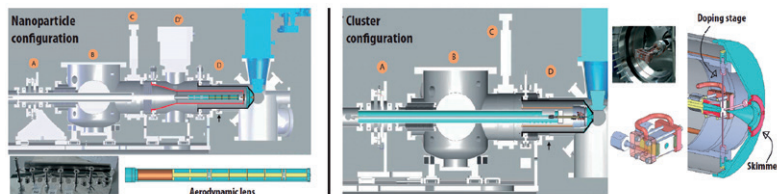
In this configuration, the system allows generation of clusters from gases and liquids (using an oven). Mixed clusters can also be created when a doping stage is inserted just after the nozzle (Fig. 1). Clustering is achieved via adiabatic

[3]. (Fig. 1). The nanoparticle beam (width < 280 μm), focused with the aerodynamic lens, crosses the interaction region where the sample is continuously renewed. The effects of charging, common with deposited nanoparticles, is absent in this case. The beam is sufficiently dense to allow the use of a conventional, hemispherical electron analyzer.

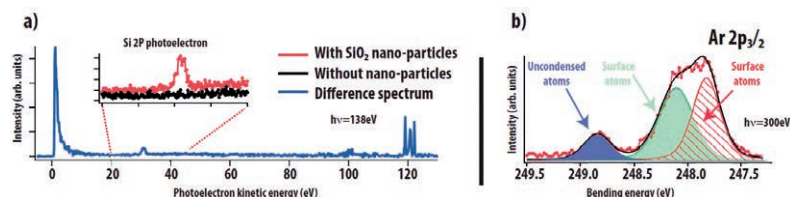
A successful bet

Figure 2 shows the first core level photoelectron spectra obtained at PLEIADES on SiO_2 nanoparticles and on argon/xenon mixed clusters. Two people can easily achieve the switch between the configurations in less than one day. Almost one third of the projects accepted by the program committee require now the use of the MPSC. Mixed atomic clusters, molecular clusters, diverse

nanoparticles, soot particles and biomolecules have already been studied with this source. Two articles linked to it are published and more than five are in preparation. The MPSC was also used to validate a new technique to obtain an online characterisation of the nanoparticle beam focussing, involving a high repetition rate ablation laser. This technique has just been patented.



1 Nanoparticle and cluster beam configurations, with details of the aerodynamic lens, the nozzle and the doping stage.



2 First XPS spectra obtained at PLEIADES for: a) Si 2p photoelectrons of 214 nm SiO_2 nanoparticles and b) Ar $2p_{3/2}$ photoelectrons of mixed Ar/Xe clusters, with an average size of 10^4 atoms.

PLEIADES beamline

ASSOCIATED PUBLICATION

A multi purpose source chamber at the PLEIADES beamline at SOLEIL for spectroscopic studies of isolated species: Cold molecules, clusters, and nanoparticles

A. Lindblad, J. Söderström, C. Nicolas, E. Robert, and C. Miron*

Review of Scientific Instruments 84 (2013), 113105

CORRESPONDING AUTHOR

* Synchrotron SOLEIL, l'Orme des Merisiers, St Aubin BP48, 91192 Gif sur Yvette Cedex, France

catalin.miron@synchrotron-soleil.fr

REFERENCES

- [1] E. Antonsson et al. Chem. Phys. Lett. 559 (2013), 1
- [2] Springer Series Chemical Physics Vol. 52, edited by H. Haberland 1994
- [3] J. T. Jayne et al. Aerosol Sci. Technol. 33 (2000), 49
- [4] R. Kambach et al. Rev. Sci. Instrum. 64 (1993), 2838

Simultaneous fast-scanning XRF, dark field, phase-, and absorption contrast tomography

The multi-technique “FLYSCAN” data acquisition scheme developed at Synchrotron SOLEIL permits to perform fast continuous scanning making scanning tomography feasible during typical user experiments. Here we present the recent results of such simultaneous hard X-ray multi-technique tomography. This fast scanning scheme will be implemented at the Nanoscopium beamline for large field of view 2D and 3D multimodal imaging.

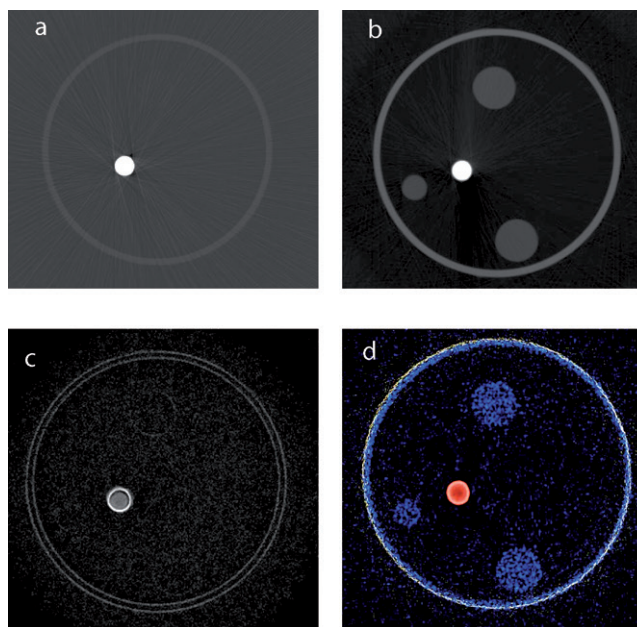
Multi-technique scanning hard X-ray imaging is a powerful technique to obtain spatially resolved and high sensitivity quantitative elemental and structural information by raster scanning the sample in the focused X-ray beam while measuring the transmitted beam and/or the secondary radiation emitted by the sample.

Complementary contrast mechanisms such as absorption, phase, dark field and X-ray fluorescence can be measured simultaneously for obtaining information on the sample structure, composition and chemistry. The combination of all these contrast modalities by scanning tomography provides a unique tool for the nondestructive quantitative study of the sample in three dimensions. The Nanoscopium beamline, (under construction), is dedicated to scanning hard X-Ray 2D/3D multimodal imaging in the 5 to 20 keV energy range. The beamline aims to provide a stable and high intensity nano-beam which can be tailored in the 30-500 nm size-range depending on the experimental needs. The study of

heterogeneous, fragile or large samples will be assured by fast and continuous scanning with sensitive and high frame rate detectors.

The multi-technique “FLYSCAN” data acquisition scheme [1] developed at SOLEIL permits to perform fast continuous multi-technique scanning. In this paper, we present the proof of principle experiments of scanning tomography by the FLYSCAN scheme together with volumetric reconstruction, performed by dedicated algorithm to each measured contrast modality.

The experiments were carried out at the Metrologie beamline of SOLEIL using a temporary scanning microprobe set-up. Monochromatic X-rays of 14 keV were focused down to 1 μm by a Fresnel Zone Plate. The read-out of a silicon photodiode (incoming beam intensity), pixel array detector (XPAD) (transmitted beam), a silicon drift detector (X-ray fluorescence) and the motor encoders were hardware synchronized by a TTL signal (Master Trigger).



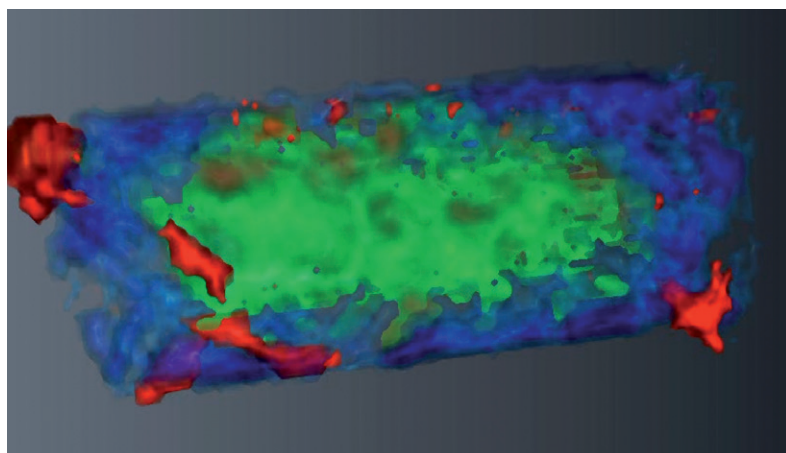
1 Multimodal tomograms : a) Attenuation, b) Phase, c) Dark field, d) X-Ray Fluorescence (red: copper, yellow: silicon, blue : compton scattering)

The tomography of a slice of a test sample (glass capillary containing two nylon fibers and a copper wire) was performed with 500 angular projections, over the full 360° range, in less than 1 hour total acquisition time which was limited by the flux available on the bending magnet beamline. Figure 1 presents the reconstructed tomogram of each contrast modality. The conventional transmission CT (fig. 1.a) reveals the copper wire and with lower contrasts the capillary itself. The phase tomogram (fig. 1.b), where the nylon fibers are visible with a very good contrast, provides complementary information about light materials. The dark field contrast (fig. 1.c) shows the capillary walls and the wires. In the XRF tomogram shown in fig. 1.d the reconstructed Si (capillary), Cu and Compton signals are overlapped. 3D imaging was performed on an 80 µm-thick polished geological sample section consisting of calcium carbonate and organic material layers. The sample also contained small pyrite crystals. The 2D projection images, of 300 x 10 pixels (pixel size: 3 x 3 µm²), were recorded at 6° rotational intervals over 360°. The total acquisition time was less than 2 hours. Figure 2 presents the volume rendering of the absorption, Fe and Ca reconstructions. The pyrite clusters having high Fe content, can be clearly identified.

The performance and the potential of the FLYSCAN architecture for fast multi-technique scanning tomographic imaging have been demonstrated. Simultaneous acquisition of 3D tomographic data sets of X-ray fluorescence, transmission, phase contrast and dark field has been performed in 1-2 hours total acquisition time using a prototype FZP-based microprobe set-up. This experiment performed in step scan mode in the same experimental conditions would take several days.

At the Nanoscopium beamline, where the available flux will be 10³-10⁴ times higher than at the Metrology beamline, the presented experiments will be done in less than half an hour. This will permit the use of scanning tomography techniques routinely during a user experiment.

The authors are grateful to Pascal Phillipot and Marie Sforna from the Institut de Physique du Globe de Paris for providing and preparing the geological sample. We acknowledge G. Baranton (Nanoscopium), P. Da Silva (Metrology) and our colleagues from the Informatics and Electronics (ICA/ECA) Support Groups of SOLEIL who helped with the test experiments.



2 Volume rendering of the 3D tomograms combining the sample absorption (green), the Ca (blue) and the Fe (red) distributions.

NANOSCOPIUM beamline & Informatics-Electronics Group

ASSOCIATED PUBLICATION

Simultaneous fast scanning XRF, dark field, phase-, and absorption contrast tomography

K. Medjoubi*, A. Bonissent, N. Leclercq, F. Langlois, P. Mercère and A. Somogyi

Proceeding: X-Ray Nanoimaging: Instruments and Methods, San Diego (US), August 25, 2013, Proceedings of SPIE, 2013, 8851:art.n° 88510P

CORRESPONDING AUTHOR

* Synchrotron SOLEIL, l'Orme des Merisiers, St Aubin BP48, 91192 Gif sur Yvette Cedex, France

kadda.medjoubi@synchrotron-soleil.fr

REFERENCE

- [1] Medjoubi et al. J. Synchrotron Rad. 20 (2013), 293

The secondary source of NANOSCOPIUM

A new system of slits, designed at SOLEIL, is deployed on the NANOSCOPIUM beamline to define a second, more stable light point source, with better resolution. The very high precision required of these slits ($<0.5 \mu\text{m}$ on the position, $<0.1 \mu\text{m}$ on the mechanical resolution) makes it a real challenge to design them, from the design/manufacture standpoint. In addition, their tremendous stability will allow Zone Plate and Kirkpatrick-Baez optical focusing configurations to be used for experiments with a spatial resolution of 30 nm. This set of (horizontal and vertical) slits is located in a vacuum of the order of 10^{-9} mbar.



The NANOSCOPIUM beamline is one of the long beamlines at SOLEIL. This multi-mode beamline will be used in the 5-20 keV energy range, and dedicated to scanning x-ray micro- and nano-probe experiments with a spatial resolution of 30 nm to 1 μm .

Both mirrors M1 and M2 of the NANOSCOPIUM beamline have a fixed curvature and focus on a system of slits that defines a secondary source. This system is located 85 m from the main source, which is a U20 in-vacuum undulator. This beamline currently operates with a double-crystal monochromator. By 2016, it could also operate with another, multilayer-type monochromator, which will provide up to 5 W power according to the energy range chosen. The power currently received by this secondary source is less than a milliwatt. To prepare for this future monochromator, we have decided to cool the secondary source with water, via copper braids.

These slits have positioning precision of $< 0.5 \mu\text{m}$ with actuator resolution $< 0.1 \mu\text{m}$. The opening value in operating mode is **5 to 50 μm** . The maximum vertical positioning travel to align the slit on the incident beam is **$\pm 3 \text{ mm}$** . The maximum horizontal travel is **30 mm**. This movement also allows for a 'clearance' position, which allows the direct beam to pass through with a 20 mm horizontal and 6 mm vertical opening. The opening of the two horizontal slits is **2 mm**.

The focal plane of mirrors M1 and M2 is located **at the secondary source with a beam size of $1.5 \times 0.066 \text{ mm}^2$ (H \times V) FWHM and divergence of $0.03 \times 0.02 \text{ mrad}$ (H \times V) FWHM**.

The secondary source assembly can translate manually along the axis of the beam for the purpose of adjustment of the order of $\pm 500 \text{ mm}$.

This adjustment is necessary for the alignment of the slits and to compensate for defects in mirrors M1 and M2 located upstream along the beamline.

This assembly must be perfectly stable, with the slits having an eigenmode greater than 60 Hz and the stand having an eigenmode greater than 100 Hz. The maximum vertical variation is less than 100 nm.

This secondary source is located in an air-conditioned room whose temperature is regulated to within $\pm 0.2^\circ\text{C}$.

This assembly is securely attached to a flange with alignment reference. The flange is mounted on three feet to allow the various tests on a bench in the laboratory, with offset acquisitions between the two slits and an alignment reference securely attached to the flange.

The linear actuator operates in-vacuum and consists of a stepper gearmotor that provides 24 mm travel in translation. It translates a wedge, which is guided with respect to the fixed platform by a ball rail. This wedge is symmetrical to allow symmetrical action with respect to the slit. An arm guided by the wedge via another ball rail actuates a sine bar arm. This means that a translation of the wedge actuates the sine bar arm with respect to an axis securely attached to the fixed platform.

This sine bar arm pushes against one of the two knife-edges of the slit. This knife-edge translates along its guide, a deformable parallelogram, whose base is securely attached to the fixed platform. The main advantage of this set-up is that the mechanical errors introduced by the various guide elements are reduced, thanks to the gear reduction ratio of the sine bar arms, which takes place only via flexible elements without play or friction.

NANOSCOPIUM beamline – Design Office

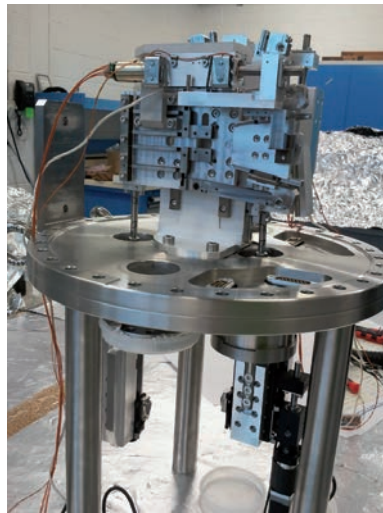
ASSOCIATED PUBLICATION

M. Ribbens*, J. M. Dubuisson and A. Somogyi

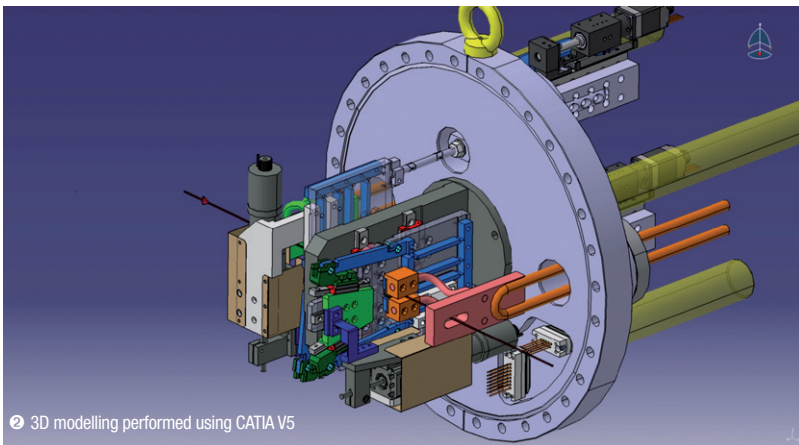
CORRESPONDING AUTHOR

*Synchrotron SOLEIL, l'Orme des Merisiers,
St Aubin BP48, 91192 Gif sur Yvette Cedex,
France

marc.ribbens@synchrotron-soleil.fr

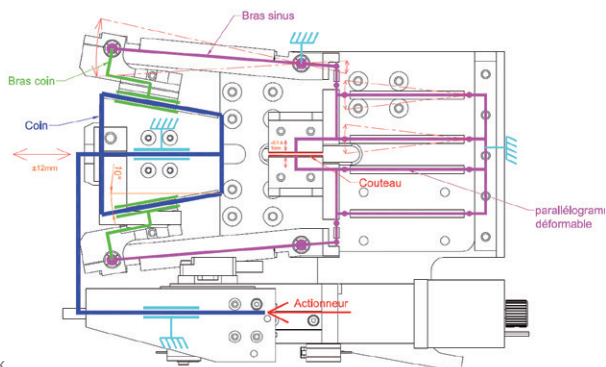


1 Assembly being mounted in the laboratory



2 3D modelling performed using CATIA V5

Bloc Fente



3 Kinematics of a slit block



SOURCES AND ACCELERATORS DIVISION

- 134** Storage ring operation status: performance and evolutions
- 136** News on the storage ring optics: operation performance improvement
- 138** W164: one insertion device for two purposes

SOURCES AND ACCELERATORS DIVISION

Up to twenty-seven beamlines have been using the photon beams in 2013. The installation of the FEMTOSLICING project, both outside and inside the storage ring went without a hitch and the first equipment tests began in late 2013. The W164 wiggler, which will serve as "modulator" for this FEMTOSLICING operation and as photon source for the PUMA beamline, was set up in October 2013. Two new beamline front ends were installed for the future PUMA and ROCK beamlines. In order to save space on the beamline, the first ROCK beamline mirror was positioned in the beamline front end, inside the storage ring tunnel, which is very unusual.

In addition to the daily maintenance work, several heavy reliability actions are underway, notably concerning the redesign of the Booster power supplies, the storage ring magnet power supplies as well as the storage ring radiofrequency system (cavity couplers, power amplifiers and cryogenic system).

Twenty-six very different types of insertion devices are now present in the storage ring. Others are being designed or under construction, such as the U18 cryogenic undulator for the ANATOMIX beamline, a spare U20 in-vacuum undulator for high energy beamlines, a spare HU60 undulator for soft X-ray beamlines and two exotic insertion devices in the context of the collaboration between SOLEIL and MAX IV: an aperiodic WSV50 in-vacuum wiggler and a 3m-long U15 cryo-ready in-vacuum undulator with a 3 mm minimum gap.

Among the R&D projects currently being undertaken in our division, the design of a multipolar injection kicker, that allows injection without disturbing the stored beam, is at an advanced stage. Its construction should begin in 2014 with an installation in the MAX IV storage ring scheduled in 2015.

At the end of 2013, a know-how license agreement for the manufacture of RF solid state amplifiers was signed between the company SIGMAPHI ELECTRONICS and SOLEIL. This cutting-edge technology is a competitive, efficient, reliable and effective alternative for providing a power source to radiofrequency cavities, and was developed by SOLEIL's "RF and Linac" group.

One of the priorities among the many objectives for 2014 is the commissioning with beam of the FEMTOSLICING project and the fact that users of the CRISTAL beamline will use radiation from this ultra-short electron bunch before the end of 2014. Very stringent specifications on the stability of the position and size of the photon beam for the NANOSCOPIUM beamline will be evaluated and additional resources will be made available to meet them.

Also worth noting: the transition to a stored current of 500 mA with uniform filling pattern will be offered to users in 2014.

Finally, feasibility studies will begin in order to optimize optics with an horizontal emittance at least 10 times lower than the present one.

Amor Nadji

Director of the "Sources and Accelerators Division"

DIVISION SOURCES ET ACCÉLÉRATEURS

Vingt-sept lignes de lumière ont utilisé le faisceau en 2013. L'installation du projet FEMTOSLICING, à l'extérieur comme à l'intérieur de l'anneau de stockage, s'est très bien déroulée et les premiers tests des équipements ont commencé fin 2013. Le wiggler W164, qui servira de « modulateur » pour cette opération FEMTOSLICING et de source de lumière pour la ligne PUMA, a été mis en place en octobre 2013. Deux nouvelles têtes de lignes ont été installées pour les futures lignes PUMA et ROCK. De façon inhabituelle et pour gagner de l'espace sur la ligne, le premier miroir de la ligne ROCK est positionné dans la tête de ligne, à l'intérieur de l'anneau.

En plus du travail quotidien de maintenance, plusieurs actions lourdes de fiabilisation sont en cours, notamment concernant les tiroirs de puissance des alimentations du Booster dont la conception est modifiée, les alimentations de l'anneau ainsi que le système radiofréquence (RF) de l'anneau (coupleurs de cavités, amplificateurs de puissance et cryogénie).

Vingt-six éléments d'insertions de types très différents sont maintenant présents dans l'anneau. D'autres sont en cours de conception ou de construction, comme l'onduleur cryogénique U18 de la ligne ANATOMIX, un onduleur sous vide U20 de rechange pour les lignes de haute énergie, un onduleur HU60 de rechange pour les lignes X-mous et deux insertions exotiques dans le cadre de la collaboration entre SOLEIL et MAX IV : un wiggler sous vide de type WSV50 apériodique et un onduleur sous vide cryo-ready U15 de 3 m de long avec un entrefer de 3 mm.

Parmi les sujets de R&D en cours autour de l'anneau, la conception du kicker d'injection multipolaire, qui permet d'injecter sans perturber le faisceau stocké, est bien avancée. Sa construction doit débiter en 2014 pour une installation sur l'anneau de MAX IV courant 2015.

Fin 2013, un accord de licence de savoir-faire pour la fabrication d'amplificateurs de puissance RF à transistors a été signé entre l'entreprise SIGMAPHI ELECTRONICS et SOLEIL. Cette technologie originale est une alternative compétitive, performante, fiable et efficace pour fournir une source de puissance aux cavités radiofréquences ; elle a été développée par le groupe « RF et Linac » de SOLEIL.

Parmi les nombreux objectifs de 2014, citons le commissioning avec faisceau du projet FEMTOSLICING, qui est une priorité, et le fait que les utilisateurs de la ligne CRISTAL exploiteront le rayonnement issu des paquets ultra-courts ainsi produits avant fin 2014. Les spécifications très serrées sur la stabilité de la position et la taille du faisceau de photons sur la ligne NANOSCOPIUM seront quantifiées et des moyens supplémentaires seront mis en œuvre pour les satisfaire.

A noter également que le passage à un courant stocké de 500 mA en remplissage uniforme sera proposé aux utilisateurs.

Enfin, vont débiter cette année les études de faisabilité d'un réglage de l'anneau permettant d'atteindre une émittance horizontale au moins 10 fois plus faible que celle du réglage actuel.

Amor Nadji

Directeur de la Division « Sources et Accélérateurs »

Storage ring operation status: performance and evolutions

In 2013, the number of beamlines (BLs) benefitting from the SOLEIL high flux and high brilliance photon beams hit a new record of 27. Among them three BLs are now under commissioning (NANOSCOPIUM, HERMES and ROCK). Two additional beamlines are under heavy construction (ANATOMIX and PUMA).

Five electron filling patterns are routinely used during user operation; all of them with Top-up injection and high beam stability (see Table 1). Figure 1 gives their distribution during 2013.

The multibunch hybrid filling pattern is overwhelmingly requested: 83.2 % of the total number of shifts. The time allocated to Low-Alpha operation has been increased from 2.3 % in 2012 to 3.3 % in 2013.

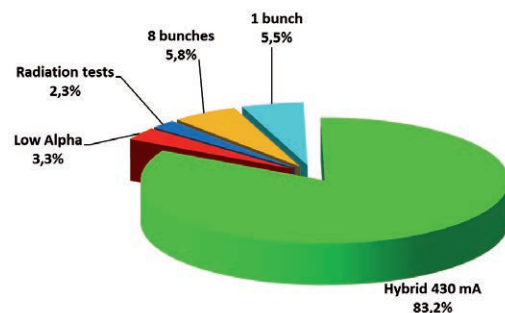
The statistics of the different quality metrics of the operation are rather good for the year 2013. First, the availability

of the photon beams for the beamlines has reached 98 %, which corresponds to a total of 4 912 hours out of the 5 015 scheduled hours. As shown in Figure 2, electrical power drops are once again the main source of beam interruption (29 % of the total) with 18 beam trips. Even if the latter were shorter than one second long, there resulted in a total of 30 hours of beam interruption. The second main source of beam interruption (28 %) was erratic and short transient current spikes of a few quadrupole power supplies. This problem occurred mainly during the first week of the year, just after the Christmas shutdown; nevertheless, besides numerous investigations, the origin is not yet fully understood. This led in turn to 21 hours of beam loss during the first week of the year. Hopefully the rest of the year, and particularly its end, was conversely of exceptionally high beam quality. The record for the longest user beam was broken twice in a row during the last run of the year as illustrated by Figure 3.

Table 1: FIVE DIFFERENT FILLING PATTERNS FOR SOLEIL USERS

FILLING PATTERN	2013 USER OPERATION	ULTIMATE PERFORMANCE ACHIEVED
Uniform (416 bunches)	430 mA	500 mA
Hybrid (312 + 1 bunches)	425 + 5 mA	420 + 10 mA
8 bunches	88 mA	110 mA
1 bunch	15 mA	20 mA
Hybrid Low-Alpha (bunch length, bunch current)	4.7 ps RMS, 65 μ A/bunch	3 ps RMS, 15 μ A/ bunch

Beamline and radiation tests beam time (4912 hours) repartition according to the filling modes in 2013



1 Distribution of the filling patterns delivered to users in 2013

This record level of 542 hours of uninterrupted user beam time significantly exceeded the 360 hours reached during the year 2011.

Three other record levels were exceeded: 1/ the highest efficiency during a run (99.4 %); 2/ the longest mean time between failures during a single run (332 hours) and 3/ during a year (68 hours). Throughout the 35 weeks of operation, an efficiency above 99 % has been obtained during 21 weeks, 9 of which reaching 100 %. The praiseworthy reliability and performance have to be credited to the teams working around the accelerator facilities.

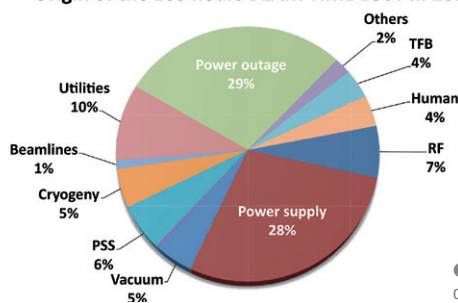
With respect to the storage ring equipment, an unexpected high rate of radiation-induced damages was discovered. Detailed investigations enabled us to understand that the dipole synchrotron radiation (less than 10 %) is intercepted by the so-called aluminium "quadrupole" vacuum chambers; X-ray fluorescence is then emitted by the material components of their NEG coating; the energy of these X-rays is too high to be significantly attenuated by the aluminium material [1]. In order to have a full characterisation of this phenomenon and to devise ways to reduce this

detrimental effect, a dedicated free dipole exit port has been recently equipped with diagnostics and different types of vacuum chamber material with and without NEG coating.

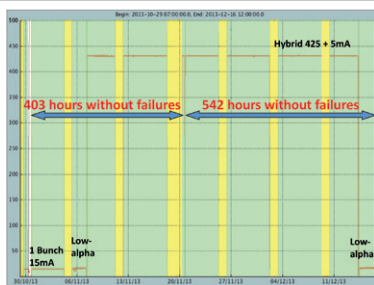
Concerning the insertion devices, the commissioning of the fast switching Apple-II type 65 mm period EMPHU undulator [2] has required a lot of efforts in order to reach satisfactory results in term of beam position stability for all its modes of operation. The commissioning of the newly installed W164 wiggler (cf page 138) is going on; it will serve both as a radiation source for the PUMA beamline and as a modulator for the femtoslicing project.

Finally, since October 2013 a new optics is in operation allowing the suppression of the excess of activation in the short straight section (SDC15) region induced by particle losses due to the beam lifetime. In addition, the sensitivity to possible skew quadrupole failures has been discarded and the routinely injection efficiency and beam lifetime are around 80 % and 13 h (for a 430 mA stored current) respectively exhibiting an increase by about 20 % with respect to the previous optics settings (cf page 136).

Origin of the 103 hours BEAM TIME LOST in 2013



② Pie chart of the distribution per domain of the beam loss origin in 2013



③ Two subsequent record levels of uninterrupted user beam reached during the last run of 2013 (yellow parts are machine dedicated periods)

Machine Operation

ASSOCIATED PUBLICATION

J.-F. Lamarre*, X. Delétoile, L. S. Nadolski and A. Nadji

CORRESPONDING AUTHOR

*Synchrotron SOLEIL, l'Orme des Merisiers, St Aubin BP48, 91192 Gif sur Yvette Cedex, France

jean-francois.lamarre@synchrotron-soleil.fr

REFERENCES

- [1] Radiation Damages and Characterization in the SOLEIL Storage Ring, N. Hubert et al., 644 (IBIC2013)
- [2] Highlights SOLEIL 140 (2012)

News on the storage ring optics: operation performance improvement

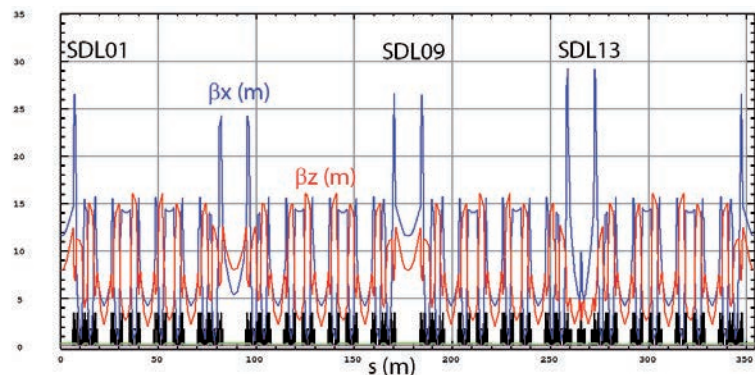
One year ago, the SOLEIL storage ring optics went through the most significant upgrade since its commissioning in 2006. The four-fold symmetry of the storage ring was broken in order to incorporate the new focusing optics for the two long beamlines ANATOMIX/Nanoscopium taken their photon beams from canted insertion devices hosted in a long straight section. Besides these major modifications, the year 2013 was an opportunity to tune even further more the optics (quadrupole and sextupole magnets) in order to make the operation of the light source less sensitive to the configurations of the insertion devices freely controlled by users and to the settings of the skew quadrupoles used to correct and maintain the coupling between the horizontal and vertical plane. Significant performance improvement (injection efficiency and lifetime) and ease of operation were successfully reached.

During the year 2011, a new storage ring optics was commissioned. The optical functions were significantly 2011 with the addition of a quadrupole triplet in the middle of one long straight section (SDL13). This is the so-called ANATOMIX-Nanoscopium optics creating a double minimum of the vertical beta function in order to focus the electron beam in the center of both canted insertion devices (ID) [1]. Since the beginning of 2012, the storage ring was operated daily in this configuration with good performances. Nevertheless, this new optics is not trivial since the four-fold symmetry of the storage ring lattice is broken and the machine performance (the injection efficiency and beam lifetime strongly linked to non-linear beam dynamics) is still sensitive to the increasing number of IDs. A second important point was to improve the too high sensitivity of the optics to the betatron coupling. This latter is minimized using special correctors, namely the skew quadrupole correctors. A large drop of the injection efficiency was observed, to a value close to or even below the radiation safety threshold, when these skew correctors were turned off. This could jeopardize the Top-up operation in case of a skew corrector failure. In addition, the machine was suffering from electron losses mainly localized in the SDC15 short straight section due to lifetime losses

when particles get scattered and change their energies by a few percent, as well as during beam losses when the beam is interrupted by the machine interlock or the personal safety systems. In both cases, large off-momentum non-linear dynamics is involved (enhanced by the broken symmetry) and is coupled to a specific horizontal physical aperture reduction in the inner side of SDC15.

A second iteration of optics optimization was then undergone during the year 2013 in order to reduce this machine sensitivity. The first step was to increase the horizontal beta function in the injection long straight section (SDL01) from 5 to 11 m keeping the rest of the lattice as well as the beamline source point dimensions unchanged (Figure 1). This increase mechanically enlarged the dynamic aperture at the injection amplitude by pushing away dangerous resonances (from Figures 2 to 3). The result was a substantial gain for the injection efficiency in presence of the IDs, relaxing the critical betatron coupling dependence. The injection efficiency is now affected by less than 10% for any ID configurations. However, the electron losses were still important in SDC15.

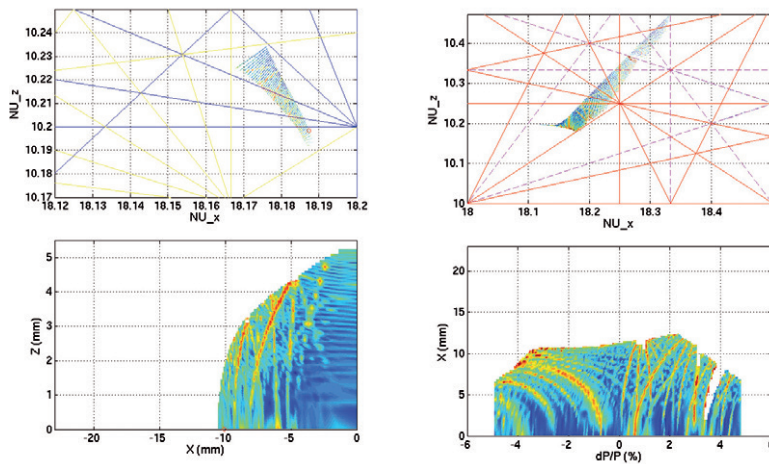
To cope with this point, as a second step, the horizontal beta function in the opposite free long straight section (SDL09) was also increased from 5 to 11 m without



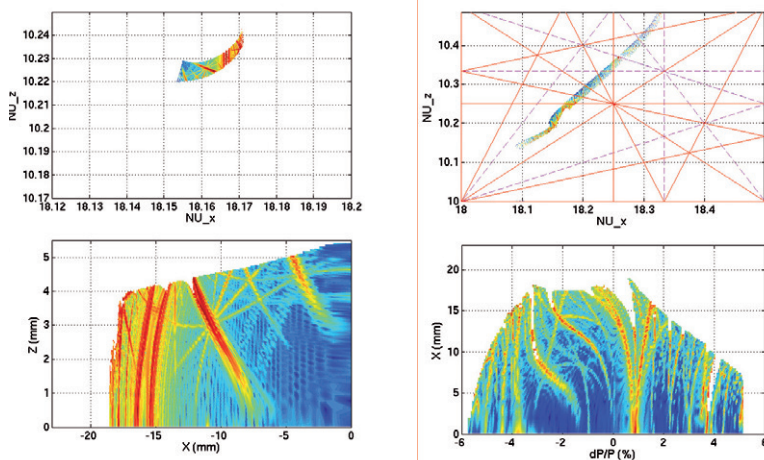
1 SOLEIL storage ring optical functions.

modifying the rest of the optics (Figure 1). This new optics setting redistributes the large off-momentum particle orbits; the amplitudes are now much reduced at the SDC15 location, while they are increased at the horizontal scraper location which is dedicated to collect the beam losses. The last step keeps the previous advantages (gain in the performance and the reduced betatron coupling dependency) along with suppressing losses in the SDC15 straight section.

Since October 2013, this new optics has been in operation. The previous excess of activation in the SDC15 region has effectively been suppressed; the sensitivity to a possible skew corrector failure has been discarded; today for whatever ID configuration, during operation, the injection efficiency and beam lifetime are routinely kept around 80% with a 13 h electron beam lifetime (for 430 mA stored current in hybrid filling pattern), exhibiting a 20% increase, for both parameters, as compare to the 2012 optics.



② Frequency map analysis of the 2012 optics, on-momentum left and off-momentum right. (The working point is 18.176/10.234, chromaticities are 1.4/2.4).



③ Frequency map analysis of the new optics, on-momentum left and off-momentum right. (The working point is 18.155/10.229, chromaticities are 1.2/2.0).

Accelerator Physics Group

ASSOCIATED PUBLICATION

Alexandre Loulergue*

CORRESPONDING AUTHOR

* Synchrotron SOLEIL, l'Orme des Merisiers, St Aubin BP48, 91192 Gif sur Yvette Cedex, France

alexandre.loulergue@synchrotron-soleil.fr

REFERENCE

[1] A. Loulergue, SOLEIL Highlights 122 (2011)

W164: one insertion device for two purposes

An out-vacuum wiggler, W164, was designed, built and installed on the SOLEIL storage ring with the double objective to produce high energy photons for the PUMA beamline (10 keV to 70 keV) and to be used as a modulator for the FEMTOSLICING project [1]. The insertion device requires simultaneously reaching high critical energy of photons (above 10 keV) and low resonant energy (1.55 eV). The wiggler is composed of 20 periods of 164.4 mm made of NdFeB magnets and Vanadium Permendur poles. The maximum total field reaches 1.85 T at the minimum gap and 1.66 T at the FEMTOSLICING operation gap. The size of the poles, the carriage and the girders were optimized to minimize the deformation resulting from the magnetic forces (8 tons at minimum gap).

The SOLEIL FEMTOSLICING [2] is a multi-user project focused on the production of ultra-short photon pulses (~100 fs). It is based on the exchange of energy resulting from the interaction inside a wiggler (“modulator”) of electron bunches and an external short pulse laser. The wiggler resonant wavelength matches the 800 nm laser wavelength (in fact the energy exchange is optimum when the wiggler operates at 780 nm). The other specificity

of the SOLEIL modulator is that it is also used as a high energy photon source (10 keV to 70 keV) for the PUMA beamline [3]. The construction of W164 gathers thus two goals. The first is to reach low photon energy which is not the predilection spectral range of medium/high energy storage rings such as SOLEIL. The second is to operate the modulator at high critical energy. Both constraints require building a wiggler with high field and large period.

Description of W164

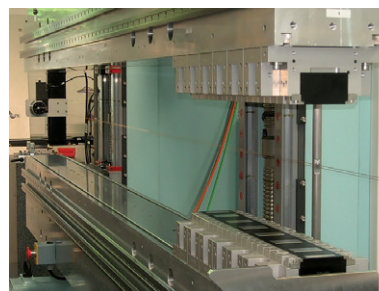
Magnetic design

The magnetic system is composed of 20 periods of 164.4 mm generating a maximum field of 1.85 T at a minimum gap of 14.5 mm. Each period consists of NdFeB permanent magnets and Vanadium Permendur poles assembled on aluminum holders and mounted on two aluminum beams (Fig. 1). The magnetic field is changed by moving the gap between the beams from 14.5 mm to 240. Particular

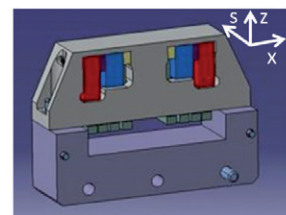
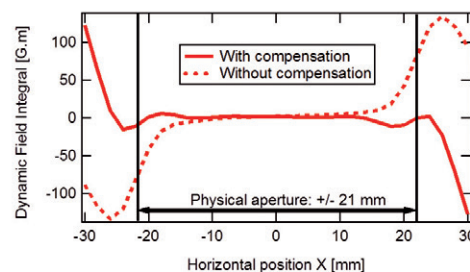
care has been taken in the design of the carriage to avoid excessive deformations which result from high magnetic forces between magnet arrays (up to 8 tons). Thanks to the stiffness of the girders (300 mm), the rigidity of the frame and the small transverse size of the poles (50 mm), their planarity and parallelism remain within 0.1 mm under load. However, the small transverse size of the poles impacts strongly the transverse homogeneity of the magnetic field and generates an off-axis strong field integral (“Dynamic field integral”) [4] which could be responsible for nasty effects on the beam dynamics.

Compensation system

Four dedicated compensation systems were designed and built at SOLEIL to reduce the off-axis dynamic field integral (Fig. 2, left). Each of them is composed of four vertically polarized permanent magnets mounted in an aluminum box (Fig. 2, right).



1 W164 during assembling.



2 Calculated reduction of the dynamic field integral (Left) resulting from the effect of the compensation system (Right) at minimum gap (14.5 mm).

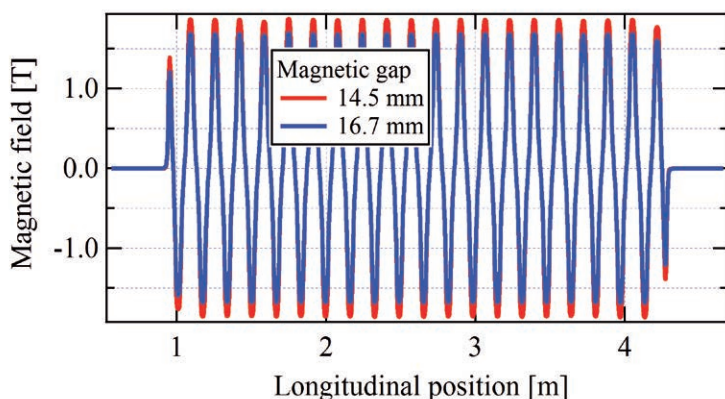
Magnetic measurements

Hall probe measurements

The magnetic field is measured with a Hall probe system moving along the wiggler axis in order to find the gap (FEMTOSLICING operational gap) corresponding to a resonant energy of 780 nm. The magnetic field reaches 1.85 T at the minimum gap and 1.66 T at the 16.7 mm FEMTOSLICING operation gap (Fig. 3).

Field integral measurements

Field integral measurements enable to deduce the kick angle experienced by the electron beam at the exit of the wiggler which should vanish if the wiggler is perfect. A six meter air coil travelling transversally in the median plane of the wiggler is used to evaluate both the residual horizontal and vertical field integrals and their transverse homogeneity.



3 Measured magnetic field of W164 at minimum gap (14.5 mm) and FEMTOSLICING operational gap (16.7 mm).

On beam commissioning

The characterization of the wiggler using the electron beam has started just after its installation (October 2013) in the ring. It has been verified first that the wiggler can be closed at minimum gap with a 500 mA stored beam without damaging the front end absorber. A special tuning of the storage ring optics has been optimized to operate the wiggler at 16.7 mm gap for the FEMTOSLICING experiments. As expected, due to the high field value, the horizontal emittance is increased by 10% at minimum gap. The effects on the main

electron beam parameters (tunes and chromaticities) have been measured and the very good agreement with expected values confirms the high quality of the magnetic measurements. In a second step it is intended on the one hand to study the effect of the wiggler on beam lifetime and injection rate, in order to evaluate the efficiency of the compensation system. On the other hand optical performances of the wiggler such as laser-synchrotron radiation overlap, spatial and spectral photon distribution will be measured.

Magnetism & Insertions group

ASSOCIATED PUBLICATION

O. Marcouillé*, H. Abualrob, P. Brunelle, L. Chapuis, M.-E. Couprie, T. Elajjouri, M. Labat, J.-L. Marlats, A. Mary, A. Nadji, K. Tavakoli and M.-A. Tordeux

CORRESPONDING AUTHOR

*Synchrotron SOLEIL, l'Orme des Merisiers, St Aubin BP48, 91192 Gif sur Yvette Cedex, France

olivier.marcouille@synchrotron-soleil.fr

REFERENCES

- [1] A. Zholents & Zoloterev, Phys. Rev. Lett 76 (1996), 912
- [2] A. Nadji et al. Proc. of EPAC2004 conference, Lucerne, Switzerland 2332 (2004)
- [3] PUMA website: www.synchrotron-soleil.fr/Recherche/IPANEMA/methodessynchrotron#puma
- [4] J. Safranek et al. Phys. Rev. ST Accel. Beams 2002 Vol. 5, 010701

Acknowledgements to all the authors
Edition: Communication Unit

Design & printing
 Poussières d'Étoiles

Copyrights : SOLEIL

Photos credits : SOLEIL, C. Mennéglier,
V. Moncorgé, L. Persin – CAVOK Production,
N. Piroux, J. Rangapanaiken – CNRS
© SOLEIL - May 2014

Communication Unit
SOLEIL Synchrotron
L'Orme des Merisiers Saint-Aubin - BP 48
91192 Gif-sur-Yvette Cedex - France
webcom@synchrotron-soleil.fr

www.synchrotron-soleil.fr

SURFACES, INTERFACES
AND NANOSYSTEMS

CHEMISTRY AND PHYSICAL CHEMISTRY,
NANOCHEMISTRY

BIOLOGY
AND HEALTH SCIENCES

ATOMIC AND MOLECULAR PHYSICS,
DILUTE MATTER, UNIVERSE SCIENCE

PHYSICS AND CHEMISTRY
OF CONDENSED MATTER, EARTH SCIENCES

MODELING, METHODOLOGY
AND INSTRUMENTATION

SOURCES AND ACCELERATORS DIVISION



SOLEIL Synchrotron
L'Orme des Merisiers Saint-Aubin - BP 48
91192 Gif-sur-Yvette Cedex - France
www.synchrotron-soleil.fr